UNIVERSITY OF SOUTHAMPTON

Faculty of Engineering and Physical Sciences

School of Physics and Astronomy

Testing Heavy Scale Seesaw Models at Future Colliders

by

YI LIU

ORCiD: 0009-0005-0466-743X

A thesis for the degree of

Doctor of Philosophy

March 2024

University of Southampton

Abstract

Faculty of Engineering and Physical Sciences

School of Physics and Astronomy

Doctor of Philosophy

Testing Heavy Scale Seesaw Models at Future Colliders

by YI LIU

In this thesis, we introduce the Standard Model (SM) and give motivations for extending it. Amongst the many possible Beyond SM (BSM) scenarios, Supersymmetry (SUSY) combined with a seesaw mechanism is a promising portal to new physics able to remedy several flaws of the SM, which we highlight. Specifically, we discuss SUSY models with high scale seesaw from a phenomenological perspective and test these at future colliders. We start by studying the Next-to-Minimal Supersymmetric Standard Model with right-handed neutrinos (NMSSMr) at the International Linear Collider (ILC) when the lightest right-handed sneutrino is the Dark Matter (DM) candidate. By exploiting a 'dijet + dilepton + Missing Transverse Energy (MET or $\not{E}_T$)' signature, we estimate the size of the neutrino Yukawa coupling. In addition, we show that, in some SUSY scenarios combined with selected seesaw models, the large Yukawa couplings produced can leave their fingerprints in Higgs-slepton couplings entering hadro-production processes. For example, in Type-I and Type-III seesaw, we can potentially observe $\tilde{\nu}_2 \to \tilde{\nu}_1 h$ and $\tilde{\ell}_2^{\pm} \to \tilde{\ell}_1^{\pm} h$ decays, respectively. Unfortunately, the current exclusion bounds make it impossible to observe a significant signal of these even at the High-Luminosity Large Hadron Collider (HL-LHC), with luminosity $\mathcal{L} = 1$ ab^{-1}. Thus, we highlight that the High-Energy LHC (HE-LHC), with energy $\sqrt{s} = 27$ TeV, could provide some sensitivity to such signals in the single lepton channel. The final part of this thesis is instead focused on CP-violation effect in the B-L Supersymmetric Standard Model (BLSSM) with inverse seesaw by measuring Triple Product Asymmetries (TPAs) in 'lepton + jet' final states induced by Z' state at the Future Circular Collider operating in hadron-hadron mode (FCC-hh), with $\sqrt{s} = 80$ TeV.

Contents

List of Figures

List of Tables

Declaration of Authorship

I declare that this thesis and the work presented in it is my own and has been generated by me as the result of my own original research.

I confirm that:

1. This work was done wholly or mainly while in candidature for a research degree at this University;
2. Where any part of this thesis has previously been submitted for a degree or any other qualification at this University or any other institution, this has been clearly stated;
3. Where I have consulted the published work of others, this is always clearly attributed;
4. Where I have quoted from the work of others, the source is always given. With the exception of such quotations, this thesis is entirely my own work;
5. I have acknowledged all main sources of help;
6. Where the thesis is based on work done by myself jointly with others, I have made clear exactly what was done by others and what I have contributed myself;
7. Parts of this work have been published as: [2],[3]

Signed:..... Date:.....

Acknowledgements

First and foremost, I would like to thank my supervisors, Professor Stefano Moretti and Doctor Harri Waltari, for their guidance, support, and patience. It is a pleasure to collaborate with them. I am inspired by their passion and rigor in physics. We solve problems together, we contribute to papers together, and we helped each other during the COVID time.

Then I would like to thank the members of the Southampton High Energy Physics group at the University of Southampton. It is a supportive and friendly community to wander with in the world of particle physics. Especially, I would like to thank my friend Muyuan Song for interesting and inspiring discussions.

Last, but certainly not least, I would like to thank my family. I am truly grateful for their care and dedication. I am fortunate to have them in my life.

To my family

Definitions and Abbreviations

ALICE	A Large Ion Collider Experiment
ATLAS	A Toroidal LHC Apparatus
BLSSM	B-L Supersmmetric Standard Model
BPs	Benchmark Points
BR	Branching Ratio
BSM	Beyond the Standard Model
CKM	Cabibbo–Kobayashi–Maskawa
CMB	Cosmic Microwave Background
CMS	Compact Muon Solenoid
CSC	Cathode Strip Chamber
DAQ	Data Acquisition System
DM	Dark Matter
DR	Damping Rings
DT	Drift Tube
ECAL	Electromagnetic Calorimeter
EW	Electro-Weak
EWSB	Electro-Weak Symmetry Breaking
FCC	Future Circular Collider
GCT	Global Calorimeter
GMT	Global Muon Trigger
GR	General Relativity
GT	Global Trigger
GUT	Grand Unification Theory

HCAL	Hadronic Calorimeter
HE-LHC	High-Energy LHC
HF	Forward Calorimeter
HH	Higgs boson pair
HL-LHC	High-Luminosity LHC
HLT	High-Level Trigger
ILC	International Linear Collider
ILD	International Larger Detector
IRs	Insertion Regions
LEIR	Low Energy Ion Ring
LEP	Large Electron-Positron (collider)
LEP	Large Electron-Positron collider
LH	Left-Handed
LHC	Large Hadron Collider
LHCb	Large Hadron Collider beauty
LS	Long Shutdown
LSP	Lightest Supersymmetric Particle
MC	Monte Carlo
MSSM	Minimal Supersymmetric Standard Model
MSSMr	MSSM with right-handed neutrinos
MU	Muon System
nEDM	neutron electric dipole moment
NLSP	Next-to-LSP
NMSSM	Next-to-Minimal Supersymmetric Standard Model
NMSSMr	NMSSM with right-handed neutrinos
PMNS	Pontecorvo–Maki–Nakagawa–Sakata matrix
PS	Proton Synchrotron
PSB	Proton Synchrotron Booster
PU	Pile-Up
QFT	Quantum Field Theory
RCT	Regional Calorimeter Trigger

RF	Radio Frequency
RGE	Renormalisation Group Evolution
RH	Right-Handed
RPC	Resistive-Plate Chamber
SCRF	Superconducting Radio-Frequency
SM	The Standard Model
SPS	Super Proton Synchrotron
SSB	Spontaneous Symmetry Breaking
SUSY	Supersymmetry
TPAs	Triple Product Asymmetries
TRK	Tracker
TTC	Timing and Control
VEV	Vacuum Expectation Value
WIMPs	Weak Interacting Massive Particles

Chapter 1

Introduction

1.1 Standard Model

Particle physics is an important branch of modern physics that focuses on describing the fundamental forces and elementary particles that constitute our universe. The SM [4; 5] provides the most precise description of the fundamental world. The SM is self-consistent from a theoretical standpoint and has demonstrated great success in making experimental predictions. According to the current understanding, the SM describes three of the four known fundamental forces (EM, weak and strong interactions, thus excluding gravity), three generations of matter (quarks and leptons), four gauge bosons and one Higgs boson, as shown in figure 1.1. The mathematical framework of the SM is established by Quantum Field Theory (QFT) [4; 5; 6; 7; 8; 9].

The elementary constituents of matter are quarks and leptons, which obey Fermi-Dirac statistics and are known as fermions. Particles that follow Bose-Einstein statistics are called bosons. The six quarks and six leptons together form three generations. Particles in the first generation are more stable and have lighter masses compared to their corresponding particles in the second and third generations. In the universe, all stable matter is composed of particles from the first generation. Heavier particles decay into stable particles.

There are four known fundamental forces in the universe: the EM force, the strong force, the weak force and the gravitational force. These forces have different ranges and strengths. Gravity and the EM force have infinite ranges, with the EM force being much stronger than gravity (at small distances), which is the weakest among the four forces. Furthermore, the strong force and the weak force have a subatomic-level range. The strong force is the strongest of all fundamental interactions, while the weak force, as its name suggests, is the weakest (except for gravity).

In the SM, three of the fundamental forces (EM, strong and weak) are described by QFT with their interactions mediated by gauge bosons. Specifically, the photon serves as the gauge boson for the EM interaction, the $W^{\pm}$ and Z bosons are responsible for the weak interaction and there are eight gluons for the strong interaction. Furthermore, the gravitational force is described by GR and is not currently included in the SM.

There is one Higgs boson, a neutral and unstable elementary particle with spin 0. The Higgs boson is produced by the quantum excitation of the Higgs field, which is giving mass to all fundamental particles through the Higgs mechanism, This mechanism is the remarkable offspring of the marriage of local gauge invariance and SSB [10; 11; 12]. Specifically, SSB gives mass to the $W^{\pm}$ and Z bosons, while fermions gain mass through Yukawa couplings between the fermion fields and the Higgs field.

1.2 Beyond the SM (BSM)

Although the SM is the most successful theory in particle physics to date, there are some phenomena and theoretical problems that cannot be explained.

The most direct evidence for the incompleteness of the SM is its inability to explain gravity. Gravity is described by GR which regards gravity as the curvature of space-time. Like Wheeler said: 'Spacetime tells matter how to move; matter tells space-time how to curve' [13]. From a theoretical perspective, gravity is perturbatively non-renormalizable because space-time is dynamic in GR, which makes it mathematically challenging to build a quantum gravity model. From an experimental

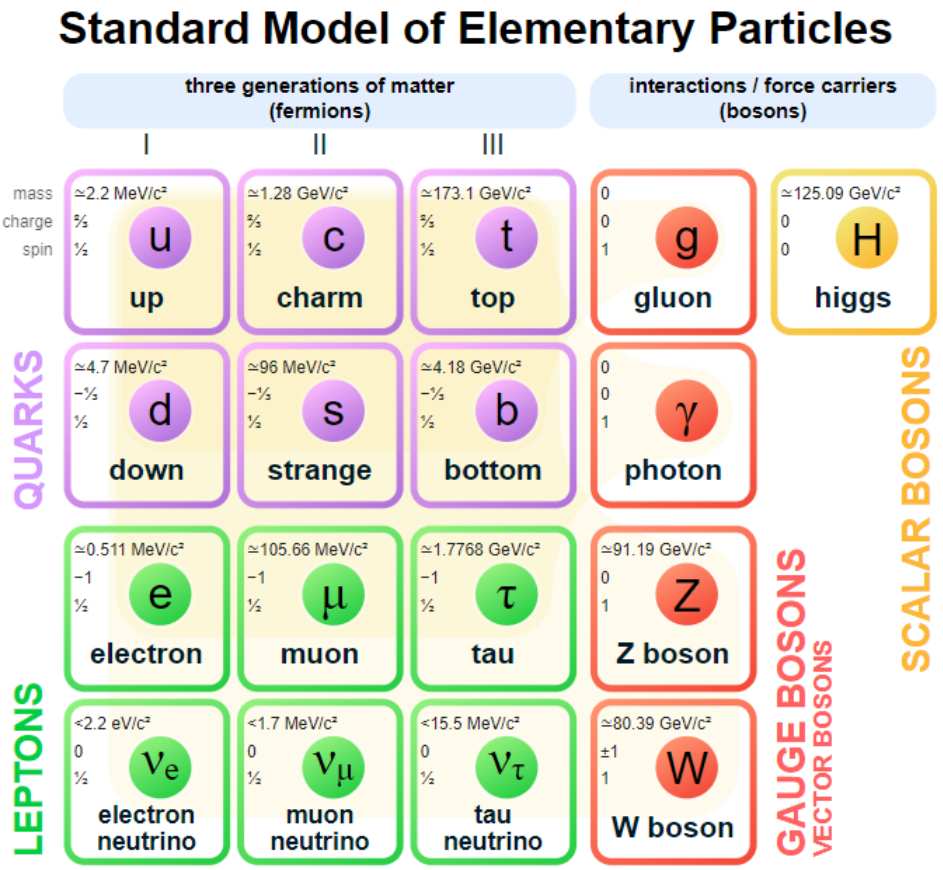

FIGURE 1.1: The SM of elementary particles.

standpoint, it is challenging to detect gravitational effects on a microscale, as gravity's strength is much weaker than the other three fundamental forces. Furthermore, the field quantizations of gravity, known as gravitons, are difficult to observe. In essence, in most current particle physics research, the gravitational effect can be ignored.

The SM implies that neutrinos are exactly massless. In the SM, for a massive Dirac particle, one can find a LH reference frame and a RH reference frame. Therefore, in order to have non-zero mass neutrinos, the LH neutrino field in the SM should couple with a RH field [14]. However, in the SM, there is no RH neutrino field to couple with a LH neutrino and obtain a mass as typical Dirac particles. If the neutrino has a Majorana nature, the lepton number will be violated and the mass term of the neutrino will break the global L symmetry and $B - L$ symmetries by two units. In the SM, there are no sources that violate L or $B - L$ symmetry by two units. However, observations of neutrino oscillations have provided evidence for non-zero neutrino masses from various experimental groups [15; 16; 17; 18]. Adding neutrino masses to

the SM framework without affecting other well-observed particles properties thus poses a challenge. Detecting such tiny neutrino mass is extremely difficult from an experimental standpoint. Currently, the nature of neutrinos (Dirac or Majorana) and the origin of mass are still hidden beneath a veil. Several experiments with higher precision are being conducted to further investigate this topic, though [19; 20; 21].

DM is a hypothetical form of matter that does not interact with light, it is therefore invisible across the entire EM spectrum, making it extremely hard to detect. Currently, DM can only be detected through its gravitational effects. It is estimated that DM constitutes 27% of the entire universe, an amount which is five times greater than visible matter [1; 22]. The rest of the universe is composed of dark energy. Some theories propose that the DM can be generated in particle colliders, despite evading detection by conventional apparatus. In fact, the DM particle would carry energy and momentum, prompting physicists to search for "missing" energy and/or momentum after a collision, specifically, in any direction transverse to the collider beam (where there was no energy in the first place). So far, the DM has not been detected, although WIMPs are promising candidates [23; 24].

Our universe is dominated by matter, but the SM cannot explain this, ie, why there is a matter-antimatter asymmetry [25]. The Sakharov conditions [26; 27] outline three necessary requirements to explain such a matter-antimatter asymmetry. The first condition is baryon number violation, which leads to the production of more baryons than anti-baryons. The second condition is the violation of charge conjugate symmetry (C-symmetry) and charge conjugate parity symmetry (CP-symmetry). The former one is necessary for the interaction that generates more baryons to dominate over the interaction which generates more anti-baryon. The latter has a similar effect, favoring processes involving LH baryons and RH anti-baryons over their respective opposites processes. The final condition is that the interaction should be out of thermal equilibrium, otherwise the (assumed) CPT symmetry will compensate for the baryon number changing processes [25]. In the SM, charge conjugate symmetry is broken by weak interactions [28] and CP-violation was observed by kaon decay in 1964 [29], which can be explained only via a phase in CKM matrix [30; 31]. However,

there is no evidence for baryon number violation in the SM. The out-of-equilibrium condition further requires the existence of very heavy gauge (larger than $10^{15} - 10^{16}$ GeV) and scalar bosons ($10^{10} - 10^{16}$ GeV) [32], which are currently beyond our observation possibilities.

The hierarchy problem arises when certain fundamental physical parameters, such as coupling constants, exhibit a significant disparity between their experimentally measured values and the values expected from fundamental theories. Typically, the effective value of a parameter is related to its fundamental value through a correction method known as renormalization. However, in some cases, the process of renormalization is unnatural. One of the most important hierarchy problems is why the Higgs boson (125 GeV) is much lighter than the Planck mass (10^{19} GeV). The large quantum contribution from virtual particles, primarily a virtual top quark, requires almost perfect cancellation with the fundamental value, resulting in the observed mass of 125 GeV [33]. The origin of this cancellation mechanism is still being pursued by particle physicists.

In addition to the experimental phenomena and theoretical problems mentioned above, some hints of new physics can be found in current data. The anomalous magnetic dipole moment of the muon, well known as 'muon g-2', shows a non-negligible difference between the experimentally measured value and the theoretically calculated value within the SM [34; 35]. Thus, it may imply new physics beyond the SM. The latest result from Fermilab strengthens the evidence for the existence of BSM physics, with a standard deviation as large as $\sigma = 4.2$ [36] (the theoretical predictions within the SM are continuously improved[35] with $a_\mu^{SM} = 116591810(43) \times 10^{-11}$).

As a result of all this, we can safely conclude that the SM is not the ultimate theory of Nature. Conversely, some 'new physics' should exist and be able to explain and address the deficiencies mentioned above. Particle colliders, especially the LHC and, its successors, will play a key role in proving and testing the predictions of such new theory.

1.3 Supersymmetry with a seesaw mechanism

One of the solutions to extend the SM using SUSY. This is a spacetime symmetry that proposes a relationship between bosons and fermions. SUSY predicts that each particle in the SM has a partner with a half-unit difference of spin, known as a superpartner, as shown in figure 1.2. An advantage of a SUSY model is that the production of supersymmetric particles (known as sparticles) may be observed in a detector.

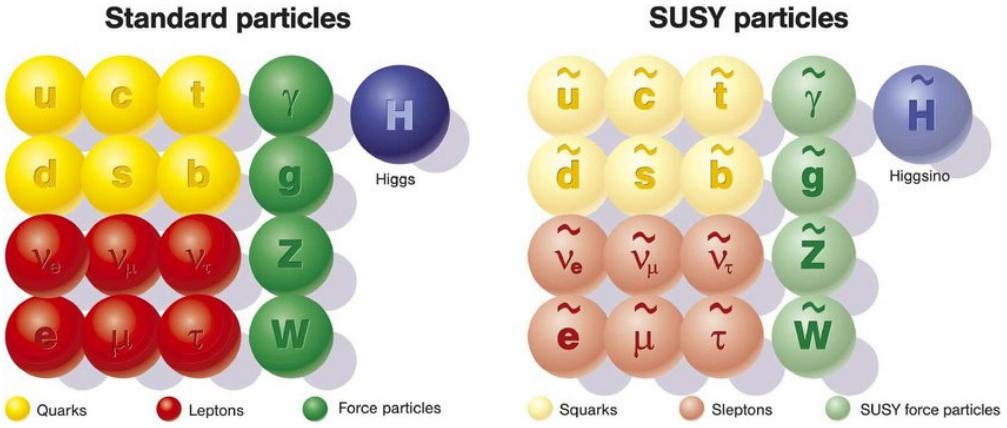

FIGURE 1.2: The SM particles and corresponding superpartners.

SUSY provides a solution to the Higgs hierarchy problem. Since fermions and bosons have opposite sign loop corrections, SUSY can produce a cancellation between the top quark and its superpartner ($\tilde{t}$), as shown in figure 1.3. This offers a natural explanation for the gap between electro-weak (EW) scale and Planck scale without requiring significant fine-tuning.

In some SUSY models, such as the MSSM, if sparticles do not mix with the SM particles, which means *R*-parity [37] (a symmetry with quantum number +1 for all SM

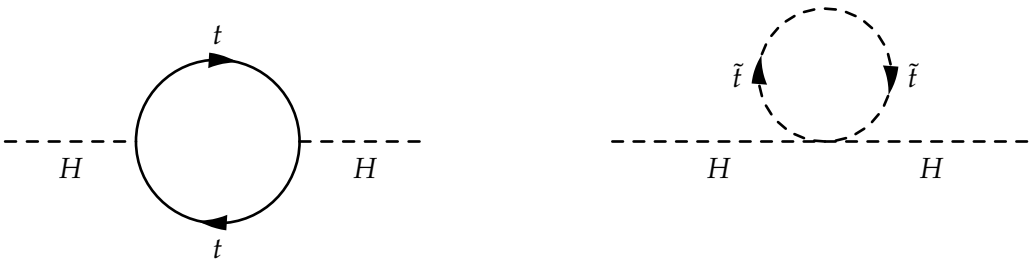

FIGURE 1.3: Representative Feynman diagrams enabling cancellations in the Higgs boson mass renormalization between the top quark loop and the top squark loops.

particles while -1 for all SUSY particles), is exactly conserved, the lightest sparticle, known as the LSP, is absolutely stable. If the LSP is electrically neutral, it can serve as a WIMP candidate for DM [38].

Although SUSY has shown its potential to remedy some flaws of the SM, it still lacks ways to explain the origin of neutrino mass. Since a neutrino with Majorana nature will break the $B - L$ symmetry by two units. Weinberg introduced a dimension-5 operator to parameterize the $B - L$ breaking effect in the following form (known as the Weinberg operator [39]):

$$\lambda LL'\Phi\Phi/\Lambda, \tag{1.1}$$

where L and Φ represent the SM lepton doublet and Higgs doublet, respectively. There are three types of products used to obtain the Weinberg operator at tree-level, considered as three different types of seesaw mechanisms [40; 41; 42; 43; 44; 45].

- The product of L and Φ forms a fermion singlet: $(L^T\Phi)(L'^T\Phi)/\Lambda$. This is known as the Type-I seesaw mechanism [40; 42; 44; 46; 47] which is described diagrammatically in figure 1.4. The fermion singlet transforms as $(1, 1, 0)$ under the SM gauge group $SU(3)_c \times SU(2)_L \times U(1)_Y$, and is considered a RH neutrino, denoted as ν_R with a Majorana mass M_R. The fermion singlet interacts with a SM lepton through a Yukawa coupling y_ν. The light neutrino mass m_ν can be obtained by $m_\nu \sim y_\nu^2 v_0^2/M_R$ where the v_0 is the VEV of Higgs boson. To comply with the mass of the light neutrino, M_R can reach the order of 10^{15} GeV when the seesaw scale is high $(y_\nu^2 \approx 1)$. A lower Yukawa coupling balances a lighter RH neutrino.

- The product of L and L' forms a scalar triplet: $(L^T\sigma L')(\Phi^T\sigma\Phi)/\Lambda$, where σ denotes the Pauli matrices. This mechanism is known as the Type-II seesaw mechanism [42; 43; 44; 48; 49]. In figure 1.5, the scalar triplet is the Higgs field Δ with mass M_Δ, which belongs to the representation of $SU(2)_L$. The light neutrino mass is given by eq. 1.2, where Y_v is the Yukawa coupling and v_Δ is the Vacuum Expectation Value (VEV) of the scalar triplet:

$$m_\nu \sim Y_\nu v_\Delta \qquad \text{with} \qquad v_\Delta = \langle \Delta \rangle = \frac{\mu v_0^2}{\sqrt{2} M_\Delta^2}. \tag{1.2}$$

The mass of Δ ranges from the TeV scale to 10^{15} GeV as Y_ν changes. A notable feature of the Type-II seesaw is that no RH neutrinos exists to explain the light neutrino mass.

- The product of L and Φ forms a fermion triplet: $(L\sigma\Phi)(L'\sigma\Phi)/\Lambda$. This is known as the Type-III seesaw mechanism [45]. The fermion triplet Σ_L belongs to the representation of the SM $SU(2)_L$ and transforms as $(1, 3, 0)$ under the SM gauge group. The process is depicted in figure 1.6. The neutrino mass in the Type-III seesaw has a similar form to that of the Type-I seesaw. The difference is that Σ_L carries an EM charge.

- The Inverse seesaw mechanism is constructed by adding one additional singlet fermion S to the Type-I seesaw mechanism. In contrast to the RH neutrino ν_R, the new singlet has a lepton number of +1 . The corresponding Feynman diagram is in the figure 1.7. The neutrino mass matrix can be expressed in the basis of ν_L, ν_R, S by:

$$\begin{pmatrix} 0 & m_D & M_S \\ m_D^T & \mu_R & M_R \\ M_S^T & M_R^T & \mu_S \end{pmatrix}, \tag{1.3}$$

where $m_D = y_\nu v$ is the Dirac neutrino matrix, μ_R and μ_S are the self-coupling of ν_R and S respectively. According to 't Hooft criteria [50], $M_S, \mu_R, \mu_S \ll m_D, M_R$, thus the neutrino mass can be given with a good approximation by:

$$m_\nu = \frac{m_D(m_D\mu_S - 2M_R M_S)}{M_R^2}. \tag{1.4}$$

A seesaw mechanism provides a plausible explanation for the smallness of the neutrino mass compared to the masses of other fermions in the SM [51]. Moreover, adding a seesaw mechanism to a SUSY model provides more options for a DM

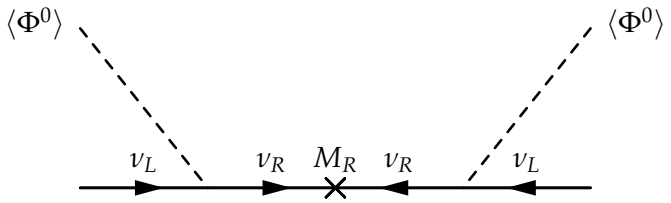

FIGURE 1.4: Type-I seesaw mechanism. The RH neutrino serves as intermediate heavy particle.

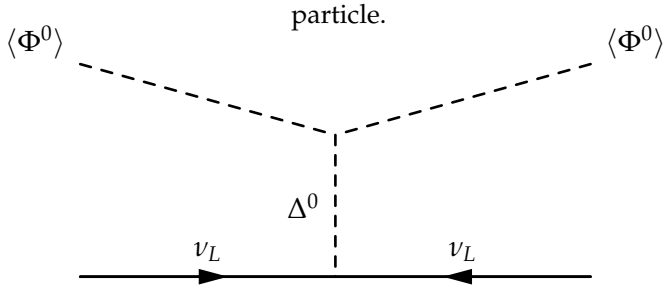

FIGURE 1.5: Type-II seesaw mechanism. The intermediate heavy particle is the scalar triplet Δ.

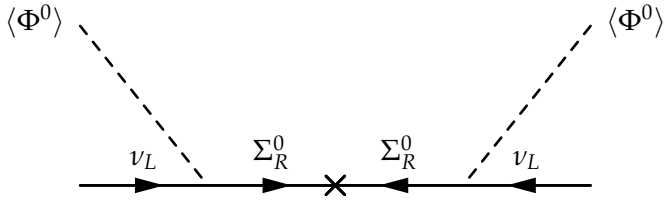

FIGURE 1.6: Type-III seesaw mechanism. A fermion triplet Σ serves as intermediate heavy particle.

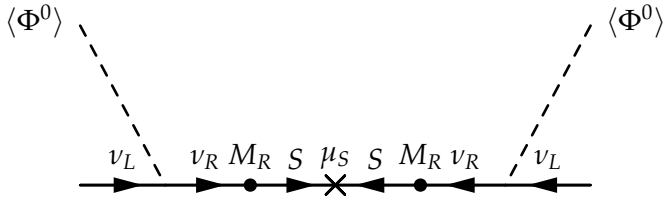

FIGURE 1.7: Inverse seesaw mechanism. The RH neutrino and singlet fermion S serve as intermediate heavy particles.

candidate, especially considering the RH sneutrino, which has been studied for years as such [52; 53; 54].

1.4 Structure of thesis

In this thesis, we discuss the phenomenology of SUSY models with different seesaw mechanisms and their potential detection at different future colliders. We first present the NMSSMr [55] with a Type-I seesaw mechanism and study a rare chargino decay which can be a handle to estimate the neutrino Yukawa couplings at the ILC. Then we compare the Type-I seesaw and Type-III within the MSSM at the HE-LHC [56; 57]: a

signal that includes a Higgs particle can be identified at 27 TeV. We also investigate CP-violation effects through TPAs in the BLSSM with an inverse seesaw mechanism [58].

More specifically, the structure of the thesis is as follows. After having discussed the motivations for SM extension in Chapter 1, we provide a brief overview of the SM in Chapter 2. Chapter 3 presents a concise discussion of SUSY. We then introduce particle colliders, in particular, the LHC and ILC, in Chapter 4. In Chapter 5, we discuss the NMSSMr, wherein a rare chargino decay at the ILC can be used to estimate neutrino Yukawa couplings [2]. In Chapter 6, we illustrate the phenomenology of the MSSM with a type-III seesaw and a type-I seesaw at the HE-LHC, wherein a signal containing the Higgs particle can be observed by the presence of two b-jets plus a single lepton and missing transverse energy ($\not{E}_T$) [3]. Chapter 7 finally focuses on CP-violation effect through TPAs in the BLSSM with an inverse seesaw mechanism. In the conclusion part, we provide a summary of past work and outline future work.

Chapter 2

The Standard Model

2.1 Gauge theory

Symmetry is a key concept in modern physics. It describes a physical system that remains unchanged under some transformation. Symmetry can be classified as global and local. A global symmetry is one that preserves invariance for a transformation applied to all point in spacetime. A local symmetry maintains invariance when the transform is independently performed at each point in space-time. This implies that local symmetry transformations can be applied to specific regions of space-time without affecting other regions. This forms the basis of gauge field theory.

The term 'gauge' refers to any specific mathematical formalism used to regulate the redundant degrees of freedom in the Lagrangian of a physical system. The transformation between gauges is called a gauge transformation, which forms a Lie Group [59]. Gauge symmetry or gauge invariance is not an inherent property of nature, but rather a choice we make to observe nature. It is merely a redundancy in our description that we introduce in order to describe the theory with a local Lagrangian[5].

Gauge field theory is important in particle physics because it provides a unified mathematical framework for quantum electrodynamics, weak interaction, and strong interaction which is known as the SM. The SM accurately predicts the experimental

results for the three fundamental forces and is formulated as a gauge field theory with gauge group $SU(3)_c \times SU(2)_L \times U(1)_Y$. The general expressions for the elements in the Lagrangian are similar for each group. Consider any continuous group of transformations represented by a set of $n \times n$ unitary matrices V. Then, the field $\psi(x)$ transforms according to:

$$\psi(x) \to V(x)\psi(x), \qquad \text{where} \quad V(x) = \exp\left(i\alpha^a(x)t^a\right). \tag{2.1}$$

The x dependence of V makes the transformation local. The quantity α^a represent phase rotation that is an arbitrary function of x. The t^a denote the group generators, and $V(x)$ can be expanded in terms of t^a in infinitesimal form, shown in eq. 2.2.

$$V(x) = 1 + i\alpha^a(x)t^a + \mathcal{O}(\alpha^2). \tag{2.2}$$

In order to write an invariant Lagrangian involving derivatives of $\psi(x)$, it is necessary to introduce a new definition: the covariant derivative D_μ. The general form is shown below:

$$D_\mu = \partial_\mu - igA^a_\mu t^a \tag{2.3}$$

where g is the gauge coupling constant. The A^a_μ are vector fields for each independent generator of the local symmetry. In the SM, A^a_μ represents different gauge fields for each gauge group $SU(3)$, $SU(2)$ and $U(1)$. It can be proven that covariant derivative of ψ transforms in the same way as the field ψ in eq. 2.1. We can construct a gauge-invariant Lagrangian with permissible terms up to dimension 4 [4].

2.2 The SM Lagrangian

The Lagrangian description of a particle consists of a dynamical term plus a mass term. The dynamical term includes the particle's self-coupling and its interaction with

gauge bosons. The mass term describes how the particle get their mass. The SM Lagrangian is shown below:

$$\begin{aligned}\mathcal{L} = &-\frac{1}{4}F_{\mu\nu}F^{\mu\nu} \\ &+ i\bar{\psi}\not{D}\psi + h.c \\ &+ \bar{\psi}_i y_{ij}\psi_j\phi + h.c \\ &+ |D_\mu(\phi)|^2 - V(\phi).\end{aligned} \tag{2.4}$$

2.2.1 The term: $-\frac{1}{4}F_{\mu\nu}F_{\mu\nu}$

The first term is a dynamical term of gauge field, which describes the interaction between gauge particles. It is a scalar product of the gauge field strength tensor $F_{\mu\nu}$ where μ and ν are Lorentz indices correspond to the space-time components from 0 to 3. The definition of $F_{\mu\nu}$ is as follows:

$$F^a_{\mu\nu} = -\frac{1}{igt^a}[D_\mu, D_\nu] = \partial_\mu A^a_\nu - \partial_\nu A^a_\mu + g f^{abc} A^b_\mu A^c_\nu \tag{2.5}$$

where g is a coupling constant. The f^{abc} is the structure constant of the gauge group, which is defined by the commutator relation:

$$[t_a, t_b] = i f^{abc} t_c \tag{2.6}$$

In the case of the Abelian group, such as the weak hypercharge $U(1)$ group, the generator t can be written as eq. 2.7. In this case, the generators commute with each other, resulting in a vanishing structure constant. Here Y represents the weak hypercharge, Q denotes the electric charge and T_3 is the third component of the weak isospin.

$$t = \frac{Y}{2} = Q - T_3. \tag{2.7}$$

For non-Abelian group, such as Weak isospin $SU(2)$ group and color $SU(3)$ group, the generator $t_i = \frac{\sigma_i}{2}$ can be expressed using the Pauli matrices (as shown in eq. 2.8) for SU(2). The generators $t_i = \frac{\lambda_i}{2}$ can be expressed by the Gell-mann matrices (as shown in eq. 2.9) for SU(3). In these cases, the generators do not commute, leading to non-zero structure constants. This theory is known as Yang-Mills theory [4].

$$\sigma^1 = \begin{pmatrix} 0 & 1 \\ 1 & 0 \end{pmatrix}, \sigma^2 = \begin{pmatrix} 0 & -i \\ i & 0 \end{pmatrix}, \sigma^3 = \begin{pmatrix} 1 & 0 \\ 0 & -1 \end{pmatrix} \tag{2.8}$$

$$\begin{aligned} \lambda_1 &= \begin{pmatrix} 0 & 1 & 0 \\ 1 & 0 & 0 \\ 0 & 0 & 0 \end{pmatrix}, \lambda_2 = \begin{pmatrix} 0 & -i & 0 \\ i & 0 & 0 \\ 0 & 0 & 0 \end{pmatrix}, \lambda_3 = \begin{pmatrix} 1 & 0 & 0 \\ 0 & -1 & 0 \\ 0 & 0 & 0 \end{pmatrix} \\ \lambda_4 &= \begin{pmatrix} 0 & 0 & 1 \\ 0 & 0 & 0 \\ 1 & 0 & 0 \end{pmatrix}, \lambda_5 = \begin{pmatrix} 0 & 0 & -i \\ 0 & 0 & 0 \\ i & 0 & 0 \end{pmatrix}, \lambda_6 = \begin{pmatrix} 0 & 0 & 0 \\ 0 & 0 & 1 \\ 0 & 1 & 0 \end{pmatrix} \\ \lambda_7 &= \begin{pmatrix} 0 & 0 & 0 \\ 0 & 0 & -i \\ 0 & i & 0 \end{pmatrix}, \lambda_8 = \frac{1}{\sqrt{3}} \begin{pmatrix} 1 & 0 & 0 \\ 0 & 1 & 0 \\ 0 & 0 & -2 \end{pmatrix} \end{aligned} \tag{2.9}$$

For a general gauge group, we need to introduce gauge fields whose number is equal to the dimension of the adjoint representation ($N^2 - 1$). Consequently, there are eight gluons for the color $SU(3)$ group, three W bosons (W_1, W_2, W_3) for the weak isospin $SU(2)$ group and one (B) for the $U(1)$ group. The physical state of gauge bosons can be expressed using the weak gauge field in eq. 2.10 and 2.11, where θ_w represents Weinberg angle [60].

$$W_\mu^\pm = \frac{1}{\sqrt{2}}(W_\mu^1 \mp iW_\mu^2) \tag{2.10}$$

$$\begin{pmatrix} Z_\mu \\ A_\mu \end{pmatrix} = \begin{pmatrix} \cos\theta_W & -\sin\theta_W \\ \sin\theta_W & \cos\theta_W \end{pmatrix} \begin{pmatrix} W_\mu^3 \\ B_\mu \end{pmatrix} \tag{2.11}$$

The associated gauge field tensors are below:

- $G_{\mu\nu}^a$ stands for the gluon field tensor, where the index a corresponds to the elements of the 8 representation of color $SU(3)$. The gauge boson vector potentials G_μ and G_ν are composed of 3×3 traceless Hermitian matrices. $G_{\mu\nu}^a$ is as follows with the strong coupling constant g_s.

$$G_{\mu\nu}^a = \partial_\mu G_\nu^a - \partial_\nu G_\mu^a + g_s f^{abc} G_\mu^b G_\nu^c \tag{2.12}$$

  The gauge invariant gluon dynamical term can be written as $G_{\mu\nu}G^{\mu\nu}$.

- $W_{\mu\nu}^i$ is labeled for the gauge field tensor of $SU(2)$ of weak isospin. It is composed of 2×2 traceless Hermitian matrices. The index i runs from 1 to 3. The coupling is g_w and structure constant is ϵ^{ijk}.

$$W_{\mu\nu}^i = \partial_\mu W_\nu^i - \partial_\nu W_m u^i + g_w \epsilon^{ijk} W_\mu^j W_\nu^k \tag{2.13}$$

- $B_{\mu\nu}$ represent the gauge field tensor for the $U(1)$ group of weak hypercharge with a coupling to the matter field g_b.

$$B_{\mu\nu} = \partial_\mu B_\nu - \partial_\nu B_\mu \tag{2.14}$$

The gauge boson dynamical term can be written as below.

$$\mathcal{L}_{gaugekin} = -\frac{1}{4} F_{\mu\nu} F_{\mu\nu} = -\frac{1}{4} B_{\mu\nu} B^{\mu\nu} - \frac{1}{2} tr(W_{\mu\nu} W^{\mu\nu}) - \frac{1}{2} tr(G_{\mu\nu} G^{\mu\nu}) \tag{2.15}$$

2.2.2 The term: $i\bar{\psi}\not{D}\psi + h.c$

The second and third term represent fermion dynamical term and its Hermitian conjugate term. These terms describe how quarks and leptons propagate and interact with gauge fields. The symbol ψ represents a Dirac spinor that represents quarks and leptons. The symbol $\bar{\psi}$ is defined in eq. 2.16, which ensures that the Lagrangian density is scalar and real. The term $h.c$ stands for the Hermitain conjugate of the preceding term.

$$\bar{\psi} \equiv \psi^{\dagger}\gamma^{0} \tag{2.16}$$

The $\not{D}$ is a short-hand notation of $\gamma_{\mu}D^{\mu}$. The γ_{μ} represents four Dirac matrices (also known as Gamma matrices) expressed below:

$$\gamma^{0} = \begin{pmatrix} 1 & 0 & 0 & 0 \\ 0 & 1 & 0 & 0 \\ 0 & 0 & -1 & 0 \\ 0 & 0 & 0 & -1 \end{pmatrix} \gamma^{1} = \begin{pmatrix} 0 & 0 & 0 & 1 \\ 0 & 0 & 1 & 0 \\ 0 & -1 & 0 & 0 \\ -1 & 0 & 0 & 0 \end{pmatrix}$$

$$\gamma^{2} = \begin{pmatrix} 0 & 0 & 0 & -i \\ 0 & 0 & i & 0 \\ 0 & i & 0 & 0 \\ -i & 0 & 0 & 0 \end{pmatrix} \gamma^{3} = \begin{pmatrix} 0 & 0 & 1 & 0 \\ 0 & 0 & 0 & -1 \\ -1 & 0 & 0 & 0 \\ 0 & 1 & 0 & 0 \end{pmatrix}$$

When a projection operator act on the 4-component Dirac spinor ψ, it separates it into left-hand and right-hand state. Eq. 2.17 shows some of the projection operator where the definition of $\gamma^{5} \equiv i\gamma^{0}\gamma^{1}\gamma^{2}\gamma^{3}$. Since right-handed fermion (left-handed anti-fermion) form singlets in weak isospin space, W boson only couple with the left-handed fermion as observed. We can express the compact term in a more specific form.

$$\psi_L = \frac{1-\gamma^5}{2}\psi \qquad \psi_R = \frac{1+\gamma^5}{2}\psi \tag{2.17}$$

$$(\bar{\nu}_L, \bar{e}_L)\tilde{\sigma}^\mu i D_\mu \begin{pmatrix} \nu_L \\ e_L \end{pmatrix} \qquad D_\mu = \left[\partial_\mu - i g_b B_\mu \frac{Y}{2} + i g_w W_\mu \frac{\sigma_i}{2}\right] \tag{2.18}$$

$$(\bar{u}_L, \bar{d}_L)\tilde{\sigma}^\mu i D_\mu \begin{pmatrix} u_L \\ d_L \end{pmatrix} \qquad D_\mu = \left[\partial_\mu + i g_w W_\mu \frac{\sigma_i}{2} + i g G_\mu \frac{\lambda_i}{2}\right] \tag{2.19}$$

$$\bar{e}_R \sigma^\mu i D_\mu e_R \qquad D_\mu = \left[\partial_\mu - i g_b B_\mu \frac{Y}{2}\right] \tag{2.20}$$

$$\bar{u}_R \sigma^\mu i D_\mu u_R \qquad D_\mu = \left[\partial_\mu + \frac{i g_b}{3} B_\mu Y + i g_s G_\mu \frac{\sigma_i}{2}\right] \tag{2.21}$$

$$\bar{d}_R \sigma^\mu i D_\mu d_R \qquad D_\mu = \left[\partial_\mu - \frac{i g_b}{3} B_\mu Y + i g_s G_\mu \frac{\sigma_i}{2}\right] \tag{2.22}$$

2.2.3 The term: $\bar{\psi}_i y_{ij} \psi_j \phi + h.c$

This term represents the mass term for quarks and leptons. It describes how the quark and lepton couple to the Higgs field (ϕ). The y_{ij} denotes Yukawa coupling. The Higgs field ϕ is a 2-component complex field of the $SU(2)$ weak isospin group, we can choose a gauge called unitary gauge (eq. 2.23) to transform Higgs field into a basis where three Goldstone bosons (massless field that arise through SSB) are eaten by W and Z boson.

$$\phi = \begin{pmatrix} \phi^+ \\ \phi^0 \end{pmatrix} \rightarrow \frac{1}{\sqrt{2}} \begin{pmatrix} 0 \\ v + h(x) \end{pmatrix} \tag{2.23}$$

the VEV of ϕ is denoted by $v = \langle \phi^0 \rangle$ where ϕ^0 represents the neutral component of the Higgs field. The field h represents the residual Higgs field, which is the fluctuation

around the VEV. As the fermion mass eigenstates are linear combination of gauge eigenstates, and we can write the term $\psi_i y_{ij} \psi_j \phi$ in a new basis to get real fermion mass.

The electron, muon and tau mass term:

$$-\frac{\sqrt{2}}{v}\Big[(\bar{\nu}_L, \bar{e}_L)\phi M^e e_R + \bar{e}_R \bar{M}^e \bar{\phi} \begin{pmatrix} \nu_L \\ e_L \end{pmatrix}\Big] \tag{2.24}$$

The down, strange and bottom quark mass term:

$$-\frac{\sqrt{2}}{v}\Big[(\bar{u}_L, \bar{d}_L)\phi M^d d_R + \bar{d}_R \bar{M}^d \bar{\phi} \begin{pmatrix} u_L \\ d_L \end{pmatrix}\Big] \tag{2.25}$$

The up, charmed and top mass term:

$$-\frac{\sqrt{2}}{v}\Big[(-\bar{d}_L, \bar{u}_L)\phi^* M^u u_R + \bar{u}_R \bar{M}^u \phi^T \begin{pmatrix} -d_L \\ u_L \end{pmatrix}\Big] \tag{2.26}$$

The quantities M^e, M^ν, M^d and N^u are 3×3 fermion mass matrices which defined by $M^{ij} = y^{ij}\frac{v}{\sqrt{2}}$. The matrix M can be diagonalized as follows and the two basis are connected by a unitary transformation in eq. 2.30.

$$M^e = (U_L^e)^\dagger \begin{pmatrix} m_e & 0 & 0 \\ 0 & m_\mu & 0 \\ 0 & 0 & m_\tau \end{pmatrix} U_R^e \tag{2.27}$$

$$M^u = (U_L^u)^\dagger \begin{pmatrix} m_u & 0 & 0 \\ 0 & m_c & 0 \\ 0 & 0 & m_t \end{pmatrix} U_R^u \tag{2.28}$$

$$M^d = (U_L^d)^\dagger \begin{pmatrix} m_d & 0 & 0 \\ 0 & m_s & 0 \\ 0 & 0 & m_b \end{pmatrix} U_R^d \tag{2.29}$$

.

$$\begin{aligned} e_L &= U_L^{e\,\dagger} e'_L, \qquad e_R = U_R^{e\,\dagger} e'_R, \qquad \nu_L = U_L^{\nu\,\dagger} \nu'_L \qquad u_L = U_L^{u\,\dagger} u'_L \\ u_R &= U_R^{u\,\dagger} u'_L, \qquad d_L = U_L^{d\,\dagger} d'_L, \qquad d_R = U_R^{d\,\dagger} d'_L. \end{aligned} \tag{2.30}$$

In the new basis, the U matrix cancels in all the pure kinetic terms, electromagnetic current, and Z boson current. Only the terms in the W boson charge current interaction remain: $\bar{u}'_L U_L^u \tilde{\sigma}^\mu W_\mu^\pm U_L^{d\,\dagger} d'_L$ and $\bar{\nu}'_L U_L^\nu \tilde{\sigma}^\mu W_\mu^\pm U_L^{e\,\dagger} e'_L$. That is, the W boson charge weak current connects u_L quark with a unitary rotation of the d_L quark, the rotation given by the unitary matrix:

$$V^q = U_u^\dagger U_d \tag{2.31}$$

The matrix V is known as CKM matrix. It contains the information about the mismatch in the quantum state of quarks freely propagating and participating in weak interaction.

2.2.4 The term $|D_\mu(\phi)|^2 - V(\phi)$

This is the Higgs dynamical and mass term. The dynamical part describes how the gauge field interacts with the Higgs field and acquire mass. The scalar potential shows the self-interaction of the Higgs boson as below:

$$V(\phi^\dagger \phi) = -\mu^2 \phi^\dagger \phi + \lambda (\phi^\dagger \phi)^2. \tag{2.32}$$

We can expand ϕ around the vacuum state (eq. 2.23) to get the minimum of potential which occurs at

$$v^2 = \frac{\mu^2}{\lambda}. \tag{2.33}$$

The scalar potential becomes with omitted a constant term:

$$V = \frac{1}{2}(2\lambda v^2)h^2 + \lambda v h^3 + \frac{\lambda}{4}h^4. \tag{2.34}$$

The quantum field of $h(x)$ get a mass:

$$m_h = \sqrt{2\lambda}v. \tag{2.35}$$

The expansion of the kinetic term in the unitary gauge can lead to gauge bosons mass term. Explicitly:

$$(D^\mu\phi)^\dagger D_\mu\phi = \frac{1}{2}(\partial_\mu h)^2 + \left[\left(\frac{g_w v}{2}\right)^2 W^{\mu+}W^-_\mu + \frac{1}{2}\frac{(g_w^2+g_b^2)v^2}{4}Z^\mu Z)\mu\right]\left(1+\frac{H}{v}\right)^2 \tag{2.36}$$

The W and Z boson obtain masses and photon stays massless.

$$m_w = \frac{gv}{2}, \qquad m_z = \frac{\sqrt{(g_s^2+g_b^2)}v}{2} \tag{2.37}$$

2.2.5 CP-violation in the SM

In particle physics, the CP-violation is a violation of CP-symmetry. The CP-symmetry describes that the physics process should be the same when a particle is changed by its corresponding anti-particle (C-symmetry) while the coordinates are inverted. As

mentioned earlier, CP-violation plays a key role when we attempt to explain the matter-antimatter asymmetry.

There are at least three sources of CP-violation in the SM. The first one is from the CKM matrix in the quark sector. The CKM matrix in eq. 2.38 is a unitary matrix describing the strength of weak interaction between up-type and down-type quark.

$$V_{\text{CKM}} = \begin{pmatrix} |V_{ud}| \approx 0.97 & |V_{us}| \approx 0.22 & |V_{ub}| \approx 0.0038 \\ |V_{cd}| \approx 0.22 & |V_{cs}| \approx 0.98 & |V_{cb}| \approx 0.041 \\ |V_{td}| \approx 0.008 & |V_{ts}| \approx 0.038 & |V_{tb}| \approx 1.00 \end{pmatrix} \tag{2.38}$$

The CKM matrix can be parametrised by three Euler angles $\theta_{12,13,23}$ and one CP-violation phase δ_{13}

$$V_{\text{CKM}} = \begin{pmatrix} c_{12}c_{13} & s_{12}s_{13} & s_{13}e^{-i\delta_{13}} \\ -s_{12}s_{23} - c_{12}s_{23}s_{13}e^{i\delta_{13}} & c_{12}c_{23} - s_{12}s_{23}s_{13}e^{i\delta_{13}} & s_{23}s_{13} \\ s_{12}s_{23} - c_{12}c_{23}s_{13}e^{i\delta_{13}} & -c_{12}s_{23} - s_{12}c_{23}s_{13}e^{i\delta_{13}} & c_{23}c_{13} \end{pmatrix} \tag{2.39}$$

where c_{ij}, s_{ij} stands for the cosine and sine of the mixing angle. The CP-violation effect from the CKM matrix has been observed in the decay of neutral kaons. This source only contributes a small portion to explain matter-antimatter asymmetry. The second source of CP-violation comes from strong interaction, but it also contribute a small portion for the necessary CP-violation as no obvious evidence of non-zero neutron electric dipole moment (nEDM). The third source of CP-violation is from Pontecorvo–Maki–Nakagawa–Sakata (PMNS) matrix in the lepton sector. Some current long -baseline experiment, such as T2K [61] are trying to find evidence of CP-violation in lepton sector. If experiment proves the lepton sector can not contribute enough to the CP-violation, we need to introduce new source from the BSM by adding new particles or interactions.

Many experiments have proven that the SM is an extremely successful fundamental theory. However, it is still far from being a complete framework of the universe. An increasing number of phenomena indicates the existence of new physics beyond the

SM, which motivates us to extend the SM. In addition to this, precision measurements also serve as a portal for understanding our nature deeper. In the next Chapter, we will provide a brief introduction to one of the most promising BSM theories: SUSY.

Chapter 3

Supersymmetry

Supersymmetry (SUSY) is a space-time symmetry which transforms fermion into boson and vice versa. SUSY is an extension of the Poincaré algebra and is constrained by Haag–Łopuszański–Sohnius extension [62] of Coleman-Mandula theorem [63]. It provides a theoretical framework to unify the SM gauge coupling $SU(3) \times SU(2) \times U(1)$ at Grand Unification Theory (GUT) scale (10^{16} GeV) and stabilize the hierachy between EW scale (100 GeV) and Planck scale (10^{19} GeV) [64; 65; 66; 67]. As a local symmetry, SUSY also has a potential to connect with gravity. If R-parity is conserved, SUSY also provides cold dark matter candidate. In this chapter, we will discuss the above topics in detail.

3.1 Supermultiplet

The transformation operator Q and $Q^\dagger$ (hermitian conjugate of Q) are fermionic operators and carry $1/2$ spin angular momentum. They obey an algebra of commutation and anticommutation relations:

$$\begin{aligned} \{Q, Q^\dagger\} &= P^\mu, \\ \{Q, Q\} &= \{Q^\dagger, Q^\dagger\} = 0, \\ [P^\mu, Q] &= [P^\mu, Q] = 0, \end{aligned} \tag{3.1}$$

where P^μ is the four-momentum generator of spacetime translation.

In SUSY theory, the single-particle state fall into irreducible representation of the supersymmetry algebra, called a supermultiplets. It contains fermion and boson states in each supermultiplet, which are referred to as superpartners of each other. Since the SUSY generators commute with the generators of gauge transformations, particles and their superpartners share same representation of the gauge group, which means they have the same electric charge, weak isospin and color. Each supermultiplet has an equal number of fermionic and bosonic degrees of freedom which is an axiom when constructing supermultiplet. There are two kinds of supermultiplets that form the contents of SUSY particles. A chiral supermultiplet, also known as a matter or scalar supermultiplet, consists of a two-component Weyl fermion and a complex scalar field. A gauge (or vector) supermultiplet contains a spin-1 gauge boson and its superparner, a spin-1/2 gaugino. Other combinations of particles with spin can also satisfy the requirement of an equal numbers of fermionic and bosonic degree of freedom. However, they are always expressed by the combination of chiral and vector supermuiltiplets (gravitino supermultiplet excluded), except in 'extended' supersymmetry theory. The theory of extended SUSY has more than one pair of generators Q, $Q^\dagger$, but the extended SUSY prohibits chiral fermion and parity violation in four-dimensional field, which has been observed in the SM. As a result, the extended SUSY is not interesting phenomenologically. Thus, this thesis will focus on $N = 1$ SUSY theory, where the value of N refers to the number of supersymmetries (the number of distinct copies of generator Q, $Q^\dagger$)[37].

supermultiplets	Superfield	Spin 0	Spin 1/2	$SU(3)_C, SU(2)_L, U(1)_Y$
Squarks, quarks ($\times$3 families)	Q	$(\tilde{u}_L \quad \tilde{d}_L)$	$(u_L \quad d_L)$	$(3, 2, \frac{1}{6})$
	$\bar{u}$	$\tilde{u}_R^*$	$u_R^\dagger$	$(\bar{3}, 1, -\frac{2}{3})$
	$\bar{d}$	$\tilde{d}_R^*$	$d_R^\dagger$	$(\bar{3}, 1, \frac{1}{3})$
Sleptons, leptons ($\times$3 families)	L	$(\tilde{\nu} \quad \tilde{e_L})$	$(\nu \quad e_L)$	$(1, 2, -\frac{1}{2})$
	$\bar{e}$	$\tilde{e}_R^*$	$e_R^\dagger$	$(1, 1, 1)$
Higgs, higgsino	H_u	$(H_u^+ \quad H_u^0)$	$(\tilde{H_u^+} \quad \tilde{H_u^0})$	$(1, 2, \frac{1}{2})$
	H_d	$(H_d^0 \quad H_d^-)$	$(\tilde{H_d^0} \quad \tilde{H_d^-})$	$(1, 2, -\frac{1}{2})$

TABLE 3.1: Chiral supermultiplets in MSSM.

Names	spin 1/2	spin 1	$SU(3)_C, SU(2)_L, U(1)_Y$
gluino, gluon	$\tilde{g}$	g	$(8, 1, 0)$
winos, W boson	$\tilde{W}^\pm \tilde{W}^0$	$W^\pm W^0$	$(1, 3, 0)$
bino, B boson	$\tilde{B}^0$	B^0	$(1, 1, 0)$

TABLE 3.2: Gauge supermultiplet in MSSM

3.2 The MSSM

SUSY can be interpreted in a geometric way by using superspace. It extends the ordinary spacetime coordinate by adding new anticommuting fermionic coordinates θ and $\theta^\dagger$. The supermultiplet can be expressed by superfield which is a function of the superspace coordinates. The minimal supersymmetric extension of the SM (MSSM) includes two Higgs doublet extension and the superparner of SM. The superpotential for the MSSM is

$$W_{MSSM} = \bar{u} y_u Q H_u - \bar{d} y_d Q H_d - \bar{e} y_e L H_d + \mu H_u H_d. \tag{3.2}$$

The quantity $\bar{u}$, $\bar{d}$, $\bar{e}$, Q, L, H_u, H_d here is MSSM chiral superfield content which is shown in table 3.1. The Higgs supermultiplet contains two complex Higgs doublet and its fermionic superpartner, higgsino, as well as their corresponding antiparticles.

3.2.1 The MSSM parameters

The parameter of MSSM can be divided into two parts: supersymmetry- conserving sector and the supersymmetry-breaking sector.

The SUSY-conserving parameters include gauge coupling: g_s, g_w and g_b. They are the SM gauge group $SU(3) \times SU(2) \times U(1)$ respectively. The y_u, y_d and y_e are dimensionless Higgs-fermion Yukawa couplings with a 3×3 matrix form. The higgsino mass parameter μ in the term $\mu H_u H_d$ which is known as 'μ term'. It is the supersymmetric version of the Higgs mass term in the SM. After electroweak symmetry breaking (EWSB), H_u and H_d will get a non-zero vev, the parameter μ should be around the order of EW scale. However, it raised a problem that why μ is in EW scale rather than the planck scale? It is known as the μ problem. Multiple solutions to the μ problem has been proposed, involving the extension of MSSM. The core idea of the solution is similar which builds a connection between the μ term and soft soft SUSY breaking term. Specifically, before symmetrey breaking, the μ term is hidden at tree-level, and then it arise from the VEV of some new field(s) which depends on soft SUSY breaking terms. In this way, the μ term has a relation with the mechanism of SUSY breaking. It transfers the puzzle of the μ term scale into the explanation of the soft SUSY breaking scale. There are several mechanisms proposed: the Next-to-Minimal Supersymmetric Standard model (NMSSM), the Kim-Nills mechanism [68], and the Giudice-Masiero mechanism [69]. We will discuss the NMSSM in the later of this chapter.

3.2.2 The soft SUSY-breaking parameters

In order to fully describe the MSSM we need to specify the soft SUSY breaking terms, which are added by hand to solve the degeneracy between the masses of the SM particles and their corresponding super-partners that are supposed to be much heavier. The designation "soft" refers to the fact that the terms break SUSY but do not introduce quadratic divergences [70]. The soft SUSY breaking terms within the MSSM are:

$$
\begin{aligned}
-\mathcal{L}_{soft} = & \frac{1}{2}\left(M_3\tilde{g}\tilde{g} + M_2\tilde{W}\tilde{W} + M_1\tilde{B}\tilde{B} + c.c\right) \\
& - \left(\tilde{u}a_u\tilde{Q}H_u - \tilde{d}a_d\tilde{Q}H_d - \tilde{e}a_e\tilde{L}H_d + c.c.\right) \\
& - \tilde{Q}^\dagger m_Q^2\tilde{Q} - \tilde{L}^\dagger m_L^2\tilde{L} - \tilde{u}m_{\tilde{u}}^2\tilde{u}^\dagger - \tilde{d}m_{\tilde{d}}^2\tilde{d}^\dagger - \tilde{e}m_{\tilde{e}}^2\tilde{e}^\dagger \\
& - m_{H_u}^2 H_u^* H_u - m_{H_d}^2 H_d^* H_d - (bH_uH_d + c.c.).
\end{aligned}
\tag{3.3}
$$

In the first line of eq. 3.3, M_1, M_2 and M_3 are the gaugino mass parameters which correspond to bino, wino and gluino respectively. The second line of eq. 3.3 contains three trilinear interaction terms, including two Higgs-squark-squark interaction and one Higgs-slepton-slepton interaction. The parameter a_u, a_d and a_e are 3×3 matrices in family space which maps to Yukawa coupling in one-to-one correspondence. The third line of eq. 3.3 shows the mass terms of squarks and sleptons. Five sfermion mass parameter, m_Q^2, $m_{\tilde{u}}^2$, $m_{\tilde{d}}^2$, m_L^2 and $m_{\tilde{e}}^2$ are 3×3 matrices in family space. Finally, the last line of eq. 3.3 are the terms which the soft SUSY breaking contribute to the Higgs potential. $m_{H_d}^2$ and $m_{H_u}^2$ are real squared mass parameter while b is complex squared mass parameter known as the 'B-parameter'.

3.3 MSSM spectrum

3.3.1 EWSB and the Higgs boson

The MSSM tree-level scalar Higgs potential is given by:

$$
\begin{aligned}
V = & (m_{H_d}^2 + |\mu|^2)H_d^\dagger H_d + (m_{H_u}^2 + |\mu|^2)H_u^\dagger H_u + [b(H_u^+ H_d^- - H_u^0 H_d^0) + c.cc] \\
& + \frac{1}{8}(g_w^2 + g_b^2)(H_d^\dagger H_d - H_u^\dagger H_u)^2 + \frac{1}{2}g_w^2|H_d^\dagger H_u|^2.
\end{aligned}
\tag{3.4}
$$

The Higgs potential should break the EW symmetry $SU(2) \times U(1)$ down to electromagnetism $U(1)_{EM}$. The SUSY breaking parameter $m_{H_d}^2$ and $m_{H_u}^2$ can be expressed by the Higgs VEV:

$$v_u = \langle H_u^0 \rangle, \qquad v_d = \langle H_d^0 \rangle \tag{3.5}$$

The Z^0 boson and EW gauge coupling have a relationship with the VEVs.

$$v_u^2 + v_d^2 = v^2 = \frac{2m_Z^2}{g_w^2 + g_b'^2} \approx (174\,\mathrm{GeV})^2 \tag{3.6}$$

The ratio of the VEV is:

$$\tan\beta = \frac{v_u}{v_d} \tag{3.7}$$

There is no definite value of $\tan\beta$ from observation. As $v_u = v\sin\beta$ and $v_d = v\cos\beta$ are real and positive, the parameter β is in the range $0 < \beta < \frac{\pi}{2}$.

The MSSM Higgs scalar field includes two complex $SU(2)_L$-doublet which means eight real scalar degrees of freedom. When the EW symmetry is broken, three of eight will be Nambu-Goldstone bosons G^0, $G^\pm$ and become the longitudinal components of the $W^\pm$ and Z^0 massive vector bosons. The remaining five Higgs scalar mass eigenstates consist of two CP-even neutral scalars h^0 and H^0, one CP-odd neutral scalar A^0, and a charge +1 scalar H^+ and its conjugate charge -1 scalar H^- [37]. The gauge-eigenstate fields can be expressed by the mass-eigenstate fields:

$$\begin{pmatrix} H_u^0 \\ H_d^0 \end{pmatrix} = \begin{pmatrix} v_u \\ v_d \end{pmatrix} + \frac{1}{\sqrt{2}} R_\alpha \begin{pmatrix} h^0 \\ H^0 \end{pmatrix} + \frac{i}{\sqrt{2}} R_{\beta_0} \begin{pmatrix} G^0 \\ A^0 \end{pmatrix} \tag{3.8}$$

$$\begin{pmatrix} H_u^+ \\ H_d^{-*} \end{pmatrix} = R_{\beta_\pm} \begin{pmatrix} G^+ \\ H^+ \end{pmatrix} \tag{3.9}$$

where the rotation matrices:

$$R_\alpha = \begin{pmatrix} \cos\alpha & \sin\alpha \\ -\sin\alpha & \cos\alpha \end{pmatrix} \qquad R_{\beta_0} = \begin{pmatrix} \sin\beta_0 & \cos\beta_0 \\ -\cos\beta_0 & \sin\beta_0 \end{pmatrix} \tag{3.10}$$

$$R_{\beta_\pm} = \begin{pmatrix} \sin\beta_\pm & \cos\beta_\pm \\ -\cos\beta_\pm & \sin\beta_\pm \end{pmatrix} \tag{3.11}$$

can be chosen to make the quadratic term of the Higgs potential has diagonal squared-mass:

$$V = \frac{1}{2}m_{h_0}^2(h^0)^2 + \frac{1}{2}m_{H_0}^2(H^0)^2 + \frac{1}{2}m_{G_0}^2(G^0)^2 + \frac{1}{2}m_{A_0}^2(A^0)^2 + m_{G^\pm}^2|G^+|^2 + m_{H^\pm}|H^+|^2 + \ldots, \tag{3.12}$$

If v_u v_d minimize the Higgs potential at tree-level, it leads $\beta_0 = \beta_\pm = \beta$ and $m_{G^0}^2 = m_{G^\pm}^2 = 0$, we can get:

$$m_{A^0}^2 = \frac{2b}{\sin 2\beta} = 2|\mu|^2 + m_{H_u}^2 + m_{H_d}^2 \tag{3.13}$$

$$m_{h^0,H^0}^2 = \frac{1}{2}\left(m_{A^0}^2 + m_Z^2 \mp \sqrt{(m_{A^0}^2 - m_Z^2)^2 + 4m_Z^2 m_{A^0}^2 \sin^2(2\beta)}\right) \tag{3.14}$$

$$m_{H^\pm}^2 = m_{A^0}^2 + m_W^2 \tag{3.15}$$

where the mixing angle α at tree-level is determined by:

$$\frac{\sin 2\alpha}{\sin 2\beta} = -\left(\frac{m_{H^0}^2 + m_{h^0}^2}{m_{H^0]}^2 - m_{h^0}^2}\right) \qquad \frac{\tan 2\alpha}{\tan 2\beta} = -\left(\frac{m_{A^0}^2 + m_Z^2}{m_{A^0]}^2 - m_Z^2}\right) \tag{3.16}$$

The parameter of $\sin 2\beta$ and m_Z^2 are obtained by:

$$\sin 2\beta = \frac{2b}{2|\mu|^2 + m_{H_u}^2 + m_{H_d}^2} \tag{3.17}$$

$$m_Z^2 = \frac{|m_{H_d}^2 - m_{H_u}^2|}{\sqrt{1 - \sin^2(2\beta)}} - m_{H_u}^2 - m_{H_d}^2 - 2|\mu|^2 \tag{3.18}$$

It can be seen that μ is a SUSY-respecting parameter that appears in the superpotential, while b, $m_{H_u}^2$ and $m_{H_d}^2$ are SUSY-breaking parameters. This leads to the necessity of extending the MSSM at high energy, incorporating a mechanism to relate μ with the SUSY breaking mechanism in some way. This is the idea to solve the μ problem as mentioned before.

3.3.2 The neutralinos and charginos

Due to the effect of EWSB, the combination of neutral higgsinos ($\tilde{H}_u^0$ and $\tilde{H}_d^0$) and neutral gauginos ($\tilde{B}$ and $\tilde{W}^0$) form four mass eigenstates, known as neutralinos, denoted by $\tilde{N}_i$ ($i = 1, 2, 3, 4$). These labels are defined conventionally as a ascending order mass which means $m_{\tilde{N}_1} < m_{\tilde{N}_2} < m_{\tilde{N}_3} < m_{\tilde{N}_4}$. The lightest neutralino, $\tilde{N}_1$, is commonly regarded as LSP when R-parity conserve, which is a popular dark matter candidate.

The charged higgsinos ($\tilde{H}_u^+$ and $\tilde{H}_d^-$) combine with winos ($\tilde{W}^+$ and $\tilde{W}^-$) to form two mass eigenstates called charginos. We denote these as $\tilde{C}_i^\pm$ ($i = 1, 2$) and the mass order is $m_{\tilde{C}_1} < m_{\tilde{C}_2}$.

The neutralino mass term in the Lagrangian is shown as follows, where we set the gauge eigenstate basis $\psi^0 = (\tilde{B}, \tilde{W}^0, \tilde{H}_d^0, \tilde{H}_u^0)$.

$$\mathcal{L}_{\text{neutralino mass}} = -\frac{1}{2}(\psi^0)^T M_{\tilde{N}} \psi^0 + c.c.. \tag{3.19}$$

The mass matrix $M_{\tilde{N}}$ is

$$M_{\tilde{N}} = \begin{pmatrix} M_1 & 0 & -g_b v_d/\sqrt{2} & g_b v_u/\sqrt{2} \\ 0 & M_2 & g_w v_d/\sqrt{2} & -g_w v_u/\sqrt{2} \\ -g_b v_d/\sqrt{2} & g_w v_d/\sqrt{2} & 0 & -\mu \\ g_b v_d/\sqrt{2} & -g_w v_d/\sqrt{2} & -\mu & 0 \end{pmatrix}. \tag{3.20}$$

The matrix $M_{\tilde{N}}$ can be diagonalized through a unitary matrix N to obtain mass eigenstates:

$$N^* M_{\tilde{N}} N^{-1} = \begin{pmatrix} m_{\tilde{N}_1} & 0 & 0 & 0 \\ 0 & m_{\tilde{N}_2} & 0 & 0 \\ 0 & 0 & m_{\tilde{N}_3} & 0 \\ 0 & 0 & 0 & m_{\tilde{N}_4} \end{pmatrix} \tag{3.21}$$

The mass eigenstates can be expressed by parameters:

$$m_{\tilde{N}_1} = M_1 - \frac{m_Z^2 s_W^2 (M_1 + \mu \sin 2\beta)}{\mu^2 - M_1^2} + \dots \tag{3.22}$$

$$m_{\tilde{N}_2} = M_2 - \frac{m_W^2 (M_2 + \mu \sin 2\beta)}{\mu^2 - M_2^2} + \dots \tag{3.23}$$

$$m_{\tilde{N}_3} = |\mu| + \frac{m_Z^2 (I - \sin 2\beta)(\mu + M_1 \cos^2\theta_W + M_2 \sin^2\theta_W)}{2(\mu + M_1)(\mu + M_2)} + \dots \tag{3.24}$$

$$m_{\tilde{N}_4} = |\mu| + \frac{m_Z^2 (I + \sin 2\beta)(\mu - M_1 \cos^2\theta_W - M_2 \sin^2\theta_W)}{2(\mu - M_1)(\mu - M_2)} + \dots \tag{3.25}$$

where M_1 and M_2 are real and positive, and μ is assumed to be real with a sign $I = \pm 1$. The mass eigenstate of the neutralino is similar to specific SUSY particles. $\tilde{N}_1 \approx \tilde{B}$ is 'bino-like', $\tilde{N}_2 \approx \tilde{W}^0$ is 'wino-like' and $\tilde{N}_3, \tilde{N}_4 \approx (\tilde{H}_u^0 \pm \tilde{H}_d^0)/\sqrt{2}$ are 'higgsino-like'.

The chargino mass term can be expressed in the Lagrangian as follows:

$$\mathcal{L}_{\text{chargino mass}} = -\frac{1}{2}(\psi^{\pm})^T M_{\tilde{C}} \psi^{\pm} + c.c. \tag{3.26}$$

where the mass matrix $M_{\tilde{C}}$ has a form:

$$M_{\tilde{C}} = \begin{pmatrix} 0 & X^T \\ X & 0 \end{pmatrix} \tag{3.27}$$

with

$$X = \begin{pmatrix} M_2 & g v_u \\ g v_d & \mu \end{pmatrix} = \begin{pmatrix} M_2 & \sqrt{2} s_\beta m_W \\ \sqrt{2} c_\beta m_W & \mu \end{pmatrix} \tag{3.28}$$

The mass eigenstates can be transformed from the gauge eigenstates by the matrices U and V.

$$\begin{pmatrix} \tilde{C_1}^+ \\ \tilde{C_2}^+ \end{pmatrix} = V \begin{pmatrix} \tilde{W}^+ \\ \tilde{H}_u^+ \end{pmatrix}, \qquad \begin{pmatrix} \tilde{C_1}^- \\ \tilde{C_2}^- \end{pmatrix} = U \begin{pmatrix} \tilde{W}^- \\ \tilde{H}_d^+ \end{pmatrix} \tag{3.29}$$

We can get chargino mass eigenstate $\tilde{C}_1^{\pm}$ (wino-like) and $\tilde{C}_2^{\pm}$ (higgsino-like):

$$m_{\tilde{C}_1} = M_2 - \frac{m_W^2 (M_2 + \mu \sin 2\beta)}{\mu^2 - M_2^2} + \dots \tag{3.30}$$

$$m_{\tilde{C}_2} = |\mu| + \frac{I m_W^2 (\mu + M_2 \sin 2\beta)}{\mu^2 - M_2^2} + \dots \tag{3.31}$$

where the $M_2 < |\mu|$ and I is the sign of μ. This condition is the same as the neutralino part above.

3.3.3 The squarks and sleptons

In principle, scalars can mix with any scalar containing the same electric charge, color quantum number and R-parity. It means that the mass eigenstate of squarks and sleptons in the MSSM can be obtained by diagonalizing the mass-squared matrices, including three 6×6 matrices for up-type squarks ($\tilde{u}_L, \tilde{c}_L, \tilde{t}_L, \tilde{u}_R, \tilde{c}_R, \tilde{t}_R$), down type squarks ($\tilde{d}_L, \tilde{s}_L, \tilde{b}_L, \tilde{d}_R, \tilde{s}_R, \tilde{b}_R$) and charged sleptons ($\tilde{e}_L, \tilde{\mu}_L, \tilde{\tau}_L, \tilde{e}_R, \tilde{\mu}_R, \tilde{\tau}_R$) plus one 3×3 matrix for sneutrinos ($\tilde{\nu}_e, \tilde{\nu}_\mu, \tilde{\nu}_\tau$). Most of the mixing effect can be neglected because the mixing angles are very small. Significant distinctions exist between third family squarks (sleptons) and those of the first and second generations. The reason for this lies in the effect of large soft coupling (a_t, a_b, a_τ) and Yukawa coupling (y_t, y_b, y_τ) in renormalization group equation [37]. The first and second family squarks and slepton have negligible mixing effect, leading seven unmixed and degenerate pairs ($\tilde{u}_L, \tilde{c}_L$), ($\tilde{d}_L, \tilde{s}_L$), ($\tilde{e}_L, \tilde{\mu}_L$), ($\tilde{u}_R, \tilde{c}_R$), ($\tilde{d}_R, \tilde{s}_R$), ($\tilde{e}_R, \tilde{\mu}_R$), ($\tilde{\nu}_e, \tilde{\nu}_\mu$). By contrast, the mixing effect of third family squarks and sleptons is substantial in pairs ($\tilde{t}_L, \tilde{t}_R$), ($\tilde{b}_L, \tilde{b}_R$) and ($\tilde{\tau}_L, \tilde{\tau}_R$).

Take the top squark as an example. There are several contributions to the mass. Firstly, the square mass term $\tilde{t}_L^* \tilde{t}_L$ and $\tilde{t}_R^* \tilde{t}_R$ contribute the top squark mass which equal to $m_{Q_3}^2 + \Delta_{\tilde{u_L}}$ and $m_{\tilde{u}_3}^2 + \Delta_{\tilde{u}_R}$. The first and second family squark have similar contributions. The term Δ has a general form:

$$\Delta_\phi = \frac{1}{2}(T_{3\phi} g_w^2 - Y_\phi g_b^2)(v_d^2 - v_u^2) = (T_{3\phi} - Q_\phi \sin^2\theta_W)\cos(2\beta) m_Z^2 \tag{3.32}$$

where the parameters T_ϕ, Y_ϕ and Q_ϕ represent the third component of weak isospin, the weak hypercharge and the electric charge. The second contribution comes from the F-terms [37] in the scalar potential with the form of $y_t^2 H_u^{0*} H_u^0 \tilde{t}_L^* \tilde{t}_L$ and $y_t^2 H_u^{0*} H_u^0 \tilde{t}_R^* \tilde{t}_R$. For the rest of squarks and sleptons, these contributions exist but too small to consider. The third contribution is from the F-term in the scalar potential of the form $-u^* y_t \tilde{\tilde{t}} \tilde{t} H_d^{0*} + c.c.$ which can be rewritten after H_d^0 is replaced by the VEV. It becomes $-u^* v y_t \cos\beta \tilde{t}_R^* \tilde{t}_L + c.c.$. Finally, there are contributions from the soft coupling with the form $a_t \tilde{\tilde{t}} \tilde{Q}_3 H_u^0 + c.c.$. After the H_u^0 get the VEV, the contribution becomes

$a_t v \sin\beta \tilde{t}_L \tilde{t}_R^*$. Putting all the contribution above together, the top squark mass term can be expressed with gauge eigenstate basis $(\tilde{t}_L, \tilde{t}_R)$

$$\mathcal{L}_{\text{stop mass}} = -\begin{pmatrix} \tilde{t}_L^* & \tilde{t}_R^* \end{pmatrix} m_{\tilde{t}}^2 \begin{pmatrix} \tilde{t}_L \\ \tilde{t}_R \end{pmatrix} \tag{3.33}$$

The mass matrix $m_{\tilde{t}}^2$ is:

$$m_{\tilde{t}}^2 = \begin{pmatrix} m_{Q_3}^2 + m_t^2 + \Delta_{\tilde{u}_L} & v(a_t^* \sin\beta - \mu y_t \cos\beta) \\ v(a_t \sin\beta - \mu^* y_t \cos\beta) & m_{\tilde{u}_3}^2 + m^2 + \Delta_{\tilde{u}_R} \end{pmatrix} \tag{3.34}$$

The mass eigenstate $(\tilde{t}_1, \tilde{t}_2)$ can be obtained by applying a unitary matrix to the gauge eigenstate.

$$\begin{pmatrix} \tilde{t}_1 \\ \tilde{t}_2 \end{pmatrix} = \begin{pmatrix} c_{\tilde{t}} & -s_{\tilde{t}}^* \\ s_{\tilde{t}} & c_{\tilde{t}}^* \end{pmatrix} \begin{pmatrix} \tilde{t}_L \\ \tilde{t}_R \end{pmatrix} \tag{3.35}$$

where the $c_{\tilde{t}}$ and $s_{\tilde{t}}$ are the cosine and sine of a stop mixing angle respectively. A similar result can be obtained for the rest of third family squarks (bottom squark) and sleptons (tau sleptons) in the gauge eigenstate $(\tilde{b}_L, \tilde{b}_R)$ and $(\tilde{\tau}_L, \tilde{\tau}_R)$. The corresponding squared-mass matrices are:

$$m_{\tilde{b}}^2 = \begin{pmatrix} m_{Q_3}^2 + \Delta_{\tilde{d}_L} & v(a_b^* \cos\beta - \mu y_b \sin\beta) \\ v(a_b \cos\beta - \mu^* y_b \sin\beta) & m_{\tilde{d}_3}^2 + \Delta_{\tilde{d}_R} \end{pmatrix} \tag{3.36}$$

$$m_{\tilde{\tau}}^2 = \begin{pmatrix} m_{L_3}^2 + \Delta_{\tilde{e}_L} & v(a_\tau^* \cos\beta - \mu y_\tau \sin\beta) \\ v(a_\tau \cos\beta - \mu^* y_\tau \sin\beta) & m_{\tilde{e}_3}^2 + \Delta_{\tilde{e}_R} \end{pmatrix} \tag{3.37}$$

The mass eigenstate $\tilde{b}_1, \tilde{b}_2$ and $\tilde{\tau}_1, \tilde{\tau}_2$ can be obtained by diagonalizing the squared matrix above.

Names	Spin	P_R	Gauge Eigenstates	Mass Eigenstate
Higgs bosons	0	+1	$H_u^0\ H_d^0$	$h^0\ H^0\ A^0\ H^\pm$
squarks	0	-1	$\tilde{u}_L\ \tilde{u}_R\ \tilde{d}_L\ \tilde{d}_R$ $\tilde{s}_L\ \tilde{s}_R\ \tilde{c}_L\ \tilde{c}_R$ $\tilde{t}_L\ \tilde{t}_R\ \tilde{b}_L\ \tilde{b}_R$	(same) (same) $\tilde{t}_1\ \tilde{t}_2\ \tilde{b}_1\ \tilde{b}_2$
slepton	0	-1	$\tilde{e}_L\ \tilde{e}_R\ \tilde{\nu}_e$ $\tilde{\mu}_L\ \tilde{\mu}_R\ \tilde{\nu}_\mu$ $\tilde{\tau}_L\ \tilde{\tau}_R\ \tilde{\nu}_\tau$	(same) (same) $\tilde{\tau}_1\ \tilde{\tau}_2\ \tilde{\nu}_\tau$
neutralino	1/2	-1	$\tilde{B}^0\ \tilde{W}^0\ \tilde{H}_u^0\ \tilde{H}_d^0$	$\tilde{N}_1\ \tilde{N}_2\ \tilde{N}_3\ \tilde{N}_4$
chargino	1/2	-1	$\tilde{W}^\pm\ \tilde{H}_u^+\ \tilde{H}_d^-$	$\tilde{C}_1^\pm\ \tilde{C}_2^\pm$
gluino	1/2	-1	$\tilde{g}$	(same)

TABLE 3.3: The feature of SUSY particles in MSSM assuming negligible sfermion mixing for the first two families.

The value of $\tan\beta$ determines the mass of sbottom and stau particles. If $\tan\beta$ is small (usually less than 10), the impact of mixing terms and the renormalization group (RG) effects on the sbottoms and staus is not significant. Under these circumstances, the mass eigenstate $\tilde{b}_1, \tilde{b}_2, \tilde{\tau}_1, \tilde{\tau}_2$ are nearly the same as the gauge eigenstate $\tilde{b}_L, \tilde{b}, \tilde{\tau}_L, \tilde{\tau}_R$. The third family squark and slepton (beside $\tilde{b}_L$) will almost degenerate with their counterpart of the first and second family with the same quantum number. The exceptional particle $\tilde{b}_L$, as a part of doublet containing $\tilde{t}_L$, will couple with large top Yukawa coupling, therefore the mass of $\tilde{b}_L$ can be less than the mass of $\tilde{d}_L$ and $\tilde{s}_L$ [37]. When $\tan\beta$ is large, the mixing effect in eq. 3.36 and eq. 3.37 is significant, as y_b, y_τ and a_b, a_τ are non-negligible. It shows similar trends with top squark, the lighter mass eigenstate of sbottom and stau, referred to as $\tilde{b}_1$ and $\tilde{\tau}_1$, are much lighter than the first and second family counterpart. The ν_τ is also lighter than $\tilde{v}_e$ and $\tilde{v}_\mu$ which is nearly degenerate.

We have shown how the masses and mixing angles for the particles in MSSM, The mass eigenstates are listed in table 3.3. only assuming the mixing effect in the first and second family squark and slepton is negligible. The Feynman diagrams and Feynman rules for the interaction between these particles and SM particles can be found in refs [71; 72].

3.4 Extension of the MSSM

There are several motivations to extend the MSSM. Firstly, as we discussed above, the parameter μ needs to be adjusted by hand to the EW scale. A further extension of MSSM is needed to generate μ naturally. In the MSSM, the Higgs sector is subject to significant constraints. Large quantum corrections and a top squark mass are required for the observation of the Higgs boson. Expanding the Higgs sector offers the potential to relax these restrictions and circumvent the Higgs lower bound. The Higgs sector in MSSM preserves the CP-symmetry at the tree-level. By expanding the Higgs sector in a suitable way, it becomes possible to introduce enough CP-violating phases that would fulfill part of the Sakharov criteria. We will discuss next-to-minimal supersymmetric extension of the Standard Model (NMSSM) as an example to demonstrate the advantage of MSSM extension and provide a brief model description.

The NMSSM extends the MSSM by adding a gauge singlet chiral superfield S, the NMSSM superpotential is given by:

$$W_{NMSSM} = W_{MSSM} + \lambda S H_u H_d + \frac{1}{3}\kappa S^3 \tag{3.38}$$

where κ is a dimensionless coupling. The bilinear term $\mu H_u H_d$ is forbidden by a global Z_3 symmetry. The trilinear term $\lambda S H_1 H_2$ can generate an effective μ, where $\mu = \lambda v_s$ after the singlet field acquires a VEV, denoted as $v_s = \langle S \rangle$.

From a phenomenological perspective, the NMSSM exhibits distinctive features in its Higgs sector compared to the MSSM. The bosonic component of the singlet introduces two additional Higgs bosons. Consequently, the NMSSM comprises a total of seven Higgs bosons, including three CP-even Higgs bsosons, two CP-odd ones and a pair of charged Higgs bosons. In contrast, the MSSM possesses five Higgs bosons, with the lightest one being considered SM-like. This characteristic serves as a strong constraint because of its observed production and decay patterns. However, within the NMSSM, the lightest Higgs can be considerably lighter than its SM counterpart, potentially evading detection.

The fermionic part of the singlet gives rise to an extra neutralino, reffered to as singlino. This addition means that the NMSSM has five neutralinos, in contrast to the four present in the MSSM. The singlino typically engages in mixing with the other four neutralinos. As a gauge singlet, singlino can only interact with the non-Higgs particles through this mixing with the other neutralinos. This introduces the possibility of a singlino-like neutralino serving as the LSP, which could potentially be a dark matter candidate and a source of missing transverse energy (MET) in detectors. Consequently, the neutralino sector of the NMSSM displays noteworthy differences in phenomenology when compared to the MSSM.

Chapter 4

LHC and ILC

There are two fundamental configurations of particle accelerators. One is a circular accelerator, such as the Tevatron, LEP and LHC, which propels elementary particles in a circular path. The other is a linear accelerator making particles run in a straight trajectory. Circular geometries offer distinct advantages, particularly at energies up to several GeV. The circular design enables more efficient particle acceleration over extended distances and, remarkably, only a fraction of the particles in a collision course actually collides. In the context of linear accelerators, such particles are irretrievably lost while, in the realm of ring accelerators, they continue to circulate, remaining available for future collisions.

However, circular accelerators come with a drawback: when the charged particles traverse curved trajectories, they unavoidably emit synchrotron radiation. The magnitude of energy loss via synchrotron radiation is inversely proportional to the fourth power of the particle mass. Hence, circular accelerators are particularly well-suited for heavy particles, as exemplified by hadron colliders such as the LHC for protons (or even for, e.g., lead nuclei). Attempting to achieve comparable collision energies with an electron-positron collider of the same dimensions is thus impractical. The LEP, which previously occupied the tunnel now designated for the LHC, faced limitations, with its collision energies at 209 GeV due to synchrotron radiation-induced energy loss.

Although the LHC boasts a nominal collision energy exceeding that of the ILC (14 TeV for the LHC compared to approximately 500 GeV for the ILC), the ILC excels in precision measurements. Collisions between electrons and positrons simplify analyses compared to collisions involving the energy distribution among the constituent quarks, antiquarks and gluons of baryonic particles. Consequently, one of the primary roles of the ILC lies in conducting precise measurements of particle properties discovered at the LHC.

4.1 The LHC

The LHC at CERN is the largest and most powerful particle accelerator in the world. Protons and heavy ions (such as lead) can be accelerated to nearly the speed of light. By using colliding beams rather than a moving particle on a fixed target, the LHC achieves the highest energy in the center of mass frame. Two opposite beams move in two adjacent pipes and collide. The beams are guided by a strong magnetic field produced by superconducting electromagnets [73].

The definition of luminosity

$$\mathcal{L} = \frac{N^2}{t \cdot S_{eff}} \tag{4.1}$$

in an accelerator is the number of collisions in a detector per second per area. The N in the equation 4.1 stands for the number of protons in a bunch while t is the time between each bunch. The quantity S_{eff} is the effective section which depends on the cross section area of a bunch. By increasing the luminosity, the LHC can generate more collision data in order to observe rare effects.

Before entering the LHC tunnel, particles pass through four accelerators, as shown in figure 4.1 [74]. Proton start from the linear accelerator Linac 2, while Linac 3 is for heavy ions. Then the proton is boosted by the Proton Synchrotron Booster (PSB) while the heavy ions are fed into the Low Energy Ion Ring (LEIR). In the next step, particles pass through the Proton Synchrotron (PS) and the Super Proton Synchroton (SPS). In particular, protons (with which we will be concerned) can reach 450 GeV before they

enter the LHC ring. There are four particle detectors on the LHC ring: ATLAS, CMS, LHCb and ALICE, as shown in figure 4.2 [75]. The CMS and ATLAS experiments are general detectors, which means they have a broad research range from measuring SM observables with high precision to detecting signals from BSM particles. They have different magnet systems and technical designs, each with its pros and cons. ALICE is a detector built for heavy ion research, its purpose is to investigate the quark-gluon plasma that is produced in strongly interacting matter at extreme energy densities. The LHCb detector is specifically designed for research on bottom quarks, with the goal of understanding the asymmetry between matter and antimatter.

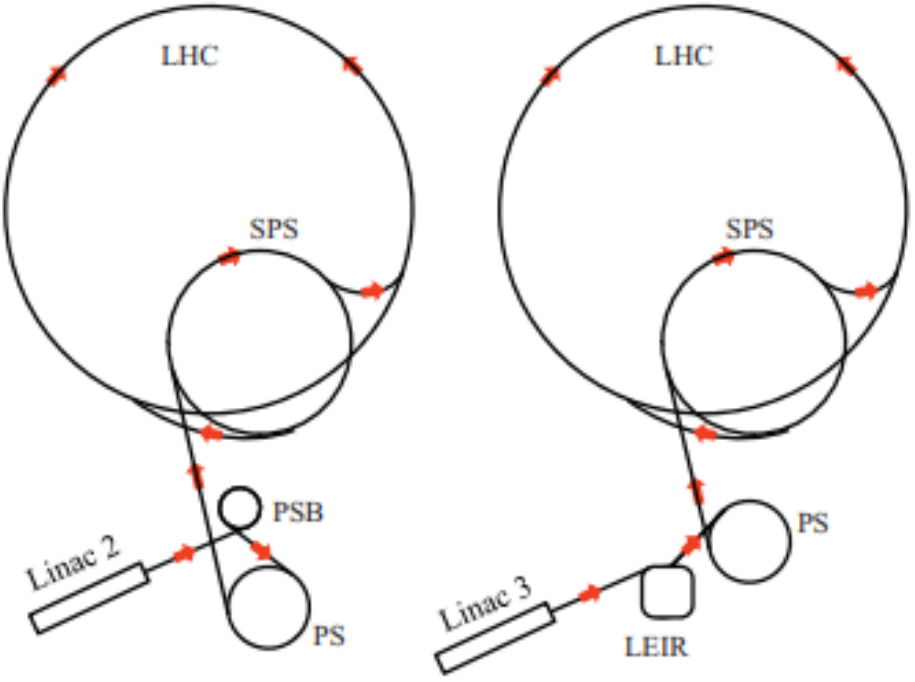

FIGURE 4.1: The schematic of the LHC injector chain for protons (left) and heavy ions (right).

The operations of the LHC effectively commenced in 2009. The operating period from 2010 to 2012 is known as Run 1, with the center of mass energy ($\sqrt{s}$) reaching 8 TeV. Following a two-year shutdown, referred to as LS1, Run 2 was initiated in 2015. It reached $\sqrt{s}$ = 13 TeV and lasted until the end of 2018. During the LS2 period, which followed Run 2 from 2019 to early 2022, several upgrades were carried out on the LHC ring and detector. These upgrades include improvement to the magnet system and a phase-1 upgrade in the CMS and the ATLAS detectors. Currently, Run 3 has just

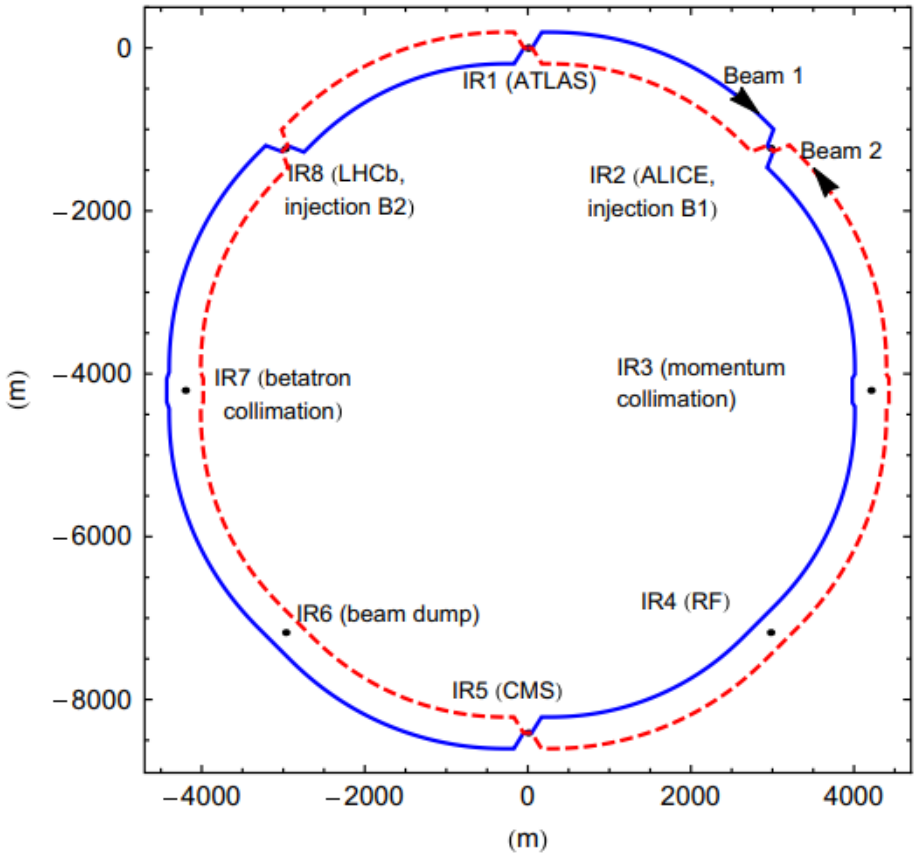

FIGURE 4.2: The schematic layout of the LHC. Eight insertion regions have different function. The beams are injected into IR2 and IR8 and extracted from IR6. IR3 is for momentum cleaning and IR7 is for betatron cleaning. The RF system is in IR4.

began (in 2022) and is expected to end in 2025. The future plan is depicted in figure 4.3. LS3 will prepare for the upgrade to the HL-LHC and the phase-2 upgrade of the CMS and ATLAS detectors.

The LHC has yielded numerous remarkable achievements. The Higgs boson was discovered in the mass region around 125 GeV by CMS and ATLAS in 2012 [76; 77]. From Run 1 and Run 2, more comprehensive analyses were conducted and deeper understanding was gathered on the properties of the Higgs boson. Additionally, the precision of many other SM results was enhanced. Now, the LHC operates during Run-3, primarily furthering the scope of previous runs but also searching for SUSY particles and other hypothetical objects.

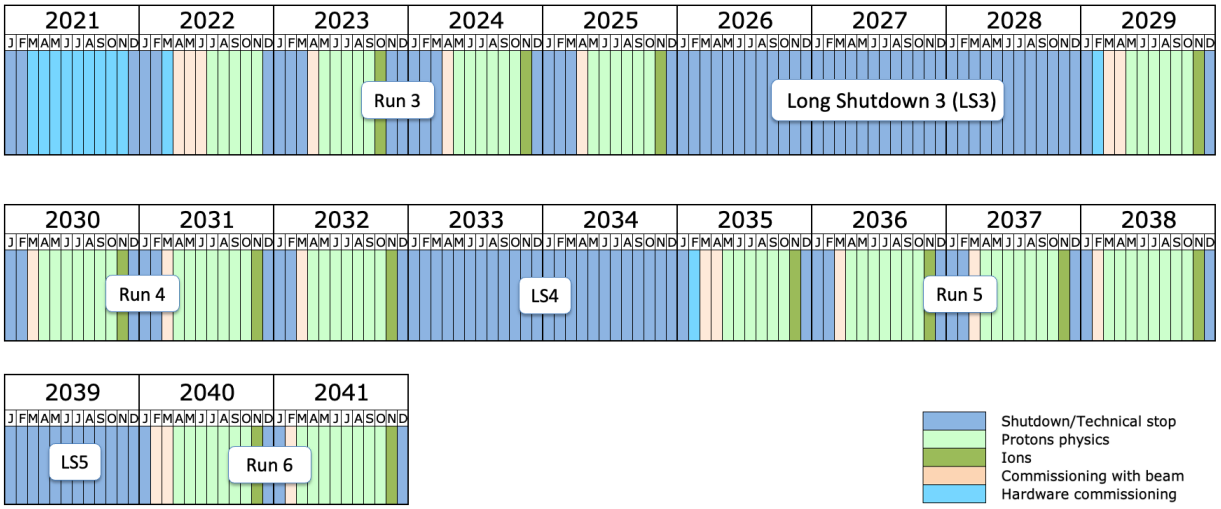

FIGURE 4.3: LHC long term schedule (updated in January 2022).

4.2 The CMS detector

The CMS is a general propose particle detector sited at one of the four collision points on the LHC rings[1]. From figure 4.4 and figure 4.5, it can be seen that the CMS detector has multiple layers with different functions. We will give an explanation in a nutshell for this design.

The CMS experiment uses a right-hand coordinate system. The origin is at the collision point, the x-axis is in the LHC plane, pointing to the centre of the LHC ring, the y-axis points up, hence it is perpendicular to the LHC plane, while the z-axis points along the anticlockwise beam direction. The azimuthal angle (ϕ) is measured from the positive x-axis in the x-y plane, and the polar angle (θ) is measured from the positive z-axis. The radius (r) represents the distance from the origin in the x-y plane, and the definition of pseudorapidity is $\eta = -\ln\tan(\theta/2)$. Finally, the angular distance is defined as $\Delta R = \sqrt{\Delta\phi^2 + \Delta\eta^2}$.

The tracker system is the nearest sub-detector to the collision point. It can detect the trajectory of a charged particle when it passes through the layers of silicon sensors. Charged particles are also deflected in the magnetic field by the Lorentz force. The higher the momentum of the particle the less its trajectory bends. Thus by collecting

[1] We concentrate on this detector as we adopted it in the forthcoming MC studies.

hits in sensors, the tracker system can rebuild the trajectory and momentum of charged particles. Here, figure 4.5 shows the layout of one quarter of the tracker.

The EM Calorimeter (ECAL) is the second nearest sub-detector from the collision point. It is made from lead tungstate crystals. Charged particles release energy in the tungstate crystals, producing secondary particles and light. Photon detectors can detect the emitted photons and calculate their energy by software. The Hadron Calorimeter (HCAL) measures the energy of hadrons, such as protons, neutron, kaons and pions. It has the same working principle as the ECAL: hadrons hit the absorber material and produce secondary particles, which can be detected and the energy calculated. The superconducting solenoid is a 13-meters-long and 6-meters-diameter coil made of niobium-titanium superconductor, and produces a magnetic field of 4 Tesla. This field bends the trajectories of charged particles, enhancing their separation and enabling momentum measurements (as mentioned). The muon system is located in the external layers of the CMS detector since muons can pass through several metres of ordinary matter and cannot be stopped by the calorimeters. When a muon passes through the muon chamber, it displaces electrons from the gas contained in the muon chamber, generating an electrical signal. In order to define the trajectory of muons, data from the tracker system and muon system can be combined.

The LHC delivers 40 Mhz proton-proton collisions, which produce a huge amount of data. It is impossible to store all the data, so a trigger system is needed. The trigger system does a pre-selection to find 'interesting' collisions and discards the rest of the data (99.99999%). At present, the CMS trigger system has two levels: the Level 1 trigger (L1 trigger) and the High-Level Trigger (HLT). The L1 trigger has hardware processors that receive data from the calorimeter and muon system, generating a trigger accept signal within 3 μs and reaching a maximum output rate of 100 kHz. The HLT decreases the data rate further, reaching about 1 kHz by using software [78].

An overview of the L1 trigger system is shown in figure 4.6. Trigger primitives are generated from the forward calorimeter (HF), HCAL, ECAL and the muon detector (resistive-plate chambers (RPC), cathode strip chambers (CSC) and drift tubes (DT)).

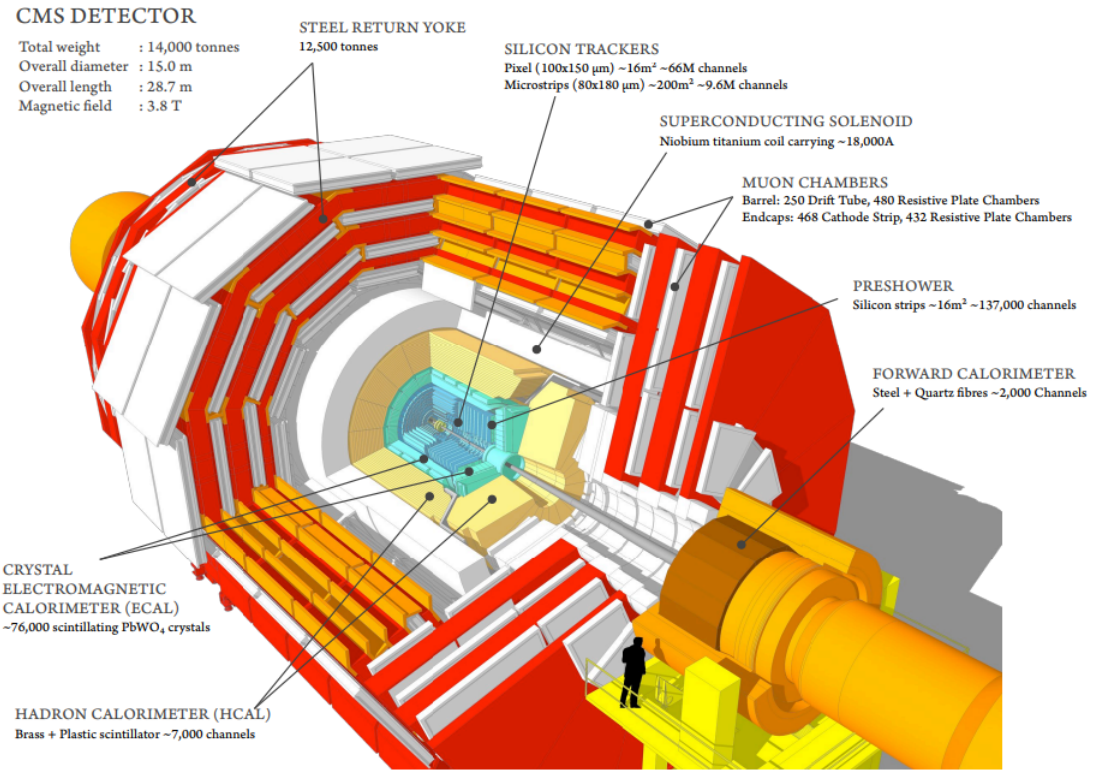

FIGURE 4.4: A cutaway schematics of the CMS detector.

Before being combined in the global trigger (GT), both the trigger primitives from the calorimeter and those from the muon detector pass through several steps [79].

4.3 The LHC upgrade

In order to exploit the full potential of the LHC, it is planned to increase the luminosity of the machine by an order of magnitude, which will require a 30 month shutdown starting around 2024. After this period, the HL-LHC will reach a peak luminosity of $5 - 7.5 \times 10^{34}$ cm^{-2}s^{-1} [80]. This corresponds to an environment of 140-200 proton-proton interactions, named pileup (PU), per LHC bunch crossing. For example, the HL-LHC can produce 15 million Higgs bosons per year, compared to the 1.2 million produced from 2011 to 2012.

The HL-LHC can thus enhance the rate of rare events and provide the highest precision in investigating the SM and BSM scenarios as well. For example, the couplinga of the Higgs boson are a crucial part of the SM. The HL-LHC will enhance

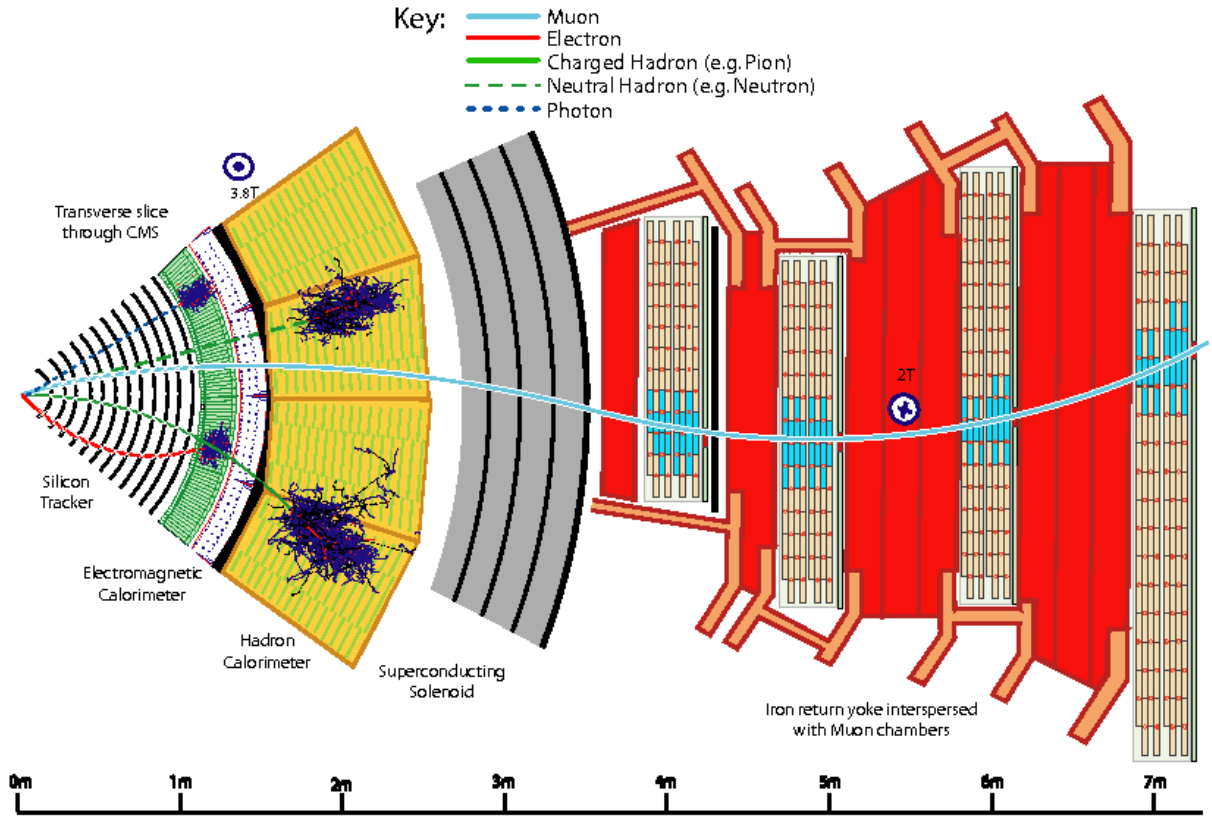

FIGURE 4.5: A segment of the CMS detector in a transverse view. The blue line is a muon track passing through the tracker and the calorimeter with a track. The red line represents an electron, it bends in the tracker and interacts in the ECAL. The trajectory of a charged hadron is represented by the solid green line. The dashed green line and dashed blue line represent a neutral hadron and photon, respectively.

the measurement precision for Higgs couplings in the CMS experiment, including the coupling to muons. The self-coupling of the Higgs boson probes the Higgs field. However, the cross section of Higgs boson pair (HH) production is about 1000 times smaller than the cross section for single Higgs boson production. The Feynman diagram of HH production is shown in figure 4.7 [81]. The HL-LHC is expected to measure these rare production modes in the near future [82].

The HE-LHC, which significantly increases energy capabilities by nearly doubling the current energy to 27 TeV is being developed. It will also offer integrated luminosity at least three times larger than that of the HL-LHC. This advanced infrastructure, combined with the four experimental detectors mentioned above, aims to deepen our understanding of the SM, enable the first precise measurement of the Higgs self-coupling (via HH production), thus expanding the discovery potential beyond the

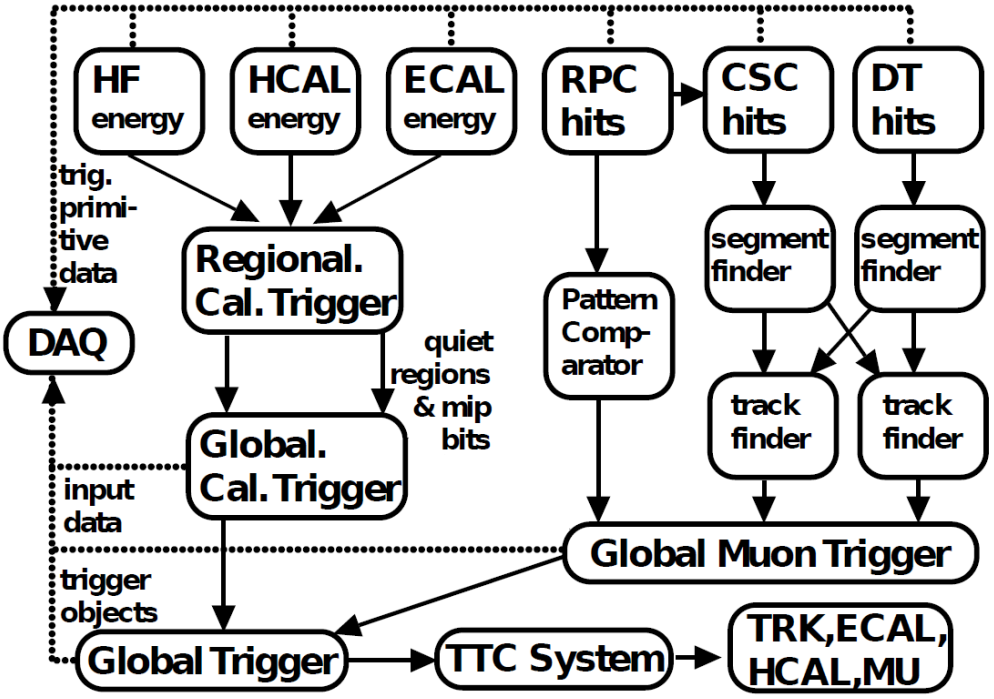

FIGURE 4.6: A schematic of the CMS L1 trigger system. The trigger primitives from HF, HCAL and ECAL are combined firstly in the regional calorimeter trigger (RCT) and then transferred to the global calorimeter trigger (GCT). The energy deposits (hits) from the RPC, CSC and DT are processed by a pattern comparator or segment-tracker finder and sent to the global muon trigger (GMT). The GT combines information from the GCT and GMT to make the final trigger decision. The decision information flows to the tracker (TRK), ECAL, HCAL and the muon system (MU) through the trigger and timing and control (TTC) system. The data acquisition system (DAQ) reads data from subsystems for offline storage.

FIGURE 4.7: Leading-order Feynman diagrams for HH production, where q stands for a quark and wherein top and bottom quarks dominate.

HL-LHC. By utilizing the existing underground infrastructure and portions of the injector chain at CERN, the HE-LHC will hopefully succeed the HL-LHC and serve the global physics community for approximately 20 years in the future.

The proposed concept includes a power-saving, low-temperature superconducting magnet system based on an evolution of the Nb3Sn technology employed in the HL-LHC, an energy-efficient cryogenic refrigeration infrastructure utilizing a neon-helium light gas mixture, a reliable and efficient cryogen distribution system,

and high-power distributed beam transfer utilizing superconducting elements. Additionally, local magnet energy recovery and re-use technologies, already being gradually introduced in other CERN accelerators, will be incorporated. Leveraging the existing LHC underground civil infrastructure, extending surface sites, and utilizing the existing injector chain will contribute to establishing a sustainable research infrastructure at the HE-LHC energy frontier.

The Future Circular Collider (FCC) [83] study is dedicated to the development of innovative designs for the next generation of high-performance particle colliders with a nearly 100 km circumference. Its purpose is to extend the scientific exploration conducted at the LHC once the HL-LHC/HE-LHC phase concludes, which is estimated to be around 2040.

The primary objective of the FCC is to push the boundaries of energy and intensity in particle colliders, with the target collision energies of 100 TeV with integrated luminosity of $20 - 30ab^{-1}$. By reaching this energy and luminosity levels, scientists aim to delve deeper into the SM and ultimately uncover BSM physics. The FCC examines scenarios for three different types of particle collisions: electron–positron collisions (FCC-ee), hadron-hadron (proton–proton and heavy ion) collisions, like in the LHC (FCC-hh), while the other option include proton–electron collisions (FCC-eh) or proton-heavy ion collisions [84].

The FCC-ee will operate with a 90-350 GeV centre-of-mass collision energy which is considered as an intermediate state before the FCC-hh. Compared to a hadron collider, the electron-positron collider has a cleaner background, creating an opportunity to measure known particles with higher precision and explore the unknown. More specifically, by using improved lepton beam and higher luminosity, the FCC-ee has a potential to measure the properties of the Higgs, top quarks and gauge bosons as well as the strong interaction with increased accuracy.

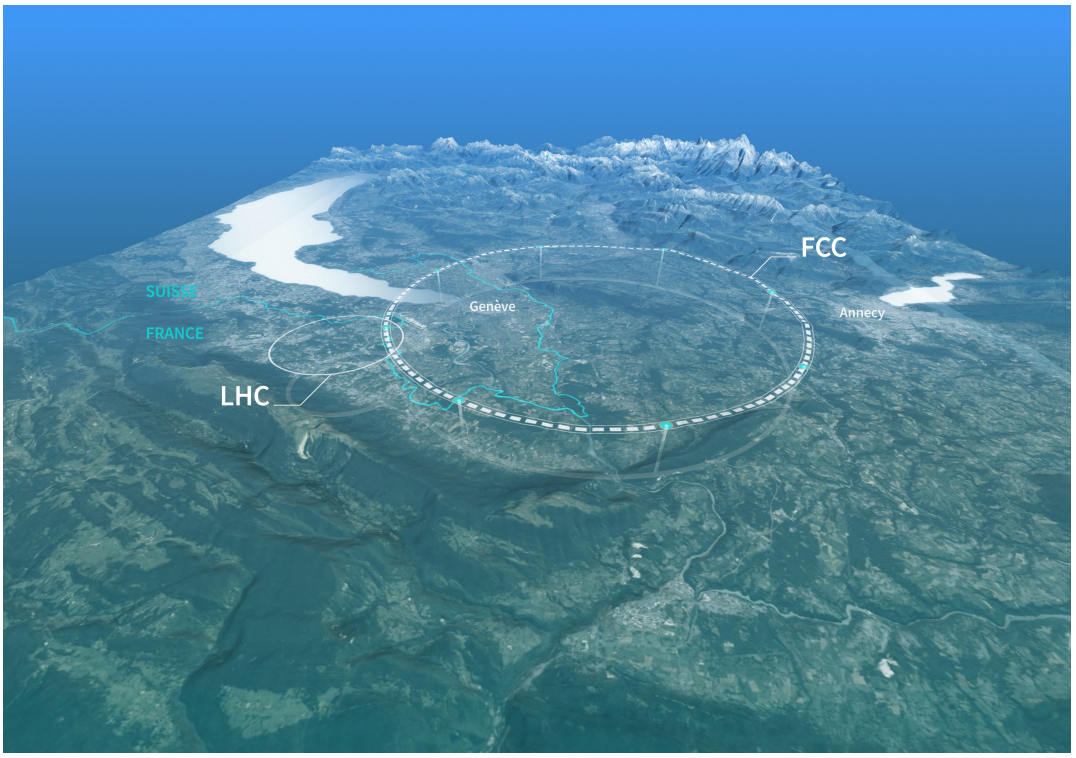

FIGURE 4.8: A schematic map showing a possible location for the FCC.

4.4 The ILC

The ILC is a 200–500 GeV (extendable to 1 TeV) centre-of-mass high luminosity linear electron-positron collider, based on 1.3 GHz Superconducting Radio-Frequency (SCRF) accelerating technology [85]. The ILC gives an opportunity to tackle many important problems in particle physics. It will provide a unique insight into the Higgs boson, the top quark and, possibly, SUSY particles. The ILC enables measurements and data collection with very high precision. A schematic view of the ILC with the major sub-system is shown in figure 4.9.

A polarised e^- source is generated on a photocathode DC gun while the polarised e^+ source is based on an undulator. Positrons are generated by converting high energy photons. Then the electron and positron are injected into damping rings (DR) with 5 GeV energy. After the DR, the beam enters into main linacs through a bunch compressor. From figure 4.9, after 11km transport in each main linac, two beams collide with 14 mrad crossing angle, enabling two detectors being located in the interaction region.

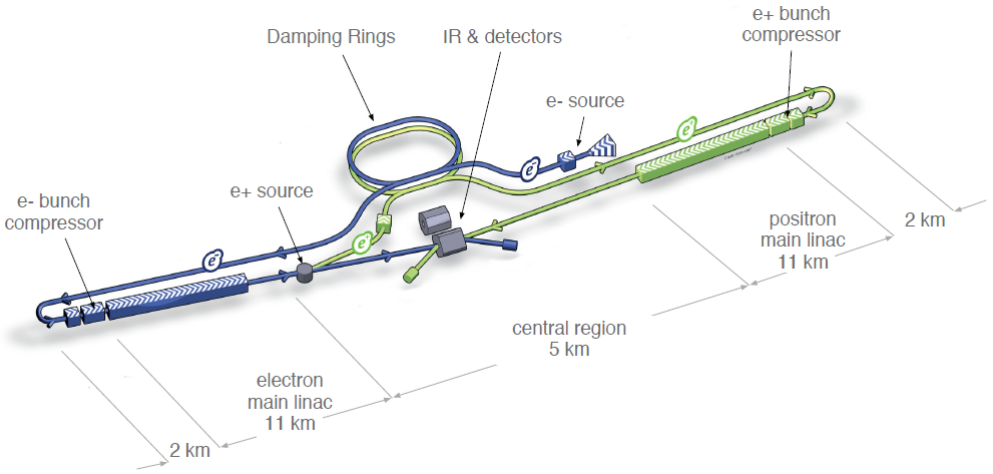

FIGURE 4.9: An overview graphic of the ILC layout with its major sub-systems.

The initial plan of ILC starts at an energy of 250 GeV, which maximizes the cross-section for the process $e^+e^- \to Zh$. In this reaction, the identification of the recoil Z boson serves as an indicator of the Higgs presence, of which it is possible to measure the rate for all decay channels with a very high precision. For example, the Higgs boson decays into quarks are shown in figure 4.10, these are hard to separate from the SM background in the LHC. These precision measurements provide a deeper insight into whether the Higgs boson generate mass independently or is combined with new additional particles (like in SUSY).

After the 250 GeV stage, the ILC will upgrade to its full designed energy (500 GeV) which provides a chance to measure the process $e^+e^- \to \nu\bar{\nu}h$ with high precision. This measurement determines the Higgs coupling strength to gauge bosons with a fraction of percent level of accuracy. The ILC may then upgrade to higher energy (1 TeV), so as to enable one to make precision measurements of the strength of the Higgs self-interaction and coupling with the top quark. The major processes to be studied at the ILC are shown in the table 4.1.

Experiments conducted at the proposed ILC are anticipated to detect effects of physics that go beyond the current SM. Additionally, the ILC is expected to contribute to the discovery and measurement of particles and interactions not described by the SM. Physicists have several key objectives they hope to accomplish at the ILC.

Energy	Reaction	Physics Goal
91 GeV	$e^+e^- \to Z$	ultra-precision EW
160 GeV	$e^+e^- \to WW$	ultra-precision W mass
250 GeV	$e^+e^- \to Zh$	precision Higgs couplings
350-400 GeV	$e^+e^- \to t\bar{t}$	top quark mass and couplings
	$e^+e^- \to WW$	precision W couplings
	$e^+e^- \to \nu\bar{\nu}h$	precision Higgs couplings
500 GeV	$e^+e^- \to f\bar{f}$	precision search for Z'
	$e^+e^- \to t\bar{t}h$	Higgs coupling to top
	$e^+e^- \to Zhh$	Higgs self-coupling
	$e^+e^- \to \tilde{\chi}\tilde{\chi}$	search for supersymmetry
	$e^+e^- \to AH, H^+H^-$	search for extended Higgs states
700-1000 GeV	$e^+e^- \to \nu\bar{\nu}hh$	Higgs self-coupling
	$e^+e^- \to \nu\bar{\nu}VV$	composite Higgs sector
	$e^+e^- \to \nu\bar{\nu}t\bar{t}$	composite Higgs and top
	$e^+e^- \to \tilde{t}\tilde{t}^*$	search for supersymmetry

TABLE 4.1: Major physics process to be studied at various energy level. The process in the low-energy state will continue to be studied at the high-energy level.

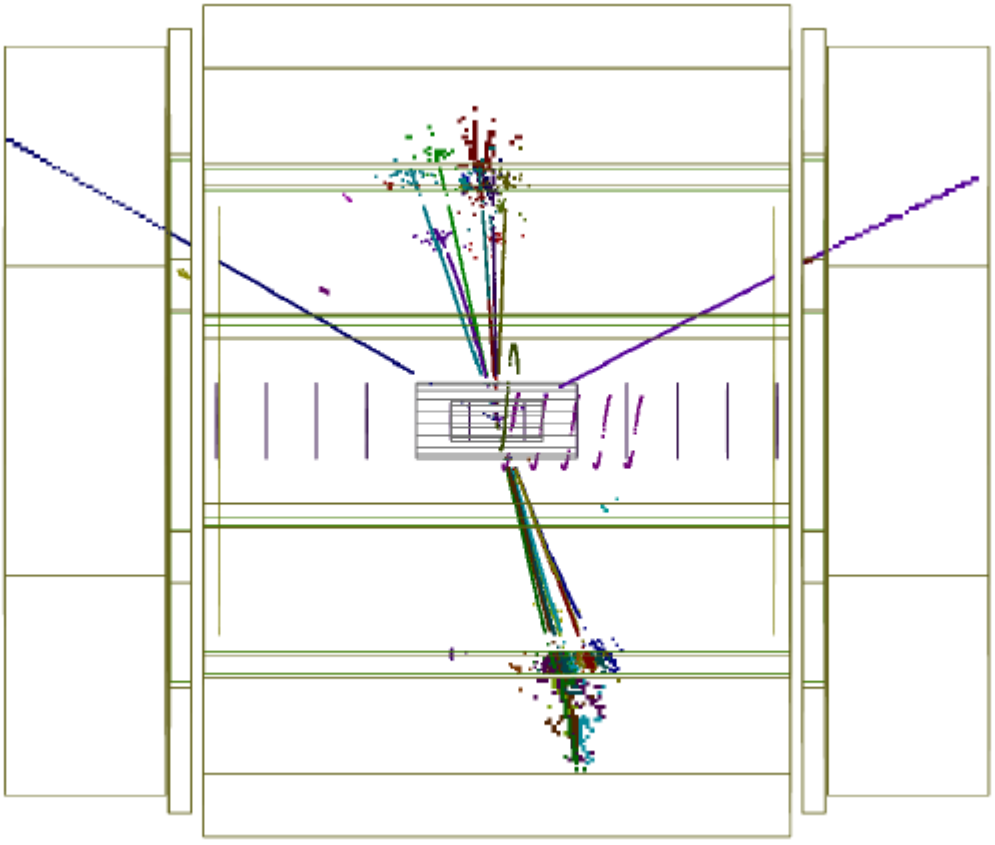

FIGURE 4.10: The process of $e^+e^- \to Zh$ with $Z \to \nu^+\nu^-$ and $h \to b\bar{b}$. It would be observed by the generic International Large Detector (ILD) at the ILC.

- Measure the mass, spin, and interaction strengths of the Higgs boson. The ILC aims to provide precise measurements of the properties of the Higgs boson, such as its mass, spin, and interaction strengths. This will help in understanding the mechanism responsible for the origin of mass and provide insights into the nature of the Higgs field.
- Explore TeV-scale extra dimensions. If additional dimensions of space exist at the TeV scale, the ILC could investigate their presence. This includes measurements related to the number, size, and shape of any hypothetical extra dimensions, which could provide evidence for string theory or brane worlds.
- Investigate SUSY particles and DM candidates. The ILC chiefly aims to study the LSP.

To achieve these scientific goals, the development of new-generation particle detectors is also crucial. These detectors will be designed to accurately measure and analyze the properties and interactions of particles produced in collisions at the ILC. While a generic ILD design is being proposed, advanced detector technologies will enhance the precision and capabilities of the experiments, allowing for more comprehensive investigations and potential breakthroughs in our understanding of the fundamental nature of the universe.

Chapter 5

Accessing neutrino dynamics in the NMSSMr with a RH sneutrino LSP at the ILC

5.1 Introduction

The LHC experiments have so far shown good agreement with the predictions of the SM. Other types of experiments instead show us that the SM needs to be extended: neutrino oscillations require neutrinos to be massive [15; 16; 17; 18; 86; 87]. Also the Cosmic Microwave Background (CMB) [88] and galactic rotation curves [89; 90] strongly support the idea that most of the mass of the Universe is in a form currently unknown to us, dubbed DM.

Neutrino oscillation experiments have measured the mixing angles of the PMNS matrix [91] and the mass splittings between neutrinos, but they offer no information on the origin of neutrino masses. As the masses are several orders of magnitude smaller than any other fermion mass, it is expected that neutrino mass generation is based on some kind of a seesaw mechanism [40; 41; 43; 44; 45; 46]. The canonical example is Type-I seesaw, where one add heavy RH neutrinos to the SM particle

spectrum, which then suppress the LH neutrino masses by a factor of m_D/m_N, where m_D is the standard Dirac mass term and m_N is the bare mass of the RH neutrino.

SUSY is one of the most studied frameworks to construct BSM theories. The MSSM however lacks a mechanism for neutrino mass generation, but it can be extended with various seesaw mechanisms. SUSY models have the advantage that the superpartners of neutrinos, sneutrinos, may in some cases decay visibly at colliders and hence studying neutrino dynamics at colliders becomes possible [92; 93]. However, current experimental constraints make it clear that non-minimal versions of SUSY are more suited to embed a neutrino mass generation mechanism [94].

Adding a seesaw mechanism to models of SUSY gives also the option of non-standard DM candidates. Especially the RH sneutrino, when is the LSP, has been of considerable interest over the years [52; 95; 96; 97; 98; 99; 100; 101; 102; 103; 104; 105; 106; 107]. In the MSSM extended with Type-I seesaw RH sneutrinos lead to overabundance of the relic density of the CMB, unless there is significant mixing between the left- and RH sneutrinos [108]. Adding a singlet to the model, (*i.e.*, considering the NMSSMr) allows a coupling between the heavy Higgses and sneutrinos, which can assist in the annihilation and lead to the correct relic abundance without the need for any left-right mixing in the sneutrino sector [53; 54].

We shall investigate here the possibility of extracting e^+e^- collider signals and of estimating neutrino Yukawa couplings in the NMSSMr with a RH sneutrino as DM candidate. Since all superpartner decay chains end with this sneutrino, we cannot rely on sneutrino decays, instead we need to find visible decays that involve the sneutrino and neutrino Yukawa couplings. Hence we need to study chargino decays to a lepton and a sneutrino. As the seesaw scale is rather low, the neutrino Yukawa couplings are tiny. Since the chargino can also decay to a virtual $W^\pm$ boson and a neutralino, the direct two-body decay of interest to us, into a lepton-sneutrino pair, is rare. However, the latter neutralino decay mode allows us to estimate the neutrino Yukawa couplings. Finally, the fact that RH sneutrinos can be rather light in the NMSSMr allows for DM signals emerging from the rare chargino decays to be sizable,

particularly at future leptonic machines, where the SM background can efficiently be vetoed thanks to the high level of control on the final state kinematics. In the end, the signature that we will pursue is the one made up by a 'dijet + dilepton + Missing Transverse Energy' (MET or $\not{E}_T$) system.

5.2 NMSSM with RH neutrinos

The NMSSM extends the MSSM with an additional gauge singlet chiral superfield S [55]. The NMSSM fixes the μ problem of the MSSM by generating an effective μ-term, but it still inherits the defect that neutrinos are massless. By adding a singlet RH neutrino superfield N, we may introduce the Type-I seesaw mechanism to generate neutrino masses. The superpotential is given by [53; 109]

$$W = W_{\text{NMSSM}} + \lambda_N SNN + y_N H_2 \cdot LN, \tag{5.1}$$

$$W_{\text{NMSSM}} = y_u H_2 \cdot Qu + y_d H_1 \cdot Qd + y_e H_1 \cdot Le - \lambda S H_1 \cdot H_2 + \frac{1}{3}\kappa S^3. \tag{5.2}$$

The flavour indices are omitted. As in the NMSSM, a $\mathbb{Z}_3$-symmetry is imposed in order to make the superpotential scale invariant. When this discrete symmetry is broken spontaneously by the VEV of the (pseudo)scalar fields, a potential domain wall problem arises. This problem can be solved like in the NMSSM, by assuming that non-renormalisable terms pick a preferred vacuum [110; 111] or by supergravity corrections during inflation [112][1].

The soft SUSY breaking terms are

$$\begin{aligned} -\mathcal{L}_{soft} = {} & m^2_{\tilde{Q}}|\tilde{Q}|^2 + m^2_{\tilde{u}}|\tilde{u}|^2 + m^2_{\tilde{d}}|\tilde{d}|^2 + m^2_{\tilde{L}}|\tilde{L}|^2 + m^2_{\tilde{e}}|\tilde{e}|^2 + m^2_{\tilde{N}}|\tilde{N}|^2 + m^2_{\tilde{S}}|S|^2 \\ & + m^2_{H_1}|H_1|^2 + m^2_{H_2}|H_2|^2 + M_1\tilde{B}\tilde{B} + M_2\tilde{W}\tilde{W} + M_3\tilde{g}\tilde{g} \\ & + A_u Y_u H_2 \tilde{Q}\tilde{u} + A_d Y_d H_1 \tilde{Q}\tilde{d} + A_e Y_e H_1 \tilde{L}\tilde{e} + y_N A_{yN} \tilde{L} H_2 \tilde{N} \\ & - \lambda A_\lambda S H_1 H_2 + \lambda_N A_{\lambda_N} S N^2 + \frac{1}{3}\kappa A_\kappa S^3 + h.c. \end{aligned} \tag{5.3}$$

[1] For an alternative formulation, called new Minimally-extended Supersymmetric Standard Model (nMSSM), where the domain wall (as well as the Peccei-Quinn axion) problem is solved by invoking a global discrete R-symmetry, see Ref. [113].

RH neutrino masses are generated when the scalar component of the singlet superfield S gets a VEV, $\langle S \rangle = v_s$. The superpotential term $\lambda_N SNN$ in eq. (5.1) leads to a Majorana mass term $M_N = 2\lambda_N v_s$. As v_s is around the EW scale, so the RH neutrino masses are naturally at the EW scale. The LH neutrino masses are obtained after the Higgs doublet fields acquire VEVs, $(v_1, v_2) = (\langle H_1 \rangle, \langle H_2 \rangle)$. The standard seesaw formula then gives $m_\nu = y_N^2 v_2^2 / M_N$. To get viable neutrino masses the neutrino Yukawa couplings y_N have to be slightly smaller than the electron Yukawa coupling, $y_N \lesssim \mathcal{O}(10^{-6})$.

The left-hand sneutrino $\tilde{\nu}_L$ and right-hand sneutrino $\tilde{N}$ can be decomposed to CP-even (real) and CP-odd (imaginary) components:

$$\tilde{\nu}_L \equiv \frac{1}{\sqrt{2}}(\tilde{\nu}_{L1} + i\tilde{\nu}_{L2}), \qquad \tilde{N} \equiv \frac{1}{\sqrt{2}}(\tilde{N}_1 + i\tilde{N}_2). \tag{5.4}$$

The sneutrino quadratic term is

$$\frac{1}{2}\ (\tilde{\nu}_{L1}, \tilde{N}_1, \tilde{\nu}_{L2}, \tilde{N}_2)\ \mathcal{M}^2_{\text{sneutrino}} \begin{pmatrix} \nu_{L1} \\ \tilde{N}_1 \\ \tilde{\nu}_{L2} \\ \tilde{N}_2 \end{pmatrix}. \tag{5.5}$$

The sneutrino mass matrix can be obtained from the quadratic terms in the scalar potential:

$$\mathcal{M}^2_{\text{sneutrino}} = \begin{pmatrix} m^2_{L\bar{L}} & \frac{m^2_{LR}+m^2_{L\bar{R}}+c.c}{2} & 0 & i\frac{m^2_{LR}-m^2_{L\bar{R}}-c.c}{2} \\ \frac{m^2_{LR}+m^2_{L\bar{R}}+c.c}{2} & m^2_{R\bar{R}} + M^2_{RR} + m^{2*}_{RR} & i\frac{m^2_{LR}-m^2_{L\bar{R}}-c.c}{2} & i(m^2_{RR} - m^{2*}_{RR}) \\ 0 & i\frac{m^2_{LR}-m^2_{L\bar{R}}-c.c}{2} & m^2_{L\bar{L}} & -\frac{m^2_{LR}+m^2_{L\bar{R}}+c.c}{2} \\ i\frac{m^2_{LR}-m^2_{L\bar{R}}-c.c}{2} & i(m^2_{RR} - m^{2*}_{RR} & -\frac{m^2_{LR}+m^2_{L\bar{R}}+c.c}{2} & m^2_{R\bar{R}} - M^2_{RR} - m^{2*}_{RR} \end{pmatrix}. \tag{5.6}$$

The parameters are defined as follows:

$$\begin{aligned} m^2_{L\bar{L}} &\equiv m^2_{\tilde{L}} + |y_N v_2|^2 + \mathrm{D-term}, \\ m^2_{LR} &\equiv y_N(-\lambda v_s v_1)^\dagger + y_N A_N v_2, \\ m^2_{L\bar{R}} &\equiv y_N v_2(-\lambda v_s)^\dagger, \\ m^2_{R\bar{R}} &\equiv m^2_{\tilde{N}} + |2\lambda_N v_s|^2 + |y_N v_2|^2, \\ m^2_{RR} &\equiv \lambda_N(A_{\lambda_N} v_s + (\kappa v_s^2 - \lambda v_1 v_2)^\dagger). \end{aligned} \tag{5.7}$$

Here, the $m^2_{\tilde{L}}$, $m^2_{\tilde{N}}$, A_{λ_N} and A_N are the soft SUSY breaking terms. Assuming thet there is no CP-violation, which means the sneutrino real part and imaginary part do not mix, eq. (5.5) can be simplified as:

$$\begin{aligned} &\frac{1}{2}(\tilde{v}_{L1}\tilde{N}_1) \begin{pmatrix} m^2_{L\bar{L}} & m^2_{LR} + m^2_{L\bar{R}} \\ m^2_{LR} + m^2_{L\bar{R}} & m^2_{R\bar{R}} + 2m^2_{RR} \end{pmatrix} \begin{pmatrix} \tilde{v}_{L1} \\ \tilde{N}_1 \end{pmatrix} + \\ &\frac{1}{2}(\tilde{v}_{L2}\tilde{N}_2) \begin{pmatrix} m^2_{L\bar{L}} & m^2_{LR} - m^2_{L\bar{R}} \\ m^2_{LR} - m^2_{L\bar{R}} & m^2_{R\bar{R}} - 2m^2_{RR} \end{pmatrix} \begin{pmatrix} \tilde{v}_{L2} \\ \tilde{N}_2 \end{pmatrix}. \end{aligned} \tag{5.8}$$

The mixing between left- and RH sneutrinos is determined by m^2_{LR} and $m^2_{L\bar{R}}$. From eq. (5.7), these two terms are proportional to the neutrino Yukawa coupling and therefore can be neglected. The mass difference between $\tilde{N}_1$ and $\tilde{N}_2$ is from the term m^2_{RR}. If $m^2_{RR} > 0$, $\tilde{N}_1$ is heavier than $\tilde{N}_2$ and vice versa. In this case, the lighter RH sneutrino mass can be determined by $m^2_{R\bar{R}} - 2m^2_{RR}$, which is defined by a set of parameters such as $m^2_{\tilde{N}}$ and λ_N.

5.2.1 RH sneutrino as a DM candidate

In the following we shall assume that the soft SUSY breaking masses for RH sneutrinos $m^2_{\tilde{N}}$ are the smallest of the SUSY breaking mass terms. Then there is a part of the parameter space where the LSP is the RH sneutrino. This parameter space can be obtained by adjusting parameters in eq. (5.7). In the MSSM with RH neutrinos

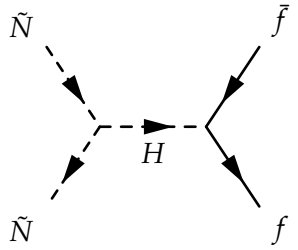

FIGURE 5.1: The dominant annihilation mechanism of sneutrino DM in the NMSSMr.

(MSSMr) it is not easy to satisfy the constraint from the relic density with a RH sneutrino LSP, since as a gauge singlet it does not annihilate efficiently enough. Enhancing the mixing between left- and RH sneutrinos is a way to remedy this [108].

The NMSSM offers an additional method to enhance the annihilation cross section. The scalar potential has a term $\lambda\lambda_N H_u H_d \tilde{N}\tilde{N}$ which, after EW Symmetry Breaking (EWSB), creates a three-point coupling between the RH sneutrinos and Higgs bosons. The coupling between the sneutrinos and the heavy Higgses H and A is larger than that with the SM-like Higgs, so the sneutrino DM annihilates mostly via the heavy Higgs portal to third generation fermions (see figure 5.1), hence, the corresponding cross section mainly depends on λ, λ_N and $m_{H,A}$. Further, in certain parts of the parameter space, coannihilations or resonant annihilation may alter the relic density largely.

The same Higgs-sneutrino couplings are mainly responsible for the effective sneutrino-nucleon interaction. In general the spin-independent direct detection cross sections are about one order of magnitude below the current experimental limit. Both constraints from the relic density and direct detection have been studied in the literature, most recently in [114].

5.3 Finding the rare chargino decay

We wish to estimate the neutrino Yukawa couplings in the presence of a RH sneutrino LSP. The decay $\tilde{\chi}^{\pm} \to \ell^{\pm}\tilde{N}$ arises from the neutrino Yukawa couplings. However, it competes with the decay $\tilde{\chi}^{\pm} \to W^{*\pm}\tilde{\chi}^0$, where the neutralino then decays to a RH

sneutrino and some other particles. Even though this is a three-body decay and hence suppressed by the propagator through $1/m_W^2$, it completely dominates over the two-body decay mode proportional to $|y_N|^2$, which can have a Branching Ratio (BR) of $\mathcal{O}(10^{-5})$. However, the fact that $\tilde{\chi}^{\pm} \to \ell^{\pm}\tilde{N}$ is a two-body decay fixes the kinematics in the rest frame of the chargino. At the LHC this is not much of a help as the relationship between the laboratory frame and the rest frame of the chargino is hard to estimated. At electron-positron colliders, instead, the situation is different: if the collision energy is chosen so that the charginos are produced almost at rest, the energy of the charged lepton will be nearly fixed in the lab frame and this can be used in the event selection.

We therefore consider the process $e^+e^- \to \gamma^*/Z^* \to \tilde{\chi}^+\tilde{\chi}^-$ with one of the charginos decaying to a lepton and a sneutrino and the other decaying to a neutralino and a virtual $W^{\pm}$ leading to a lepton plus MET or to hadrons. We assume that the difference between the neutralino and chargino masses is much smaller than the W boson mass. In this case, the W boson would decay into the SM particles so soft that would go undetected. If the neutralino decays invisibly through the neutrino Yukawa couplings, i.e., via $\tilde{\chi}^0 \to \tilde{N}\nu$, the final state with a single hard lepton and MET will get a too large background from $W^{\pm}$ bosons. If, however, the RH neutrino and sneutrino are light enough, the neutralino can decay via its singlino component through $\tilde{\chi}^0 \to \tilde{N}N$ with the RH neutrino decaying subsequently to a lepton and two jets. The Feynman diagram of this process is shown in figure 5.2. Requiring a lepton and two jets with an

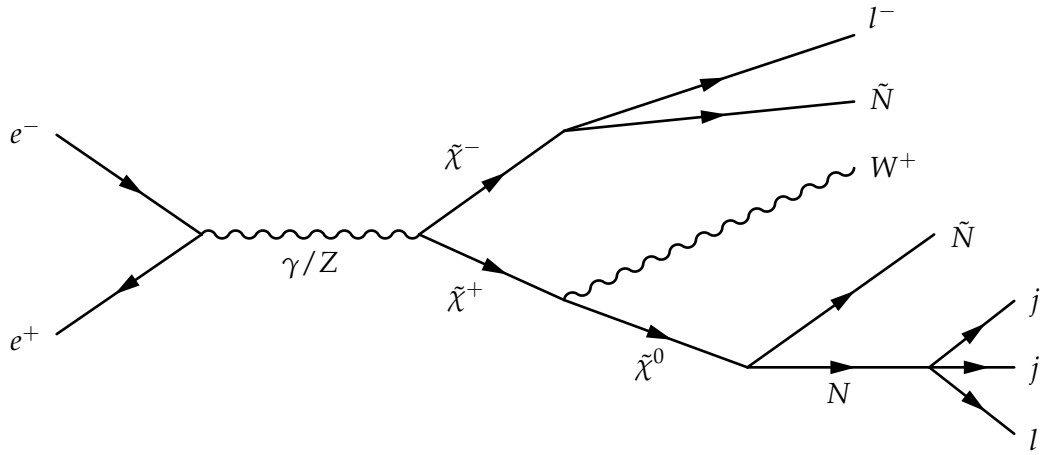

FIGURE 5.2: An example of a full process leading to the 'dijet + dilepton + $\not{E}_T$' signature, if $\Delta M = M_{chargino} - M_{neutralino} \ll M_W$.

invariant mass corresponding to the RH neutrino mass will be enough to get rid of the backgrounds, as we shall see. Finally, notice that the existence of RH neutrinos can be established already at the LHC [115].

Thus we can get the aforementioned signature: 'dijet + dilepton + MET'. The dilepton signature should emerge in both same-sign and opposite-sign dileptons due to the Majorana nature of the RH neutrino. The latter will have a smaller background from SM processes. The major SM background to this final state comes from the following processes.

- W^+W^-Z production in the case where one $W^\pm$ boson decays into two jets and the other to a lepton and neutrino while the Z boson gives two leptons, one of which is missed by the detector.
- ZZZ production, where one Z boson decays leptonically, the second to neutrinos and the third creates the two jets.
- $t\bar{t}$ production, where the top (anti)quarks decay to a $W^\pm$ boson and a b-quark, when one lepton originates from the $W^\pm$ boson and an opposite sign lepton from a B-meson.

We now proceed to describe how we performed our Monte Carlo (MC) analysis.

5.3.1 Event simulation

We prepared the model files with the Mathematica package SARAH v4.14 [116; 117], which creates the source code for SPHENO v4.0.3 [118; 119] to generate the mass spectrum. We simulate collider events with MADGRAPH5 v2.8.2 [120]. We use PYTHIA v8.2 [121] for parton showering and simulate the detector response with DELPHES3 [122], where we use the DSiD card [123] to simulate the detector at the future ILC. We use MADDM v.3.0 [124] to check that our Benchmark Points (BPs) satisfy the constraints from the relic density and direct detection experiments. Lastly, we use MADANALYSIS5 v1.8 [125] to implement the cuts.

	BP1	BP2	BP3
$m(\tilde{\chi}_1^{\pm})$	239.3 GeV	234.8 GeV	233.3 GeV
$m(\tilde{N}_1)$	130.6 GeV	127.9 GeV	127.4 GeV
$m(N_1)$	101.7 GeV	90.5 GeV	88.6 GeV
$m(\tilde{\chi}^0)$	233.3 GeV	228.7 GeV	227.3 GeV
BR($N \to \ell jj$)	60%	68%	68%
BR($W^* \to$ leptons)	28%	28%	28%

TABLE 5.1: Mass spectra and the most important parameters of our BPs. The chargino is chosen to be slightly lighter than 250 GeV in order to make the process $\tilde{\chi}^0 \to \tilde{N}N$ kinematically allowed. All the masses in these BPs have not been excluded [1].

Number of leptons	$N(\ell) = 2$
Same-sign lepton pair	$N(\ell^+)$ or $N(\ell^-) = 2$
Number of jets	$N(j) = 2$
Veto on b-jets	$N(b) = 0$

TABLE 5.2: The requirements for the final state topology.

We prepared a number of BPs, which could be probed at the $\sqrt{s} = 500$ GeV phase of the ILC. As the integrated luminosity we use 4000 fb^{-1}, which could represent the total integrated luminosity after the luminosity upgrade of the ILC [126]. We select the charginos to be slightly lighter than 250 GeV and the RH neutrino and sneutrino so light that $\tilde{\chi}^0 \to \tilde{N}N$ is kinematically allowed. We show the spectra of our BPs in table 5.1. We checked with MADDM v3.0 [124] that the BPs are acceptable with respect to constraints from the relic density and direct detetion experiments. Regarding the relic density we only imposed the upper limit $\Omega h^2 \leq 0.12$.

As a preselection we require two same-sign leptons, two jets and veto against b-jets. For the b-tagger we use a working point, where the b-tagging efficiency is 70% with a mistagging rate of 2% for c-quark jets and 0.3% for light quark (and gluon) jets. We summarise this preselection in table 5.2.

We impose several cuts. The leading lepton ℓ_1 arises from $\tilde{\chi}^{\pm} \to \tilde{N}\ell^{\pm}$, which is a two-body process. As long as the beam energy is not much larger than $2m_{\tilde{\chi}^{\pm}}$, the lepton energies in the lab frame are in a rather narrow range determined by the event kinematics as can be seen from figure 5.3. We filter the signal by requiring
30 GeV $< p_T(\ell_1) <$ 100 GeV and 60 GeV $< E(\ell_1) <$ 120 GeV.

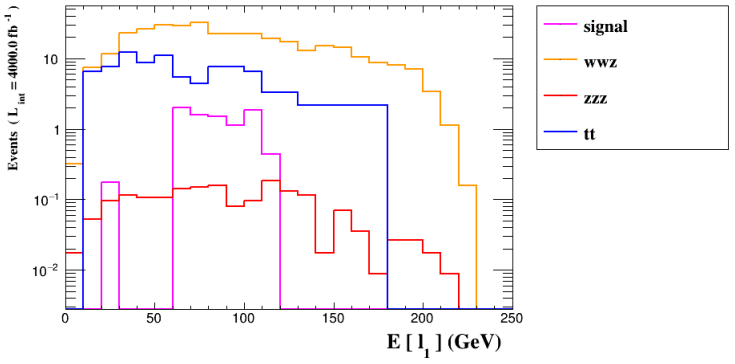

FIGURE 5.3: The energy of the leading lepton ℓ_1 for our signal and different background components. The preselection of table 5.2 has been imposed.

The second lepton and the jets arise from $N \to \ell jj$ and the momenta of the decay products are limited by the mass of the RH neutrino. Hence, the momenta are constrained from above and imposing a veto against a second hard lepton with $p_T(\ell_2) > 40$ GeV and against a hard jet with $p_T(j_1) > 70$ GeV leaves our signal untouched while rejects a reasonable fraction of the background.

As the hadronic activity in our signal events arises mainly from the hadronic decay of a $W^{\pm}$ boson emerging from the RH neutrino, we expect the total hadronic energy to be smaller than in the background events, especially $t\bar{t}$. Hence we require $H_T < 100$ GeV.

The LSPs give rise to MET for signal events. As we can see from figure 5.4, the distribution of $\not{E}_T$ for the signal is mostly in the interval $[50, 100]$ GeV, hence, we select that interval. From figure 5.6 we can see that for the signal the leading lepton is almost in the opposite direction compared to $\not{p}_T$ so we require the azimuthal angle between the leading lepton and missing transverse momentum to be greater than 2.5 radians. We also impose the condition $M(\ell_1\ell_2) < 80$ GeV for the invariant mass of the lepton pair, which rejects a fraction of the bosonic backgrounds as can be seen from figure 5.5.

Finally, we assume that the RH neutrino mass is known and require the invariant mass of the second lepton[2] and the two leading jets to be close to the RH neutrino mass. We consider all the particle stable thus their width equal to zero. We show the full list of cuts in table 5.3 and the resulting cutflow for the signal and background components in table 5.4.

[2]The leading lepton arises from the two-body decay of the chargino, the one coming from the RH neutrino is always softer.

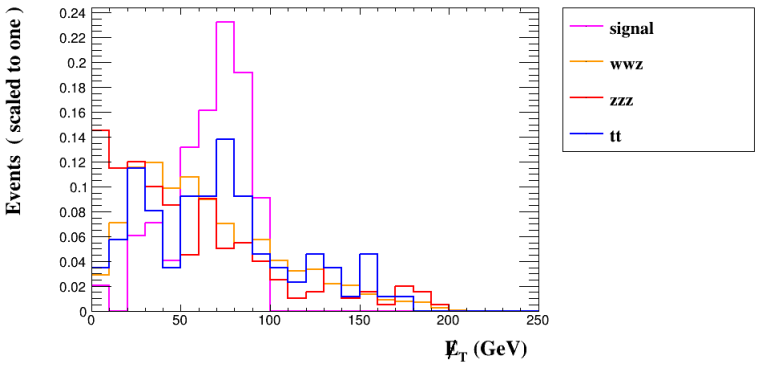

FIGURE 5.4: The distribution of missing transverse energy ($\not{E}_T$) for the signal and background components. Here we have normalised the distributions to unity.

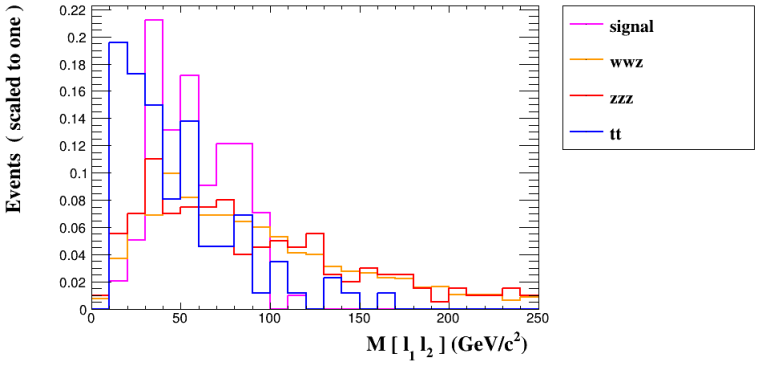

FIGURE 5.5: The distribution of invariant mass of the leading two leptons, the different distributions are normalised to unity.

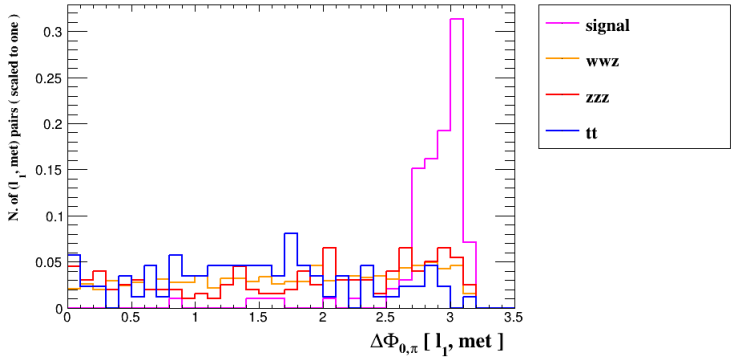

FIGURE 5.6: The distribution of the azimuthal angle between the leading lepton and missing transverse energy, the different distributions are normalised to unity.

Acceptance Cuts	
Transverse momentum of electron	$p_T(e) > 5$ GeV
Transverse momentum of muon	$p_T(\mu) > 3$ GeV
Transverse momentum of jet	$p_T(j) > 17$ GeV
Absolute pseudorapidity of electron	$\lvert\eta(e)\rvert < 2.5$
Absolute pseudorapidity of muon	$\lvert\eta(\mu)\rvert < 2.4$
Absolute pseudorapidity of jet	$\lvert\eta(j)\rvert < 2.4$
Kinematical Cuts	
Transverse momentum of leading lepton	$30 \text{ GeV} < p_t(\ell_1) < 100 \text{ GeV}$
Energy of leading lepton	$60 \text{ GeV} < E(\ell_1) < 120 \text{ GeV}$
Transverse momentum of sub-leading lepton	$3 \text{ GeV} < p_t(\ell_2) < 40 \text{ GeV}$
Transverse momentum of leading jet	$17\text{GeV} < p_t(j_1) < 70 \text{ GeV}$
Total hadronic energy	$H_T < 100$ GeV
Missing transverse energy	$50 \text{ GeV} < \not{E}_T < 100 \text{ GeV}$
Invariant mass of ℓ_1 ℓ_2	$M(\ell_1\ell_2) < 80$ GeV
Angle of leading lepton with MET	$\Delta\Phi_{0,\pi} > 2.5$
Invariant mass of two jets and sub-leading lepton	$90 \text{ GeV} < M(j_1 j_2 \ell_2) < 110 \text{ GeV}$

TABLE 5.3: The multiplicity requirements for the final state topology and the full set of cuts in our MC analysis. The first six cuts are acceptance cuts while the rest are kinematical cuts. The Invariant mass of two jets and sub-leading lepton, $M(j_1 j_2 \ell_2)$, is set between 80 GeV and 100 GeV for BP3, the corresponding result can be found in table 5.4

Overall we may see that we are able to see excesses of some level above the expected SM background, but a full discovery would need a higher integrated luminosity. Nevertheless, even if the excesses are not statistically significant enough to claim the discovery of the two-body decay of the chargino, some bounds on the neutrino Yukawa couplings can be inferred.

5.4 Estimating neutrino Yukawa couplings

The coupling between the RH sneutrino, charged lepton and lightest chargino is

$$\lambda_{\tilde{N}\ell^+\tilde{\chi}^-} = \frac{i}{\sqrt{2}} y^{\nu}_{ab} V_{12} \frac{1+\gamma_5}{2}, \tag{5.9}$$

Cut	BP1	BP2	BP3	W^+W^-Z	ZZZ	$t\bar{t}$	Total backgroun
Acceptance Cuts	87.0	139	116	158999	4400	2193599	2356998
b-jet veto	84.2	137	115	133754	2802	240648	377204
$N(\ell)$=2	38.8	54.9	42.0	11308	387	11454	23149
$N(\ell^+) = 2$ or $N(\ell^-) = 2$	17.8	26.0	20.6	792	6.07	339	1137
$N(j) = 2$	8.66	12.3	8.69	343	1.76	95.4	440
17 GeV$< p_T(j_1) <$ 70 GeV	8.66	12.0	8.35	154.5	0.625	26.3	181.4
$p_T(\ell_1) > 30$ GeV	7.87	10.2	8.11	134.5	0.519	17.6	152.6
$p_T(\ell_1) < 100$ GeV	7.17	9.05	6.38	108.6	0.37	14.3	123.3
3 GeV$< p_T(\ell_2) <$ 40 GeV	7.17	9.05	6.26	83.3	0.29	14.3	97.9
$H_T < 100$ GeV	7.17	9.05	6.26	67.9	0.20	7.68	75.8
$E(\ell_1) < 120$ GeV	7.17	8.21	5.91	34.8	0.123	4.39	39.3
$E(\ell_1) > 60$ GeV	7.17	8.21	5.91	34.8	0.123	4.39	39.3
$\Delta\Phi_{0,\pi}$ >2.5	7.00	6.96	4.40	15.58	0.035	2.19	17.8
$\not{E}_T > 50$ GeV	6.12	6.27	3.48	8.75	0.026	1.10	9.88
$\not{E}_T < 100$ GeV	6.12	5.43	3.01	7.79	0.026	1.10	8.92
$M(\ell_1\ell_2) < 80$ GeV	5.34	5.15	3.01	4.45	0.018	1.1	5.57
$M(j_1j_2\ell_2) < 110(100)$ GeV	5.25	5.15	3.01	1.91(1.27)	0.0088(0)	1.1(1.1)	3.019(2.37)
$M(j_1j_2\ell_2) > 90(80)$ GeV	3.5	3.06	1.97	0.954(0.636)	0.0088(0)	0(0)	0.963(0.636)

TABLE 5.4: The cutflow for the signal BPs and all background. The luminosity is 4000 fb^{-1} and the energy is $\sqrt{s} = 500$ GeV. The bracket stands for the cut and result corresponding to both BP2 and BP3. After these cuts, the significance for BP1 is 3.57, for BP2 is 3.83 and for BP3 is 2.47.

where a, b refer to neutrino flavours and V_{12} gives the higgsino component of the lightest chargino. For our BPs, we have $|V_{12}| \simeq 1$. This leads to the following decay width (neglecting the lepton mass):

$$\Gamma(\tilde{\chi}^\pm \to \ell_a^\pm \tilde{N}_b) = \frac{(m_{\tilde{\chi}}^2 - m_{\tilde{N}}^2)^2}{64\pi m_{\tilde{\chi}}^3} |y_{ab}^\nu|^2 |V_{12}|^2. \tag{5.10}$$

The majority of charginos decay via $\tilde{\chi}^\pm \to \tilde{\chi}^0 \ell^\pm \nu, \tilde{\chi}^0 q\bar{q}'$. This decay can in principle be mediated by several particles ($W^\pm$, $\tilde{\ell}^\pm$, $\tilde{\nu}$, $H^\pm$, $\tilde{q}$) and their contributions can interfere. In this section, we focus on the rare chargino decay $\tilde{\chi}^\pm \to \ell^\pm \tilde{N}$, so we skip the analysis about these channel, the explicit formulae are given in [127].

If we assume that all of the superpartners besides the RH sneutrino and the higgsinos are heavy, the decay width of the chargino is calculable. In such a case the measurement of the BR of the rare chargino decay would give us an estimate of the neutrino Yukawa couplings through the computed full width and eq. (5.10). The overall chargino pair production cross section is readily calculated. The problem in estimating such a BR is that the observed number of sneutrino events after the full set

of cuts does not represent the number of sneutrinos originally produced. Hence, we need to estimate how many sneutrinos are lost in the procedure.

If we assume that hadrons from the virtual $W^{\pm}$ decay cannot form a detectable jet which satisfy our final state topology, the only way the process of figure 5.2 can produce two leptons and two jets is that the $W^{\pm}$ boson from the RH neutrino decays hadronically. Then we can observe two leptons if either the virtual $W^{\pm}$ decays hadronically (including hadronic taus) and we detect all leptons or the virtual $W^{\pm}$ decays leptonically and we miss one lepton. The only way to get same-sign dileptons is that one of the leptons detected arises from the RH neutrino. Hence, the probability of detecting two leptons that can lead to a same-sign dilepton signature is[3]

$$\begin{aligned} P(N(\ell)=2) &= \epsilon(\ell_1)\epsilon(\ell_2)\times \mathrm{BR}(N\to \ell jj)\times \mathrm{BR}(W^*\to \text{hadrons}) \\ &\quad +\epsilon(\ell_1)\epsilon(\ell_2)(1-\epsilon(\ell_3))\times \mathrm{BR}(N\to \ell jj)\times \mathrm{BR}(W^*\to \text{leptons}) \\ &\quad +\epsilon(\ell_2)\epsilon(\ell_3)(1-\epsilon(\ell_1))\times \mathrm{BR}(N\to \ell jj)\times \mathrm{BR}(W^*\to \text{leptons}), \end{aligned} \tag{5.11}$$

where $\epsilon(\ell)$ is the lepton identification efficiency averaged over the detector. The probability of having two same-sign leptons is 50% due to the Majorana nature of the RH neutrino. The probability of having two jets is $\epsilon(j)^2$, where $\epsilon(j)$ is the single jet identification efficiency, while the b-veto gives us a factor of $(1-a)^2$, where a is the average mistagging rate.

We try to mimic the actual process of determining the selection efficiencies by basing the efficiency estimates on simulated data other than our primary process. We estimated the efficiencies of leading lepton and jet identification based on $e^+e^-\to W^+W^-$ data, which gives average values of $\epsilon(\ell_1)=0.89\pm0.02$ and $\epsilon(j)=0.83\pm0.02$. The identification efficiency for the sub-leading lepton is lower. We estimated it from $e^+e^-\to\tilde{\chi}^+\tilde{\chi}^-$ data, where requiring at least one lepton, four jets and a fully reconstructed RH neutrino gives us a sample with over 95% purity[4]. From the numbers of single and dilepton events one may estimate the identification

[3] If one would wish to follow the steps of the cutflow more precisely, one would have to add contributions, where the decay of the RH neutrino leads to two leptons (one being missed), which would be removed by the $N(j)=2$ requirement.

[4] Quite often the RH neutrino decay leads to a secondary vertex that can help reduce the backgrounds even further.

efficiency for the sub-leading lepton. This leads to estimate $\epsilon(\ell_2) = 0.50/0.46/0.45$ for BP1/BP2/BP3. The b-mistag rate is approximately $a = 0.008$ as one in four jets arising from a hadronically decaying $W^{\pm}$ is a c-jet. Overall this leads to a selection efficiency of 0.082/0.085/0.083 for BP1/BP2/BP3 for the basic event selection of table 5.2. The systematic error of these efficiencies is $\mathcal{O}(10\%)$. We then turn to the cut efficiencies. The cuts on the leading lepton transverse momentum and energy basically remove the cases where the leading lepton has not been identified, *i.e* the third line of eq. (5.12). This gives a selection efficiency of 98% for all of the benchmark points. Some of the further cutting efficiencies can also be estimated in a data-driven way from chargino pair data. If we look at events with two leptons and four jets, where we are able to reconstruct the RH neutrinos, we may derive estimates of some kinematical distributions. Specifically, the sub-leading lepton and all hadronic activity of our signal events arise from the decays of the RH neutrino, so the efficiencies of the cuts $p_T(j_1) < 70$ GeV and $p_T(\ell_2) < 40$ GeV can be directly inferred from data and the efficiency of requiring $H_T < 100$ GeV can be estimated by looking at the distribution of H_T for events with two RH neutrinos.

For the cut on the second lepton momentum, the data-driven estimate for the cutting efficiency is 100% for all BPs. For the leading jet momentum the efficiency is 100% for BP1 and 98% for BP2 and BP3. The total hadronic transverse momentum distribution would give an average of 67 GeV with a 10 GeV standard deviation, so that, assuming a Gaussian distribution, the signal acceptance is higher than 99.9%.

The rest of the cutting efficiencies need to be estimated by simulation. To successfully simulate events, the spectrum needs to be known. The chargino mass is easily determined from the onset energy of the chargino pair production. The problem is that the mass of the sneutrino is not too easy to determine from data. For instance, mono-X signatures, which could give the LSP mass through the endpoint of the visible spectrum at e^+e^- colliders [128; 129] cannot be used in the case of a RH sneutrino LSP as they can be produced only via the Higgs portal or SUSY cascades. Eventually, the LSP mass can be measured from the endpoint of the lepton energy spectrum (which is $\sqrt{s}/2 - m_{\tilde{N}}$) from the rare decay mode, but the number of events

is so small that this may not provide a useful bound. Another limit for the LSP mass is naturally $m_{\tilde{N}} < m_{\tilde{\chi}} - m_N$, which can be improved with the $\not{E}_T$ distribution of the chargino pair events.

Overall we expect that the simulation should be able to determine the cutting efficiencies of the remaining cuts with a reasonable accuracy, perhaps with a 20% error or so. In such a case, there would be an overall systematic uncertainty in the initial number of charginos decaying to the two-body state of about 30%. However, the statistical error would be larger, in the range of 50–70% depending on the actual number of observed events. This would lead to an overall error in the range 55–75% for the BR($\tilde{\chi}^{\pm} \to \ell^{\pm}\tilde{N}$). Since the latter is proportional to the Yukawa coupling squared, this would give an error of about 25–35% for the determination of the Yukawa couplings.

5.5 Conclusions

The RH sneutrino is an additional candidate to be the LSP in the NMSSM with RH neutrinos. If such a sneutrino is the LSP, the higgsinos need to also be at the EW scale and potentially could be produced at the LHC and future e^+e^- colliders. However, when the sneutrino is the LSP, we do not have the advantage of visible sneutrino decays as a window to neutrino physics. However, the charged higgsino has a small chance of decaying into a charged lepton and the sneutrino LSP, this decay being determined by the tiny neutrino Yukawa couplings.

In this paper, we have shown that, if the RH neutrino is so light that the neutral higgsino will decay via $\tilde{\chi}^0 \to N\tilde{N}$, this additional handle will let us find the rare two-body decay of the chargino at the ILC, $\tilde{\chi}^- \to l^-\tilde{N}$, while at the LHC such a discovery is impossible as the boost between the laboratory frame and the CM frame is unknown. This rare two-body decay would allow us to estimate the size of the neutrino Yukawa couplings but, even with the luminosity upgrade of the ILC, the measurement will be statistically limited and give at best an accuracy of 25%.

This result would probably constitute the first glimpse into the neutrino dynamics of our chosen non-minimal SUSY framework.

Chapter 6

Exploring high scale seesaw models through a SUSY portal

6.1 Introduction

Neutrino masses have been known to be non-zero for 25 years [15]. As they are so much smaller than all other SM fermion masses, one usually assumes that they are generated by some kind of a seesaw mechanism [40; 41; 45; 130; 131]. The masses are still generated through the Higgs mechanism, but suppressed by a heavy seesaw particle, which can be a singlet neutrino (Type-I), a triplet of Higgs bosons (Type-II) or a triplet of exotic leptons (Type-III) [94; 132].

The seesaw scale is a priori unknown. If the seesaw scale is around the EW scale, one may be able to produce the seesaw particles directly at the LHC [133; 134; 135; 136]. One of the original ideas [130] was that the smallness of the neutrino masses could be related to the breaking of a (GUT), *i.e.*, the relevant Yukawa couplings would be of order unity and the seesaw scale somewhere around $M_{\text{GUT}} \sim 10^{14}$ GeV. Such energy scales are obviously out of the reach of present and future colliders.

SUSY, the symmetry between fermions and bosons, is often a necessary ingredient in formulating models with large separations of scales. Different scale of mass can be reached when the SUSY is broken. Due to the cancellation between the bosonic and

fermionic loops, the separation of scales is radiatively stable [65], once it has been generated by some dynamics. Thus in the supersymmetric framework, scalar masses would not get quadratic corrections proportional to the seesaw scale and an EW scale Higgs boson would not be unnatural even if the seesaw scale was close to the GUT scale.

In the context of high scale seesaw models, supersymmetry has one remarkable property. The scalar potential, and especially its F-terms being of the form

$$V = \sum_i \left| \frac{\partial W}{\partial \varphi_i} \right|^2 , \tag{6.1}$$

leads to four-scalar interactions without the seesaw particle but with the seesaw couplings involved. If the couplings are of the order unity, they are among the largest ones in the model and could lead to observable consequences.

For definiteness, let us consider the Type-I seesaw model, where the extra superpotential terms in addition to those of the MSSM are

$$W = W_{\text{MSSM}} + y^\nu L \cdot H_u N^c + M_N N^c N^c, \tag{6.2}$$

where we assume $y^\nu \sim 1$ and $M_N \sim 10^{14}$ GeV. When differentiating with respect to N^c, one gets the term

$$\sum_k y^{\nu *}_{ik} y^\nu_{jk} \tilde{L}^\dagger_i \cdot H^\dagger_u \tilde{L}_j \cdot H_u,$$

involving only Higgs bosons and left-handed sleptons, which we assume to be at the TeV scale. If there are significant mass splittings between the sfermion generations, which could well be generated through Renormalisation Group Evolution (RGE) due to the large couplings, one might get processes like $\tilde{\nu}_i \to \tilde{\nu}_j h$ with a large BR. If the sneutrinos decay visibly, the decays can be distinguished from mono-Higgs signatures that could arise from dark matter [137; 138]. Slepton decays with Higgs bosons in the final state could offer an indication of a high scale seesaw model and thus provide us a window to scales otherwise beyond our experimental reach.

Our aim is to investigate how could one observe such slepton decay patterns

involving Higgs bosons in seesaw models of Type-I and Type-III, which have a similar structure in terms of the TeV scale Lagrangian.

Our paper is organised as follows. Higgs-slepton interactions are described in the next section, which is followed by a discussion of the production and decay modes relevant to our research. Our numerical analysis is introduced in the following section, after which we conclude.

6.2 Higgs-slepton interactions in seesaw models

We shall now look at how the Higgs-slepton interactions arise from our seesaw models in some detail. In particular, we look at Type-I and Type-III seesaw models. Both have Yukawa couplings that connect the lepton and Higgs doublets to the seesaw particles, which form a singlet and triplet under SU(2). The superpotential of Type-I seesaw is given in eq. (6.2) and for Type-III seesaw it is

$$W = W_{\text{MSSM}} + y^{\nu} L \Sigma H_u + M_{\Sigma} \text{Tr}(\Sigma^2), \tag{6.3}$$

where L is the left-chiral lepton doublet and $H_u = (H^+, H^0)^T$ is the up-type Higgs doublet. The Σ is an antilepton ($L = -1$) chiral superfield which transforms as $(1, 3, 0)$ under the SM gauge group $SU(3)_c \times SU(2)_L \times U(1)_Y$. The mass term for Σ violates lepton number by two units.

The superfield Σ can be represented

$$\Sigma = \sigma^i \Sigma^i = \begin{pmatrix} \Sigma^0/\sqrt{2} & \Sigma^+ \\ \Sigma^- & -\Sigma^0/\sqrt{2} \end{pmatrix}, \quad \Sigma^{\pm} = \frac{\Sigma^1 \mp i\Sigma^2}{\sqrt{2}}, \quad \Sigma^0 = \Sigma^3. \tag{6.4}$$

The models look very similar in what comes to neutrino mass generation, both having a lepton and a Higgs doublet coupling to the companion neutrinos. The only difference is that the L and H_u superfields combine to a singlet in the case of Type-I and to a triplet in the case of Type-III seesaw. This difference between the two seesaw

models leads to a difference in the scalar potential which contributes the processes that lead to slepton decays containing a Higgs boson.

When we expand the neutrino Yukawa terms in the superpotential, we get

$$W = y^{\nu}_{ij}\left(e^{-}_{i}H^{+}_{u} - \frac{1}{\sqrt{2}}\nu_i H^{0}_{u}\right)N^{c}_{j} + \ldots, \tag{6.5}$$

$$W = y^{\nu}_{ij}\left(\frac{1}{\sqrt{2}}e^{-}_{i}H^{+}_{u}\Sigma^{0}_{j} - \nu_i\Sigma^{-}_{j}H^{+}_{u} + \frac{1}{\sqrt{2}}e^{-}_{i}\Sigma^{+}_{j}H^{0}_{u} + \frac{1}{2}\nu_i\Sigma^{0}_{j}H^{0}_{u}\right) + \ldots, \tag{6.6}$$

for Type-I and Type-III, respectively. Here we have included a factor of $1/\sqrt{2}$ into the definition of the neutral Higgs field.

Differentiating with respect to the heavy seesaw fields leads to the scalar potentials

$$V = \sum_{k}\frac{1}{2}y^{\nu}_{ik}y^{\nu *}_{jk}\tilde{\nu}_i\tilde{\nu}^{*}_{j}H^{0}_{u}H^{0*}_{u} + \ldots, \tag{6.7}$$

$$V = \sum_{k}\frac{1}{4}y^{\nu}_{ik}y^{\nu *}_{jk}\left(\tilde{\nu}_i\tilde{\nu}^{*}_{j}H^{0}_{u}H^{0*}_{u} + 2\tilde{e}^{-}_{i}\tilde{e}^{+}_{j}H^{0}_{u}H^{0*}_{u}\right) + \ldots, \tag{6.8}$$

for Type-I and Type-III, respectively. Hence one in general gets Higgs interactions with sleptons that are non-diagonal in flavour space and, in the case of a high scale seesaw, to obtain the observed neutrino mass from the mass relation with the right-hand neutrino, Yuakwa coupling is "sizeable", $Y_\nu \sim \mathcal{O}(1)$. After EWSB we have $\langle H^0_u\rangle = v\sin\beta$ ($v = 246$ GeV), which generates a three-point coupling between sleptons and the SM-like Higgs.

One may also note that in Type-III seesaw there is a non-flavour-diagonal coupling between charged sleptons and Higgs bosons, while there is no such coupling in the case of Type-I seesaw. As we discuss below, this leads to a stronger signal arising from Type-III than Type-I seesaw. We further notice that, while the usual D-terms of the scalar potential also contain large couplings between sneutrinos, charged sleptons and Higgs bosons, such couplings are always flavour-diagonal and cannot result in decays of the type $\tilde{\nu}_2 \to \tilde{\nu}_1 h$, which is our smoking gun signature for high scale seesaw models. For the non-diagonal coupling in the D-terms, they will not contribute to our Higgs production signature.

Besides the decay modes containing Higgs bosons, there are other decay channels and the visibility of the signal depends on the branching ratios. If the LSP is a higgsino-like neutralino and the gauginos are heavier than the sleptons, the decays of the left-handed sleptons arise from the superpotential term $y^\ell L H_d E^c$, so one gets the decays $\tilde{\nu} \to \tilde{\chi}^\pm \ell^\mp$ and $\tilde{\ell}^\pm \to \tilde{\chi}^0 \ell^\pm$. These lead to partial widths

$$\Gamma(\tilde{\nu}_j \to \ell_j^\pm \tilde{\chi}_i^\mp) = |y_{jj}^\ell|^2 |U_{i2}|^2 \frac{(m_{\tilde{\nu}}^2 - m_{\tilde{\chi}}^2)^2}{32\pi m_{\tilde{\nu}}^3}, \tag{6.9}$$

$$\Gamma(\tilde{\ell}_j^\pm \to \ell_j^\pm \tilde{\chi}_i^0) = |y_{jj}^\ell|^2 |N_{i3}|^2 \frac{(m_{\tilde{\ell}}^2 - m_{\tilde{\chi}}^2)^2}{16\pi m_{\tilde{\ell}}^3}, \tag{6.10}$$

where U_{i2} gives the higgsino component of the chargino (for our benchmarks $|U_{i2}| \simeq 1$), N_{i3} gives the down-type higgsino component of the neutralino (for our benchmarks $|N_{13}| \simeq 1/\sqrt{2}$). If the soft slepton masses are not flavour diagonal, an appropriate linear combination of the leptonic Yukawas corresponding to the flavour composition of the sleptons must be used.

If the LSP is a gaugino there are additional decay channels $\tilde{\nu} \to \nu\tilde{\chi}^0$ and $\tilde{\ell}^\pm \to \tilde{\chi}^\pm \nu$ (if winos are light) and the decay widths are propotional to g^2 instead of $|y^\ell|^2$ and gaugino components instead of higgsino components. Since we have the hierarchy $y_{11}^\ell \ll y_{22}^\ell \ll y_{33}^\ell \ll g$, the strength of our signal will depend on the nature of the light neutralinos and charginos and in the case of higgsinos, the flavour of the heavier sleptons. As the electron and muon Yukawas are so tiny, in practice the mixing between the gaugino and higgsino components will be significant for the overall decay widths of the sneutrinos and charged sleptons unless the gauginos are extremely heavy.

We shall concentrate on the higgsino case, since, as we shall see, the tau Yukawa coupling is already so large that it can produce a visible signal, which can practically arise only from selectrons or smuons with a higgsino-like LSP. The signal containing Higgs bosons will have a too small branching ratio if stau is the heavy slepton that decays. Hence in all our benchmarks we make our gauginos heavier than the sleptons.

6.3 The production and decay mechanisms

To study the high-scale seesaw signatures with Higgs bosons, we build some BPs with $m(\tilde{e}^{\pm}) < m(\tilde{\mu}^{\pm}) < m(\tilde{\tau}^{\pm})$ and mass splittings between generations larger than $m_h \approx 125$ GeV (the mass of the SM-like state h). As we shall see, this will be the limiting case, where we still can see a signal. If the second slepton (assuming the third one to be too heavy to be produced efficiently) would be a selectron, the signal would be similar (as the mixing with gauginos dominates the other decay modes already for smuons), while in the case of a stau, the signal would almost vanish due to the larger partial widths from eq. (6.9) and (6.10). We consider the charged current process $pp \to \tilde{\ell}_2^{\pm}\tilde{\nu}_2$, where the subscript indicates mass ordering. The charged current portal is more promising as the final state contains charged leptons even when the sneutrino decays invisibly.

As discussed above, in Type-III seesaw both sneutrinos and charged sleptons can decay to final states with Higgs bosons. The dominant process is $\tilde{\ell}_2 \to \tilde{\ell}_1 h$ while $\tilde{\nu}_2 \to \ell^{\pm}\tilde{\chi}_1^{\mp}, \nu\tilde{\chi}^0$. The Feynman diagram for such a process is shown in figure 6.1. There is also a process, where the Higgs originates from a sneutrino decay, but that has a smaller BR as can be seen from eq. (6.8). In Type-I seesaw, only the sneutrino can decay into a Higgs boson via $\tilde{\nu}_2 \to h\tilde{\nu}_1$. The corresponding Feynman diagram is shown in figure 6.2.

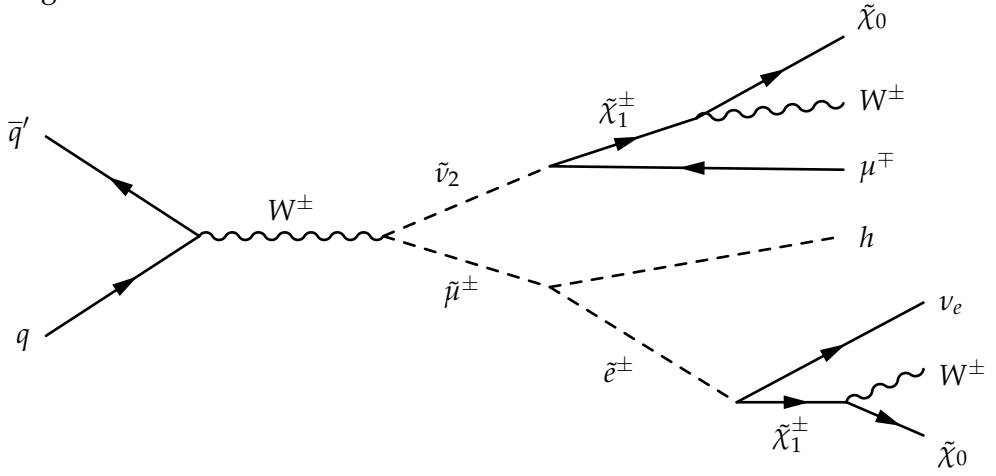

FIGURE 6.1: The dominant process for charged current slepton-sneutrino production and the subsequent decay involving a Higgs boson in Type-III seesaw. The W^+W^- pair of gauge bosons will decay into leptons and/or jets.

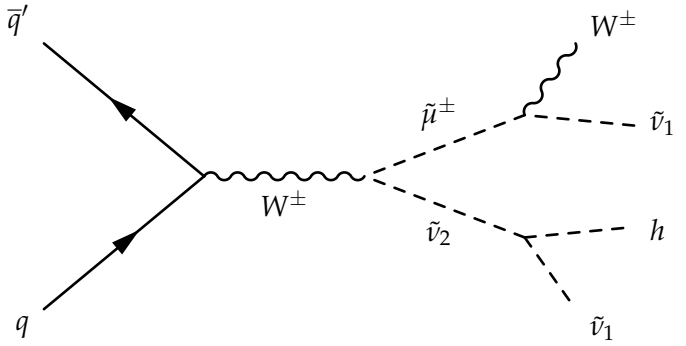

FIGURE 6.2: The dominant process for charged current slepton-sneutrino production and the subsequent decay involving a Higgs boson in Type-I seesaw. The $W^\pm$ boson will decay into leptons or jets.

These processes can lead to a variety of final state topologies. Currently the lower limit for charged slepton masses is around 700 GeV ($m(\tilde{e}^\pm), m(\tilde{\mu}^\pm)$), for neutralino masses below 350 GeV [139], which we take as our lower limit of charged slepton masses[1]. This means that the overall production rate of slepton-sneutrino pairs will be low, especially as we have to produce second generation sleptons with a large mass splitting compared to the first generation ones.

In fact, the production rate at the LHC even with nominal collision energy ($\sqrt{s} = 14$ TeV) is so low (~ 30 ab for 1 TeV sleptons), that there will not be sufficient statistics even at the High-Luminosity LHC (HL-LHC) [140]. Hence we turn to the proposed High-Energy LHC (HE-LHC) [56] with a nominal collision energy of $\sqrt{s} = 27$ TeV. This increases the production cross section by an order of magnitude compared to the standard LHC.

	Type-III	Type-I
$N(\ell) = 0$	2484	1842
$N(\ell) = 1$	2816	2940
$N(\ell) = 2$	794	1268
$N(\ell) \geq 3$	58	169

TABLE 6.1: Lepton number multiplicities for typical BPs in both seesaw models. The luminosity is 10 ab^{-1} and the energy is $\sqrt{s} = 27$ TeV.

In table 6.1 we show the lepton multiplicities for some typical benchmark points (BP1 and BP3, defined in table 6.2). We see that the single lepton final state has the highest events for both seesaw models. As we will lose a part of the signal due to different

[1] With more compressed spectra $m(\tilde{\ell}) - m(\tilde{\chi}^0) \lesssim 100$ GeV, one obviously can have significantly lighter sleptons. Such cases need a different analysis strategy than the one adopted here as we rely on large $\not{E}_T$ to suppress SM backgrounds.

BRs involved in the model, it is reasonable to look at the state with the highest events first. We also pick the Higgs decay mode to b-quarks as that has the highest BR and allows to reconstruct the Higgs boson, although not with a too high precision in mass. Unfortunately the channels with good mass resolution (*i.e.*, $\gamma\gamma$ and $ZZ^* \to 4$ leptons) are too rare to be useful with such a small event rate.

Our signal events will then consist of events with a single lepton, two b-tagged jets and missing momentum carried by the LSP. The largest SM backgrounds to this final state arise from the following processes:

- $t\bar{t}$ production where one the top (anti)quarks decays semileptonically and the other one hadronically;
- $W^{\pm}h$ production in the case where the $W^{\pm}$ boson decays into a lepton and a neutrino.

These have been considered to be the dominant backgrounds in similar types of experimental analyses (*e.g.*, [141]).

6.4 Simulation and results

In this section we will describe our numerical toolbox and the MC simulations that we have pursued with it.

6.4.1 Analysis strategy

The model files are produced by the Mathematica package SARAH v4.14 [116]. This code also generates a source code for SPHENO v4.0.4 [118; 119] to obtain the mass spectrum and couplings as well as for MADGRAPH5 v2.8.2 [120] to simulate collider events. We use PYTHIA v8.2 [121] for parton showering and hadronisation while we simulate the detector response by using DELPHES3 [122]. We simulate the analysis and present our numerical results with MADANALYSIS5 v1.8 [125].

We prepare two BPs for Type-III seesaw and two for Type-I seesaw, which can be detected in the HE-LHC with 27 TeV collision energy and the integrated luminosity 10 ab^{-1}. We simulate proton-proton collisions to produce the second generation sneutrino ($\tilde{\nu}_2$) and slepton ($\tilde{\ell}_2$), which in our cases are smuon-like, and select decays to the SM-like Higgs boson plus corresponding first generation particles. The mass of $\tilde{\nu}_2$ and $\tilde{\ell}_2$ should be heavy enough to allow for the decay kinematics. At the same time, the lower mass bound of the lightest slepton is required to be around 700 GeV [1]. The particle mass spectra and relevant BRs are shown in table 6.2.

	BP1	BP2	BP3	BP4
$m(\tilde{\mu})$ (GeV)	895.3	1001.9	885.5	993.2
$m(\tilde{e})$ (GeV)	701.9	834.0	692.9	993.2
$m(\tilde{\nu}_2)$ (GeV)	886.8	994.3	891.7	998.6
$m(\tilde{\nu}_1)$ (GeV)	692.8	826.2	697.5	830.2
BR$(\tilde{\ell}_2 \to \tilde{\ell}_1 + h)$	74.6%	63.1%	0%	0%
BR$(\tilde{\nu}_2 \to \tilde{\nu}_1 + h)$	12.2%	6.7%	30.9%	20.4%
LSP	410.4($\tilde{\chi}_0$)	410.4($\tilde{\chi}_0$)	410.4($\tilde{\chi}_0$)	410.4($\tilde{\chi}_0$)
NLSP	413.3 ($\tilde{\chi}_1^\pm$)	413.3($\tilde{\chi}_1^\pm$)	413.3 ($\tilde{\chi}_1^\pm$)	413.3 ($\tilde{\chi}_1^\pm$)

TABLE 6.2: Mass spectra and BRs of our BPs. BP1 and BP2 are for Type-III seesaw while BP3 and BP4 are for Type-I seesaw. For all of these benchmarks we have bino and wino-like neutralinos with masses of 1100 GeV and 2300 GeV, which leads to a gaugino component of about 0.3% for the LSP. The relevant neutrino Yukawas are in the range $0.3 < |y^\nu| < 0.5$ with $\sum_k y^\nu_{1k} y^\nu_{2k} \simeq 0.2$.

All of the BPs have the same LSP and Next-to-LSP (NLSP), which are higgsino-like neutralinos and charginos. BP1 has a mass spectrum similar to BP3 and the same situation arises between BP2 and BP4. However, there is a significant difference in the Higgs production cross section times BRs between Type-III seesaw and Type-I seesaw. For the sneutrino decay process, Type-I seesaw has BRs larger than the Type-III ones, which can be traced back to the factors in eq. (6.7) and (6.8). However, the charged slepton decay channel does not exist in Type-I seesaw whereas it dominates the Higgs signal in Type-III seesaw, consistent with eq. (6.7) and (6.8). As the slepton masses increase, the BR shows a decreasing trend.

The BR for $\tilde{\mu}^\pm \to \tilde{e}^\pm h$ is high in Type-III seesaw, since the competing decay mode of eq. (6.10) is proportional to the small muon Yukawa coupling squared or the small gaugino-higgsino mixing factor squared. Had the second slepton been a selectron, the BR would have been similar as the gaugino-higgsino mixing would dominate the

decays to neutralinos/charginos, while for staus the corresponding branching ratio is only a few percent as the tau Yukawa is large enough to dominate the branching ratio.

Number of leptons	$N(\ell) = 1$
Number of b-jets	$N(b) \geq 2$
Transverse momentum of electron	$p_T(e) > 5$ GeV
Transverse momentum of muon	$p_T(\mu) > 3$ GeV
Transverse momentum of jet	$p_T(j) > 17$ GeV
Absolute pseudorapidity of electron	$\|\eta(e)\| < 2.5$
Absolute pseudorapidity of muon	$\|\eta(\mu)\| < 2.4$
Absolute pseudorapidity of jet	$\|\eta(j)\| < 2.4$
Relative distance in (η, ϕ) between any two visible objects	$\Delta R \geq 0.5$

TABLE 6.3: The multiplicity requirements for our final state topology ($\ell = e$, μ), and the definitions of the various objects. Note that we allow for any number of non b-jets.

As a pre-selection, we require a single lepton and at least two b-jets, as shown in table. 6.3. We use a working point, where the b-jet tagger achieves 70% efficiency and only a 1.5% probability of misidentifying a light-parton jet as a b-one [142]. Then several cuts are imposed to select the Higgs signal as per the process in figure 6.1. The leading lepton is dominantly produced from the process $\tilde{\nu}_1 \to e + \tilde{\chi}_1^{\pm}$. As the mass difference between sneutrino and the lightest chargino is larger than 500 GeV for BP1 and 400 GeV for BP2, we choose the transverse momentum of the leading lepton to be larger than 400 GeV to preserve the single lepton signal and reduce the background, as shown in figure 6.3. The MET cut is chosen to be 500 GeV as the NLSP mass is around that value. In order handle properly the MC generation of the $t\bar{t}$ background, we add a cut at the generation level (MET above 300 GeV) so as to generate this SM process automatically in the signal region of interest. The Higgs selection is done by choosing the interval of invariant mass of the leading and next-to-leading b-jets from 100 GeV to 150 GeV. Figure 6.4 shows a peak around the SM-like Higgs mass for the signal and $W^{\pm}h$ background, while the $t\bar{t}$ noise is rather flat therein. Hence, this requirement proves effective against the latter. Finally, the 100 GeV cut on the transverse mass defined using the highest p_T lepton plus missing transverse momentum, $M_T(l_1, \not{E}_T)$, can also significantly reduce background, especially $t\bar{t}$, as evident from figure 6.5.

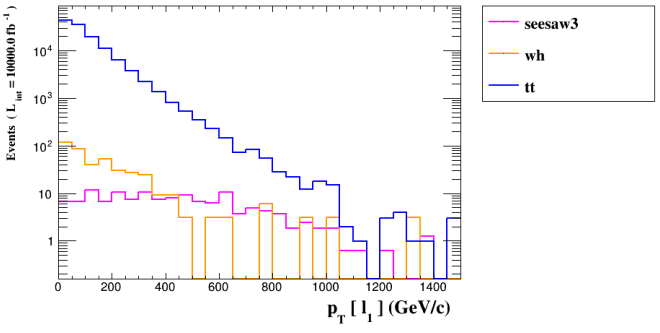

FIGURE 6.3: The distribution in transverse momentum of the leading lepton after the pre-selection (and generation-level) cuts.

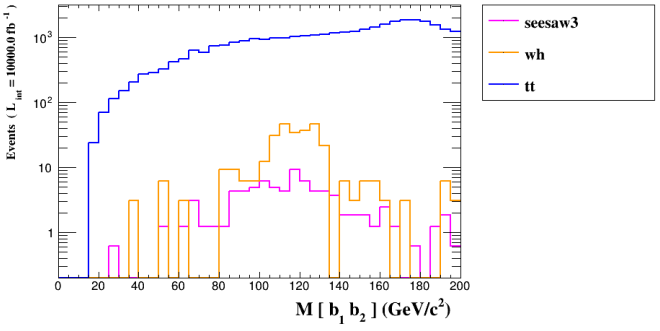

FIGURE 6.4: The distribution in invariant mass of the leading and next-to-leading *b*-jets after the pre-selection (and generation-level) cuts.

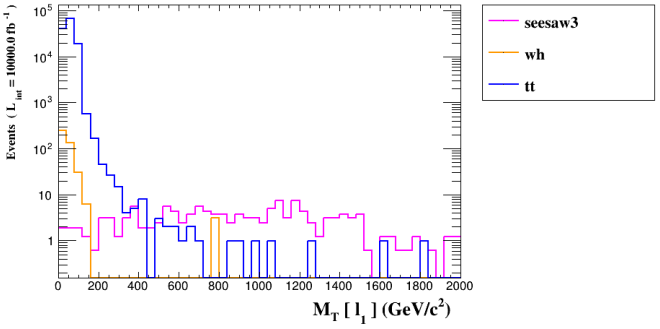

FIGURE 6.5: The distribution in transverse mass of leading lepton plus MET after the pre-selection (and generation-level) cuts.

6.4.2 Numerical analysis

We have applied the cuts of table 6.4 to all BPs as well as backgrounds and the results are presented in table 6.5, for the discussed HE-LHC energy and luminosity. As expected, Type-III seesaw preserves more signal events (25.8 for BP1 and 27.7 for BP2) than Type-I seesaw (15.5 for BP3 and 9.2 for BP4). Furthermore, BP2 and BP4 show the interesting feature of having fewer initial events (compared to BP1 and BP3,

Transverse momentum of leading lepton	$p_T(\ell_1) > 400$ GeV
Missing transverse energy	$\not{E}_T > 500$ GeV
Invariant mass of b_1, b_2	100 GeV $< M(b_1 b_2) <$ 150 GeV
Transverse mass of leading lepton and missing momentum	$M_T(\ell_1, \not{E}_T) > 100$ GeV

TABLE 6.4: The full set of cuts used in the MC analysis.

respectively) but displaying a similar final result. This is because the sneutrino and smuon in BP2(BP4) are heavier than those in BP1(BP3), leading to a larger MET and higher transverse momentum of the leading lepton ($p_T(\ell_1)$), thereby increasing the efficiency of the corresponding selections.

The significances are shown in table 6.6, for the usual HE-LHC parameters, wherein one can appreciate rather significant signal excesses above the SM backgrounds for Type-III seesaw while for Type-I seesaw the sensitivity is somewhat limited (but larger values of Yukawa couplings could be probed and there could be room to improve the analysis or increase the amount of data). We also tested a benchmark similar to BP1, but with the mass ordering $m(\tilde{e}) < m(\tilde{\tau}) < m(\tilde{\mu})$ with the smuon too heavy to be produced. This gave just 0.6 events after the cuts, so we can get a significant signal only arising from selectrons or smuons and their sneutrinos.

Cut	BP1	BP2	BP3	BP4	$W^{\pm}h$	$t\bar{t}$	Total background
Initial	6150	3650	6220	3660	9250000	2170000	11420000
$N(b) \geq 2$	1095	549	506	193	1585690	691090	2276780
$N(\ell) = 1$	482	255	238	90.4	835311	224927	1060238
$\not{E}_T > 500$ GeV	136.5	105.1	60.3	37.3	423	126239	126662
$M(b_1 b_2) > 100$ GeV	113.2	86.5	52.9	27.1	380	118569	118949
$M(b_1 b_2) < 150$ GeV	46.7	43.8	28.0	13.9	236	10706	10942
$p_T(\ell_1) > 400$ GeV	25.8	27.7	15.5	9.2	15.3	203	218
$M_T(\ell_1, \not{E}_T) > 100$ GeV	25.8	27.7	15.5	9.2	3.1	19.9	23.0

TABLE 6.5: The response of the signal BPs and backgrounds to the application of the full cutflow used in the MC analysis. The luminosity is 10 ab^{-1} and the energy is $\sqrt{s} = 27$ TeV.

	BP1	BP2	BP3	BP4
Significance	3.69σ	3.89σ	2.49σ	1.62σ

TABLE 6.6: Significance of the BPs for the HE-LHC parameters of table 6.5.

In addition it is essential for our analysis that there is a significant mass splitting between the sleptons and the LSP. With a softer MET cut the $t\bar{t}$ background would be problematic, while the cut on the transverse mass of the lepton and MET would keep $W^{\pm}h$ under control.

In summary, though, it is clear that the HE-LHC is a machine with clear potential to access high scale seesaw models (like Type-III and Type-I embedded within the MSSM) by exploiting the SM-like Higgs (eventually decaying to $b\bar{b}$) plus a hard lepton and MET signature.

6.5 Conclusions

How neutrino mass generation occurs in Nature is one of the outstanding questions in particle physics. Current probes of neutrinos hardly include colliders, as herein such particles appear as $\not{E}_T$, thereby offering no scope to identify their properties. However, in a supersymmetric world, there exist sneutrinos, which share with neutrinos their interactions. Therefore, given that sneutrinos can decay visibly at the LHC (*i.e.*, inside the detectors), it makes sense, in order to study neutrino properties in supersymmetry, to study sneutrinos. One, however, needs a paradigm for supersymmetry to do so, *i.e.*, a model realisation of it, which we assumed here to be the MSSM, supplemented with two kinds of seesaw mechanism for (s)neutrino mass generation, the so-called Type-I and Type-III. These mechanisms have a similar structure to generate neutrino masses and hence both lead to Higgs-sneutrino interactions, which are non-diagonal in flavour space.

These two are examples of high scale seesaw mechanisms, wherein the companion neutrinos (to the SM ones) can have masses of order $10^{12} - 10^{14}$ GeV. However, left-handed sneutrino and slepton masses are necessarily linked to the typical supersymmetry breaking scale, which ought to be 10 TeV or so at the most (in order to preserve gauge coupling unification, successful dynamical EWSB, etc.). In the case of a high seesaw scale the neutrino Yukawa couplings are among the largest ones in the model and, due to the structure of the supersymmetric scalar potential, they can lead

to observable consequences at the supersymmetry breaking scale. We found that the current LHC, for which $\sqrt{s} = 14$ TeV (in turn recalling that $\sqrt{\hat{s}}$ is only a fraction of that), cannot test such seesaw scenarios. However, a possible energy upgrade has been proposed for it: the so-called HE-LHC. This offers $\sqrt{s} = 27$ TeV (and $\int L\,dt = 10$ ab^{-1}), therefore, it is in a position to test the aforementioned seesaw scenarios of neutrino mass generation.

In this section, we have, in particular, tested the scope of a particular signal stemming from these two seesaw mechanisms. In fact, the signature is common to both, *i.e.*, charged current induced slepton-sneutrino production and subsequent decay into the SM-like Higgs boson (in turn decaying to $b\bar{b}$ pairs), a single lepton ($l = e, \mu$) and MET (or $\not{E}_T$). Upon assessing that the single lepton channel (as opposed to multi-lepton ones also stemming in these two scenarios) is the most sensitive one, for any number of b-jets beyond 1, we have devised a simple cut-and-count analysis, deployed identically for both Type-I and -III, that has enabled us to reach evidence to discovery significances at the HE-LHC for the Type-III case while for the Type-I case a more refined selection and/or additional data would be required. This was shown, in both cases, for BPs currently compliant with standard theoretical requirements as well as current experimental searches.

Parameterwise, the signature requires the gauginos to be heavier than the sleptons, a sufficient mass splitting ($\gtrsim 300$ GeV) between the sleptons and the higgsino-like LSP and a sufficient mass splitting between the slepton generations so that the decay with a Higgs boson is kinematically allowed.

Even though this signal is common to the two seesaw models, the fact that in Type-I seesaw only sneutrinos have decay modes containing Higgs bosons, while for Type-III also charged sleptons have such decay channels allows us to distinguish the models. This distinction might be more difficult at a hadron collider but, if there was an electron-positron collider with sufficient collision energy, the pair production of charged sleptons above $\sqrt{s} = 2m_{\tilde{\ell}}$ would lead to an enhanced signal with Higgs bosons in case of Type-III, while no such an enhancement would be present in Type-I.

As an outlook of our work, we would like to highlight that the FCC-hh [143], running at $\sqrt{s}$ values up to 100 TeV, will not improve the scope of the HE-LHC since, herein, background rates increase more that the signal ones that we pursued (although this may not be true for other channels not considered here).

Altogether, we have shown that there exist cases where, in supersymmetric theories, it is possible to probe the neutrino mass generation mechanism through sneutrino physics while the (seesaw) scale related to this mechanism is extremely high, roughly, up to 10^{14} GeV.

Chapter 7

CP-violation effects in the BLSSM with inverse seesaw

7.1 Introduction

The non-zero mass of the neutrino has been observed by several experiments, which is a firm hint for BSM physics. Neutrinos are assumed to be massless in the SM for two reasons. First, there are no RH neutrinos to couple as Dirac fermions. Second, the SM strictly conserves the Baryon minus Lepton ($B-L$) number. To address this, the SM can be extended by a new $B-L$ symmetry, allowing for the detection of the Majorana nature of neutrinos. The $B-L$ extended model leads to new testable signals, including a neutral gauge boson Z' and a new Higgs state that breaks the $U(1)_{B-L}$ gauge group.

As mentioned repeatedly, a seesaw mechanism provides an elegant explanation for neutrino masses. In the canonical seesaw mechanism, such as Type-I seesaw, RH neutrinos acquire mass at the $B-L$ symmetry breaking scale (TeV or so), which is around the SUSY breaking scale. Consequently, the Yukawa coupling is constrained to be an order of magnitude smaller than 10^{-6}. The inverse seesaw mechanism can alleviate constraints on the Yukawa coupling, making it more feasible to be tested at the LHC. By introducing two SM gauge singlet fermions, the light neutrino obtains its

mass when one of the two singlets interacts with the RH neutrino. The other singlet can serve as a DM candidate.

The origin of CP violation in the BLSSM arises from the neutrino mass generation mechanism. There are two sets of superpotential couplings required to generate neutrino masses. Either of them can be complex, resulting in CP violation in the leptonic sector. If the neutrino dynamics further includes CP-violation, the latter may eventually manifest itself in specific kinematical observables, which appears as a difference in the angular distributions of multi-body decay processes of a particle and corresponding antiparticle. The TPAs are proportional to the scalar triple product of the generic form:

$$\text{TPA} = \vec{v}_1 \cdot (\vec{v}_2 \times \vec{v}_3), \tag{7.1}$$

where the vector $\vec{v}_i$ are the three-momenta of final state particles. TPAs are generally T-odd observables and those that can violate CP symmetry are known as 'true' TPAs. TPAs can serve as an indicator of CP-violating new physics with a relatively clean background from the SM (only onset by CKM effects), which can lead to a deeper understanding of the CP-properties of any new interaction [144].

In this chapter, we plan to discuss TPAs in the SUSY version of $B-L$ extended model combined with inverse seesaw mechanism, known as the BLSSMIS. The structure of this chapter is as follows. The BLSSMIS model is described in Section 2. This is followed by a discussion about signal and background rates at the FCC-hh. Current progress and future work will be presented, finally.

7.2 Model description

The BLSSMIS extends the MSSM by adding three parts. The first part contains two SM singlet chiral Higgs superfield χ_1 and χ_2 with $B-L$ charge equal to $+1$ and -1, respectively. When the scalar components of the superfields χ_1 and χ_2 get their VEVs, they break the $U(1)_{B-L}$ symmetry spontaneously. The second part includes three SM singlet chiral superfields: N_i $(i = 1, 2, 3)$ with $B-L$ charge equal to -1. They are used

to cancel the $U(1)_{B-L}$ anomaly and the fermionic component of N_i is considered as a RH neutrino. The third part consists of two chiral SM singlet superfield S_1 and S_2 with $B-L$ charge equal to $+2$ and -2, respectively, in order to implement the inverse seesaw mechanism [145; 97]. The superpotential of the leptonic sector is

$$W = Y_E L H_1 E^c + Y_\nu L H_2 N^c + Y_S N^c \chi_1 S_2 + \mu H_1 H_2 + \mu' \chi_1 \chi_2. \tag{7.2}$$

When the EW symmetry and $B-L$ symmetry break, the Higgs fields and the χ_i ($i = 1, 2$) get a VEV. The neutrino interaction is as follows

$$\mathcal{L} = m_D \bar{\nu}_L N^c + M_N \bar{N}^c S_2, \tag{7.3}$$

where $m_D = Y_\nu v \sin\beta$ and $M_N = Y_S v' \sin\theta$, with $\tan\beta = \frac{v_2}{v_1} = \frac{\langle H_2 \rangle}{\langle H_1 \rangle}$ and $\tan\theta = \frac{v_1'}{v_2'} = \frac{\langle \chi_1 \rangle}{\langle \chi_2 \rangle}$. Specifically, $v^2 = v_1^2 + v_2^2$ and $v'^2 = v_1'^2 + v_2'^2$. The LH neutrino masses are related to a small mass term $\mu_S \bar{S}_2^c S_2 S_2$, with $\mu_S \approx \mathcal{O}(1)$ keV, which can emerge at the $B-L$ scale from the non-renormalizable term in the superpotential $\frac{\chi_1^4 S_2^2}{M_1^3}$, with M_1 an intermediate scale of the order $\mathcal{O}(10^7)$ GeV [145]. The 3×3 neutrino mass matrix of one generation has the following form (in the basis (ν_L, N^c, S_2)):

$$M_\nu = \begin{pmatrix} 0 & m_D & 0 \\ m_D & 0 & M_N \\ 0 & M_N & \mu_S \end{pmatrix}. \tag{7.4}$$

one finds the physical light and heavy neutrino masses are

$$m_{\nu_L} = \frac{m_D^2 \mu_S}{M_N^2 + m_D^2} \tag{7.5}$$

and

$$m_{\nu_{H,H'}} = \sqrt{M_N^2 + m_D^2}, \tag{7.6}$$

respectively.

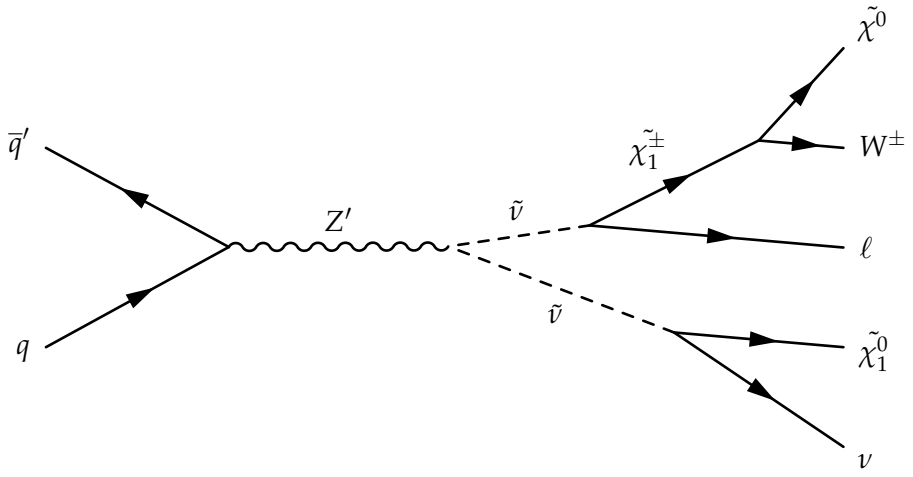

FIGURE 7.1: The process for sneutrino-sneutrino production and corresponding decay. The $W^{\pm}$ boson will decay into jets.

7.3 Simulation and results

The model files are produced by the Mathematica package SARAH v4.14 [116]. This code also generates a source code for SPHENO v4.0.4 [118; 119] to obtain the mass spectrum and couplings for MADGRAPH5 v2.8.2 [120] to simulate collider events. We use PYTHIA v8.2 [121] for parton showering and hadronisation while we simulate the detector response by using DELPHES3 [122]. We carry out the MC analysis and present our numerical results using ROOT [146].

We prepare our BPs so that they can be detected at the FCC-hh [147] with 100 TeV collision energy and integrated luminosity 3000 fb^{-1}. The Delphes card in the FCC-hh is redesigned to satisfy higher PU and enhance the tagging efficiencies. We consider the process $pp \to Z' \to \tilde{\nu}\tilde{\nu}$. One of the sneutrino decays into the lightest chargino plus lepton, then this chargino cascades into the lightest neutralino and $W^{\pm}$ boson, leading to a di-jet final state. The other sneutrino decays to neutrino plus neutralino. As a result, we get a 'di-jet + di-lepton + MET' signal (hereafter, $j_{1(2)}$) refers to the highest(lowest) p_T jet). The Feynman diagram of such a process is shown in figure 7.1, which we will then use to define T-odd observables, so as to test the TPA scope in extracting CP-violation effects. The major SM background here arises from the process: $pp \to W^{\pm} + jj$, where the $W^{\pm}$ boson decays into lepton and neutrino.

MET	$\not{E}_T > 300$ GeV
Transverse momentum of all jets	$p_T(j_{1,2}) > 100$ GeV
Transverse momentum of second leading jet j_2	$p_T(j_2) > 200$ GeV
Relative distance in (η, ϕ) between j_2 and l (either lepton)	$\Delta R \leq 1.5$

TABLE 7.1: The full set of cuts used in our MC analysis.

$T_{\not{E}_T l j_2}$	N_s	$\epsilon_s = \frac{N_s}{N}$	N_b	$\epsilon_b = \frac{N_b}{N}$	$S = \sigma_s \cdot \epsilon_s \cdot \mathcal{L}$	$S = \sigma_b \cdot \epsilon_b \cdot \mathcal{L}$	$\frac{S}{\sqrt{S+B}}$
$\lvert T_{\not{E}_T l j_2}\rvert > 0.001$	204500	0.409	840	0.0042	6418.64	2.26e+07	1.167
$\lvert T_{\not{E}_T l j_2}\rvert > 0.01$	148000	0.296	460	0.0023	4632.93	1.25e+07	1.272
$\lvert T_{\not{E}_T l j_2}\rvert > 0.05$	72000	0.144	120	0.0006	2261.93	3.16e+06	1.310
$\lvert T_{\not{E}_T l j_2}\rvert > 0.1$	43500	0.087	40	0.0002	1362.26	1.36e+06	1.349

TABLE 7.2: The $T_{\not{E}_T l j_2}$ dependent rates for signal and background following the cuts described in the text.

Despite the TPAs are formally non-zero for the CP-violating signal and strictly zero for the background (aside from tiny CKM driven effects) and since their measurement is subject to both statistical and systematic errors, we ought to minimize as much as possible the size of the background, to avoid it contaminating the signal region in the various T-odd observables. Several cuts are thus imposed. We have listed the full set of these in table 7.1. Now, it can be seen that the $\not{E}_T$ distribution of the signal differs from that of the $W^\pm + jj$ background, as per figure 7.2[1]. In order to suppress the background, we have finally chosen events with $\not{E}_T$ larger than 300 GeV. Furthermore, based on the distribution of jet transverse momentum in figure 7.3 and figure 7.4, we filter the signal and background requiring $p_T(j_{1,2}) > 100$ GeV and $p_T(j_2) > 200$ GeV. The distribution of relative distance in (η, ϕ) between j_2 and either lepton l is shown in figure 7.5. There is a different trend in the lower range between signal and background, thus we select only events with $\Delta R \leq 1.5$.

Amongst the various TPA distributions that one can construct with the selected final state, there is one allowing for a good discrimination between signal and background, which is $T_{\not{E}_T l^- j_2}$, for the, e.g., negatively charged lepton. Therefore, we exploit this distribution first to attempt extracting our CP-violating signal. By attempting various cuts away from the CP-conserving limit (i.e., $T_{\not{E}_T l^- j_2} = 0$), we extract several significances for our signal, as given in table 7.2.

[1] To effectively manage the MC generation of the background, we have implemented a generation-level cut ($\not{E}_T$ above 200 GeV) for the $W^\pm$ boson: this has allowed us to automatically generate this SM process within the desired signal region of interest.

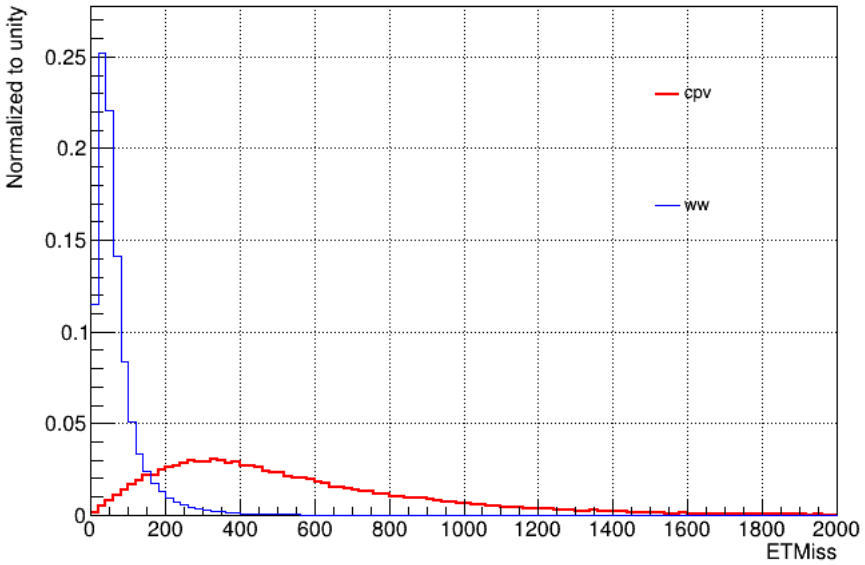

FIGURE 7.2: The distribution of the missing transverse energy for the CP-violating events and the background. Here we have normalized the distributions to unity.

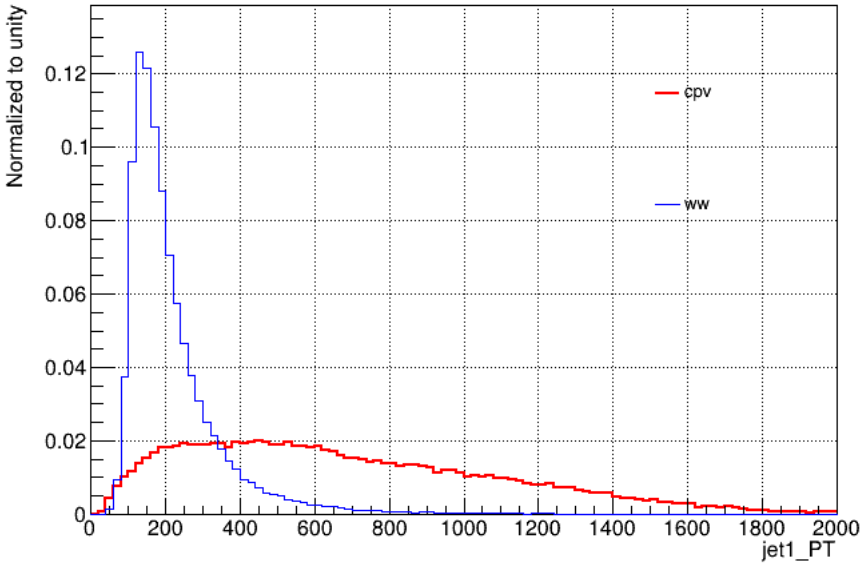

FIGURE 7.3: The distribution of the transverse momentum of the leading jet j_1 for the CP-violating events and the background. Here we have normalized the distributions to unity.

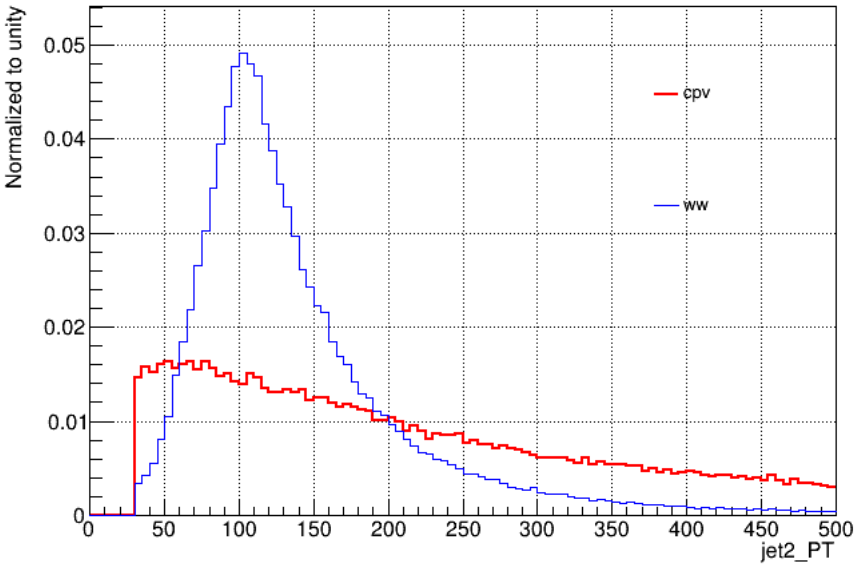

FIGURE 7.4: The distribution of the transverse momentum of second leading jet j_2 for the CP-violating events and the background. Here we have normalized the distributions to unity.

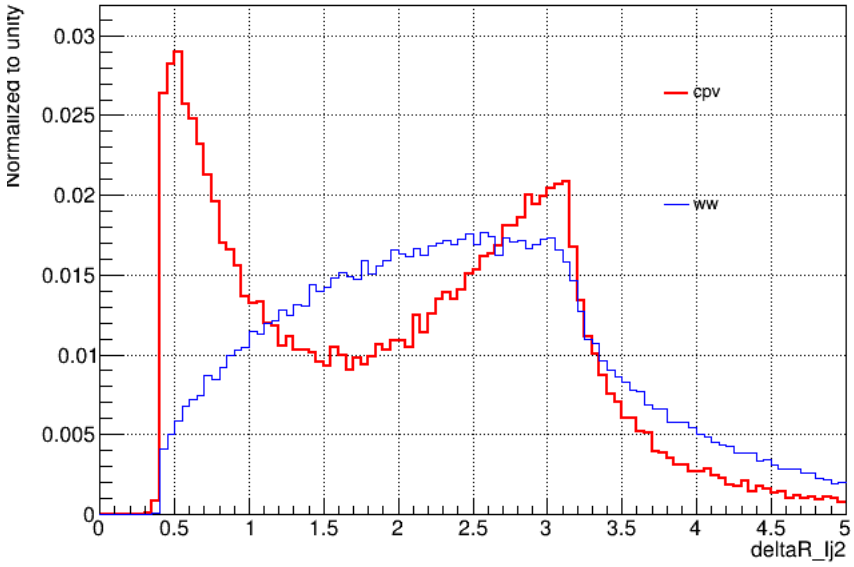

FIGURE 7.5: The distribution of the relative distance in (η, ϕ) between j_2 (the second leading jet) and l (the lepton). Here we have normalised the distributions to unity.

$T_{\not{E}_T J_1 J_2}$	N_s	$\epsilon_s = \frac{N_s}{N}$	N_b	$\epsilon_b = \frac{N_b}{N}$	$S = \sigma_s \cdot \epsilon_s \cdot \mathcal{L}$	$S = \sigma_b \cdot \epsilon_b \cdot \mathcal{L}$	$\frac{S}{\sqrt{S+B}}$
$\lvert T_{\not{E}_T j_1 j_2}\rvert > 0.001$	79600	0.398	1950	0.0039	6236.60	2.11e+07	1.321
$\lvert T_{\not{E}_T j_1 j_2}\rvert > 0.01$	148000	0.377	1750	0.0035	5905.39	1.90e+07	1.328
$\lvert T_{\not{E}_T j_1 j_2}\rvert > 0.05$	62200	0.311	1250	0.0025	4881.5	1.35e+07	1.358
$\lvert T_{\not{E}_T j_1 j_2}\rvert > 0.1$	52000	0.260	850	0.0017	4079.4	9.53e+06	1.361

TABLE 7.3: The $T_{\not{E}_T j_1 j_2}$ dependent rates for signal and background following the cuts described in the text plus the additional cut condition $p_T(j_1) > 300$ GeV.

As the significances are not very large, we attempt next another selection, based on another TPA distribution: $T_{\not{E}_T j_1 j_2}$. In table 7.3, we also exploit an additional cut, $p_T(j_1) > 300$ GeV, which yields slightly better results in comparison, yet, still not enough to claim significant sensitivity.

Therefore, our ongoing work is focusing on identifying new BPs to increase both the cross section of the signal and its significance, possibly following the implementation of a more efficient set of cuts to suppress the SM background further.

Chapter 8

Conclusions

In this thesis, we have introduced the SM and the motivations to extend it with some BSM physics. In particular, we have concentrated on SUSY models combined with high scale seesaw mechanisms which can be tested at future colliders, both hadronic and leptonic. In fact, this was the core content of this thesis. To set the stage from the phenomenological point of view, we have then introduced the LHC and ILC, including the detector prototypes that we have used in our MC analyses (CMS and ILD, respectively).

The actual realisations of SUSY combined with a seesaw mechanism that we have tackled in this thesis have been as follows. First, we have studied the NMSSMr with a RH sneutrino as DM candidate within a Type-I seesaw scenario at the ILC, through a process which allowed us to estimate the relevant Yukawa couplings. We have then introduced a method to access Higgs-slepton couplings in the minimnal SUSY setup (MSSM) in presence of the Type-I and Type-III seesaw mechanisms, both realised at high scales, at the HE-LHC. Presently, we are studying CP-violation effects in the BLSSMIS through TPAs at the FCC-hh and a paper will be oit soon.

We have demonstrated that, in the NMSSMr, the RH neutrino can be the LSP which is a candidate of DM. In this scenario, the higgsinos can be produced at the LHC and ILC at the EW scale. Although the LSP is prohibited to decay, the charged higgsino has a small chance of decaying into a charged lepton plus the RH sneutrino. This

decay is determined by the tiny neutrino Yukawa couplings. From Chapter 5, it can be seen that the neutral higgsino can decay via $\tilde{\chi}^0 \to N\tilde{N}$ when the RH neutrino is light enough. This gives us a window to find the rare two-body decay of the chargino, $\tilde{\chi}^- \to l^-\tilde{N}$, leading us to estimate the scale of neutrino Yukawa coupling. However, the measurement will be statistically limited and give at best an accuracy of 25%, even with the ILC luminosity upgrade. Even this limited accuracy should be enough, though, to test the consistency of the seesaw model, i.e., that the neutrino masses are generated by a Type-I seesaw and not by some more extended seesaw model like the inverse or linear ones. Clearly, the requirement introduced by the CM energy of the ILC being fixed at discrete values all below the TeV scale, as opposed to the LHC case where, at the partonic level, $\sqrt{\hat{s}}$ can be well beyond it, limits the region of the NMSSMr space that can be accessed. However, we can confirm that this is continuous and finite, from which we have then drawn representative BPs that can be used for experimental analysis at such a future e^+e^- linear machine.

We have then discussed the MSSM with a Type-I and Type-III seesaw at high scale. A signal generated by the two seesaw mechanism above has been then tested: charged current induced slepton-sneutrino production and cascade decay into the SM-like Higgs boson, a single lepton and MET. Compared to a multi-lepton channel, the single lepton channel is more sensitive when the number of b-jet is larger than one. This signal is common to both the Type-I and Type-III seesaw mechanism. In the Type-I case, only the sneutrino can decay into the Higgs boson whereas in the Type-III case the charged slepton also has such a decay channel, enabling us to distinguish between the two seesaw models. Conducting an identical cut-and-count analysis for both seesaw cases has allowed us to obtain evidence to observe the Type-III seesaw mechanism at the HE-LHC while the Type-I case may need more data or a more efficient selection. This signal can be enhanced at a future electron-positron collider with sufficient collision energy. In contrast, the FCC-hh will not be able to improve the significance, as the background rate increases more than the signal.

The last part of the thesis was devoted to study the BLSSMIS, this time with neutralino DM, at a future collider, specifically, the FCC-hh, in presence of (explicit)

CP-violation in the Yukawa sector. The signature we pursued was that of sneutrino pair production via a Z' portal, yielding (via light chargino decays) a 'di-jet + di-lepton + $\not{E}_T$', of which we studied T-odd observables, which are naturally zero in the absence of CP-violation, hence, typically so for the SM (apart from tiny CKM effects). The ensuing TPAs can serve as an efficient way to detect such CP-violation in the BLSSMIS, despite it manifests itself at high scales. Based on our current results, the cross sections of the signal is not very large to enable to fully exploit the powerof the TPAs, altogether making it difficult to distinguish the signal from the SM background, which leaks into the signal regions because of experimental uncertainties (both statistical and systematic) in the measurement of the T-odd observables. Thus, ultimately, we cannot presently establish the CP-violating signal presence with enough significance. However, the analysis is still ongoing and we are confident that new BPs will be found, enabling us to establish FCC-hh sensitivity to the CP-violating BLSSMIS, possibly also exploiting a more efficient set of cuts.

References

[1] R. L. Workman and Others. Review of Particle Physics. *PTEP*, 2022:083C01, 2022.

[2] Yi Liu, Stefano Moretti, and Harri Waltari. Measuring neutrino dynamics in nmssm with a right-handed sneutrino lsp at the ilc. *Journal of High Energy Physics*, 2022(1):1–17, 2022.

[3] Yi Liu, Stefano Moretti, and Harri Waltari. Exploring high scale seesaw models through a supersymmetric portal. *arXiv preprint arXiv:2307.05550*, 2023.

[4] Michael Peskin. *An introduction to quantum field theory*. CRC press, 2018.

[5] Matthew D Schwartz. *Quantum field theory and the standard model*. Cambridge university press, 2014.

[6] Steven Weinberg. *The quantum theory of fields*, volume 2. Cambridge university press, 1995.

[7] Lewis H Ryder. *Quantum field theory*. Cambridge university press, 1996.

[8] Anthony Zee. *Quantum field theory in a nutshell*, volume 7. Princeton university press, 2010.

[9] Tom Lancaster and Stephen J Blundell. *Quantum field theory for the gifted amateur*. OUP Oxford, 2014.

[10] François Englert and Robert Brout. Broken symmetry and the mass of gauge vector mesons. *Physical Review Letters*, 13(9):321, 1964.

[11] Peter Ware Higgs. Broken symmetries, massless particles and gauge fields. *Phys. Lett.*, 12:132–133, 1964.

[12] Peter W Higgs. Broken symmetries and the masses of gauge bosons. *Physical Review Letters*, 13(16):508, 1964.

[13] John Archibald Wheeler and Kenneth Ford. Geons, black holes and quantum foam: a life in physics, 2000.

[14] Yuval Grossman. Tasi 2002 lectures on neutrinos. *arXiv preprint hep-ph/0305245*, 2003.

[15] Kamiokande Collaboration et al. Evidence for oscillation of atmospheric neutrinos. *arXiv preprint hep-ex/9807003*, 1998.

[16] A Aguilar, LB Auerbach, RL Burman, DO Caldwell, ED Church, AK Cochran, JB Donahue, A Fazely, GT Garvey, RM Gunasingha, et al. Evidence for neutrino oscillations from the observation of electron anti-neutrinos in a muon anti-neutrino beam. *arXiv preprint hep-ex/0104049*, 2001.

[17] MH Ahn, S Aoki, H Bhang, S Boyd, D Casper, JH Choi, S Fukuda, Y Fukuda, W Gajewski, T Hara, et al. Indications of neutrino oscillation in a 250 km long-baseline experiment. *Physical Review Letters*, 90(4):041801, 2003.

[18] K Abe, N Abgrall, Y Ajima, H Aihara, JB Albert, C Andreopoulos, B Andrieu, S Aoki, O Araoka, J Argyriades, et al. Indication of electron neutrino appearance from an accelerator-produced off-axis muon neutrino beam. *Physical Review Letters*, 107(4):041801, 2011.

[19] Mark G Aartsen, M Ackermann, J Adams, JA Aguilar, M Ahlers, M Ahrens, D Altmann, K Andeen, T Anderson, I Ansseau, et al. The icecube neutrino observatory: instrumentation and online systems. *Journal of Instrumentation*, 12(03):P03012, 2017.

[20] Babak Abi, Roberto Acciarri, Mario A Acero, Giorge Adamov, David Adams, Marco Adinolfi, Zubayer Ahmad, Jhanzeb Ahmed, Tyler Alion, S Alonso Monsalve, et al. Deep underground neutrino experiment (dune), far detector

technical design report, volume ii: Dune physics. *arXiv preprint arXiv:2002.03005*, 2020.

[21] Ke Abe, Ke Abe, H Aihara, A Aimi, R Akutsu, C Andreopoulos, I Anghel, LHV Anthony, M Antonova, Y Ashida, et al. Hyper-kamiokande design report. *arXiv preprint arXiv:1805.04163*, 2018.

[22] Katherine Garrett and Gintaras Duda. Dark matter: A primer. *Advances in Astronomy*, 2011:1–22, 2011.

[23] Gerard Jungman, Marc Kamionkowski, and Kim Griest. Supersymmetric dark matter. *Physics Reports*, 267(5-6):195–373, 1996.

[24] Manuel Drees. Dark matter theory. *arXiv preprint arXiv:1811.06406*, 2018.

[25] Glennys R Farrar and ME Shaposhnikov. Baryon asymmetry of the universe in the minimal standard model. *Physical Review Letters*, 70(19):2833, 1993.

[26] A. D. Sakharov. Violation of CP Invariance, C asymmetry, and baryon asymmetry of the universe. *Pisma Zh. Eksp. Teor. Fiz.*, 5:32–35, 1967.

[27] Andrei D Sakharov. Violation of cp-invariance, c-asymmetry, and baryon asymmetry of the universe. In *In The Intermissions... Collected Works on Research into the Essentials of Theoretical Physics in Russian Federal Nuclear Center, Arzamas-16*, pages 84–87. World Scientific, 1998.

[28] Chien-Shiung Wu, Ernest Ambler, Raymond W Hayward, Dale D Hoppes, and Ralph Percy Hudson. Experimental test of parity conservation in beta decay. *Physical review*, 105(4):1413, 1957.

[29] James H Christenson, Jeremiah W Cronin, Val L Fitch, and René Turlay. Evidence for the 2 π decay of the k 2 0 meson. *Physical Review Letters*, 13(4):138, 1964.

[30] Nicola Cabibbo. Unitary symmetry and leptonic decays. *Physical Review Letters*, 10(12):531, 1963.

[31] Makoto Kobayashi and Toshihide Maskawa. Cp-violation in the renormalizable theory of weak interaction. *Progress of theoretical physics*, 49(2):652–657, 1973.

[32] Antonio Riotto and Mark Trodden. Recent progress in baryogenesis. *Annual Review of Nuclear and Particle Science*, 49(1):35–75, 1999.

[33] Lisa Randall and Raman Sundrum. Large mass hierarchy from a small extra dimension. *Physical Review Letters*, 83(17):3370, 1999.

[34] Thomas Blum, Achim Denig, Ivan Logashenko, Eduardo de Rafael, B Lee Roberts, Thomas Teubner, and Graziano Venanzoni. The muon (g-2) theory value: present and future. *arXiv preprint arXiv:1311.2198*, 2013.

[35] Tatsumi Aoyama, Nils Asmussen, Maurice Benayoun, Johan Bijnens, T Blum, M Bruno, I Caprini, CM Carloni Calame, M Cè, Gilberto Colangelo, et al. The anomalous magnetic moment of the muon in the standard model. *Physics reports*, 887:1–166, 2020.

[36] Babak Abi, T Albahri, S Al-Kilani, D Allspach, LP Alonzi, A Anastasi, A Anisenkov, F Azfar, K Badgley, S Baeßler, et al. Measurement of the positive muon anomalous magnetic moment to 0.46 ppm. *Physical Review Letters*, 126(14):141801, 2021.

[37] Stephen P Martin. A supersymmetry primer. In *Perspectives on supersymmetry*, pages 1–98. World Scientific, 1998.

[38] Gerard Jungman, Marc Kamionkowski, and Kim Griest. Supersymmetric dark matter. *Physics Reports*, 267(5-6):195–373, 1996.

[39] Steven Weinberg. Baryon-and lepton-nonconserving processes. *Physical Review Letters*, 43(21):1566, 1979.

[40] Peter Minkowski. $\mu \to e\gamma$ at a rate of one out of 109 muon decays? *Physics Letters B*, 67(4):421–428, 1977.

[41] W Konetschny and W Kummer. Nonconservation of total lepton number with scalar bosons. *Physics Letters B*, 70(4):433–435, 1977.

[42] Rabindra N Mohapatra and Goran Senjanović. Neutrino mass and spontaneous parity nonconservation. *Physical Review Letters*, 44(14):912, 1980.

[43] M Magg and Ch Wetterich. Neutrino mass problem and gauge hierarchy. *Phys. Lett. B*, 94(CERN-TH-2829):61–64, 1980.

[44] J Schechter and José WF Valle. Neutrino masses in su (2) u (1) theories. *Physical Review D*, 22(9):2227, 1980.

[45] Robert Foot, H Lew, X G He, and Girish C Joshi. See-saw neutrino masses induced by a triplet of leptons. *Zeitschrift für Physik C Particles and Fields*, 44:441–444, 1989.

[46] T Yanagida and Japan Tsukuba. Rn mohapatra and g. senjanovic. *Phys. Rev. Lett*, 44:912, 1980.

[47] Murray Gell-Mann, Pierre Ramond, and Richard Slansky. Complex spinors and unified theories. Technical report, 2013.

[48] TP Cheng and Ling-Fong Li. Neutrino masses, mixings, and oscillations in su (2)$\times$ u (1) models of electroweak interactions. *Physical Review D*, 22(11):2860, 1980.

[49] George Lazarides, Q Shafi, and Ch Wetterich. Proton lifetime and fermion masses in an so (10) model. *Nuclear Physics B*, 181(2):287–300, 1981.

[50] G't Hooft. Naturalness, chiral symmetry, and spontaneous chiral symmetry breaking. In *Recent developments in gauge theories*, pages 135–157. Springer, 1980.

[51] Carlo Giunti and Chung W Kim. *Fundamentals of neutrino physics and astrophysics*. Oxford university press, 2007.

[52] Takehiko Asaka, Koji Ishiwata, and Takeo Moroi. Right-handed sneutrino as cold dark matter. *Physical Review D*, 73(5):051301, 2006.

[53] David G Cerdeno, Carlos Munoz, and Osamu Seto. Right-handed sneutrino as thermal dark matter. *Physical Review D*, 79(2):023510, 2009.

[54] David G Cerdeno and Osamu Seto. Right-handed sneutrino dark matter in the nmssm. *Journal of Cosmology and Astroparticle Physics*, 2009(08):032, 2009.

[55] Ulrich Ellwanger, Cyril Hugonie, and Ana M Teixeira. The next-to-minimal supersymmetric standard model. *Physics Reports*, 496(1-2):1–77, 2010.

[56] Asmaa Abada, Marcello Abbrescia, Shehu S AbdusSalam, I Abdyukhanov, Jose Abelleira Fernandez, A Abramov, M Aburaia, AO Acar, PR Adzic, P Agrawal, et al. He-lhc: the high-energy large hadron collider: future circular collider conceptual design report volume 4. *The European Physical Journal Special Topics*, 228:1109–1382, 2019.

[57] Frank Zimmermann. He-lhc overview, parameters and challenges. *ICFA Beam Dyn. Newsl.*, 72:138–141, 2017.

[58] S Khalil and S Moretti. The b- l supersymmetric standard model with inverse seesaw at the large hadron collider. *Reports on Progress in Physics*, 80(3):036201, 2017.

[59] Anthony Zee. *Group theory in a nutshell for physicists*, volume 17. Princeton University Press, 2016.

[60] Steven Weinberg. Mixing angle in renormalizable theories of weak and electromagnetic interactions. *Physical Review D*, 5(8):1962, 1972.

[61] K Abe, N Abgrall, H Aihara, Y Ajima, JB Albert, D Allan, P-A Amaudruz, C Andreopoulos, B Andrieu, MD Anerella, et al. The t2k experiment. *Nuclear Instruments and Methods in Physics Research Section A: Accelerators, Spectrometers, Detectors and Associated Equipment*, 659(1):106–135, 2011.

[62] Rudolf Haag, Jan T Łopuszański, and Martin Sohnius. All possible generators of supersymmetries of the s-matrix. *Nuclear Physics B*, 88(2):257–274, 1975.

[63] Sidney Coleman and Jeffrey Mandula. All possible symmetries of the s matrix. *Physical Review*, 159(5):1251, 1967.

[64] Edward Witten. Dynamical breaking of supersymmetry. *Nuclear Physics B*, 188(3):513–554, 1981.

[65] Savas Dimopoulos and Howard Georgi. Softly broken supersymmetry and su (5). *Nuclear Physics B*, 193(1):150–162, 1981.

[66] N Sakai. Naturalnes in supersymmetric guts. *Zeitschrift für Physik C Particles and Fields*, 11:153–157, 1981.

[67] Leonard Susskind. The gauge hierarchy problem, technicolor, supersymmetry, and all that. *Physics Reports*, 104(2-4):181–193, 1984.

[68] Jihn E Kim and Hans Peter Nilles. The μ-problem and the strong cp-problem. *Physics Letters B*, 138(1-3):150–154, 1984.

[69] Gian F Giudice and Antonio Masiero. A natural solution to the μ-problem in supergravity theories. *Physics Letters B*, 206(3):480–484, 1988.

[70] I Jack and DRT Jones. Non-standard soft supersymmetry breaking. *Physics Letters B*, 457(1-3):101–108, 1999.

[71] Howard E Haber and Gordon L Kane. The search for supersymmetry: probing physics beyond the standard model. *Physics Reports*, 117(2-4):75–263, 1985.

[72] John F Gunion and Howard E Haber. Higgs bosons in supersymmetric models (i). *Nuclear Physics B*, 272(1):1–76, 1986.

[73] Lyndon Evans and Philip Bryant. Lhc machine. *Journal of instrumentation*, 3(08):S08001, 2008.

[74] A Jeff, A Boccardi, E Bravin, AS Fisher, T Lefevre, A Rabiller, F Roncarolo, and CP Welsch. First results of the lhc longitudinal density monitor. *Nuclear Instruments and Methods in Physics Research Section A: Accelerators, Spectrometers, Detectors and Associated Equipment*, 659(1):549–556, 2011.

[75] R Bruce, RW Assmann, V Boccone, G Bregliozzi, H Burkhardt, F Cerutti, A Ferrari, M Huhtinen, A Lechner, Y Levinsen, et al. Sources of machine-induced background in the atlas and cms detectors at the cern large hadron collider. *Nuclear Instruments and Methods in Physics Research Section A: Accelerators, Spectrometers, Detectors and Associated Equipment*, 729:825–840, 2013.

[76] Serguei Chatrchyan, Vardan Khachatryan, Albert M Sirunyan, Armen Tumasyan, Wolfgang Adam, Ernest Aguilo, T Bergauer, M Dragicevic, J Erö, C Fabjan, et al. Observation of a new boson at a mass of 125 gev with the cms experiment at the lhc. *Physics Letters B*, 716(1):30–61, 2012.

[77] Atlas Collaboration et al. Observation of a new particle in the search for the standard model higgs boson with the atlas detector at the lhc. *arXiv preprint arXiv:1207.7214*, 2012.

[78] Alexandre Zabi, Jeffrey Wayne Berryhill, Emmanuelle Perez, and Alexander D. Tapper. The Phase-2 Upgrade of the CMS Level-1 Trigger. 2020.

[79] CMS collaboration et al. The cms trigger system. *arXiv preprint arXiv:1609.02366*, 2016.

[80] Giorgio Apollinari, O Brüning, T Nakamoto, and Lucio Rossi. High luminosity large hadron collider hl-lhc. *arXiv preprint arXiv:1705.08830*, 2017.

[81] Georges Aad, Brad Abbott, Jalal Abdallah, S Abdel Khalek, O Abdinov, Rosemarie Aben, Babak Abi, Maris Abolins, OS AbouZeid, Halina Abramowicz, et al. Search for higgs boson pair production in the $\gamma\ \gamma$ b b^{-} final state using p p collision data at s= 8 tev from the atlas detector. *Physical review letters*, 114(8):081802, 2015.

[82] CMS collaboration et al. Technical proposal for the phase-ii upgrade of the cms detector. *CERN, CERN-LHCC-2015-010. LHCC-P-008*, 2015.

[83] M Benedikt, A Chance, B Dalena, D Denisov, M Giovannozzi, J Gutleber, R Losito, M Mangano, T Raubenheimer, W Riegler, et al. Future circular hadron collider fcc-hh: overview and status. *arXiv preprint arXiv:2203.07804*, 2022.

[84] Asmâa Abada, Marcello Abbrescia, Shehu S AbdusSalam, Ildar Abdyukhanov, Jose Abelleira Fernandez, A Abramov, M Aburaia, AO Acar, PR Adzic, P Agrawal, et al. Fcc-hh: The hadron collider. *The European Physical Journal Special Topics*, 228(4):755–1107, 2019.

[85] Ties Behnke, James E Brau, Brian Foster, Juan Fuster, Mike Harrison, James McEwan Paterson, Michael Peskin, Marcel Stanitzki, Nicholas Walker, and Hitoshi Yamamoto. The international linear collider technical design report-volume 1: Executive summary. *arXiv preprint arXiv:1306.6327*, 2013.

[86] C Athanassopoulos, LB Auerbach, RL Burman, DO Caldwell, ED Church, I Cohen, JB Donahue, A Fazely, FJ Federspiel, GT Garvey, et al. Evidence for nu_mu-¿ nu_e neutrino oscillations from lsnd. *arXiv preprint nucl-ex/9709006*, 1997.

[87] FP An, JZ Bai, AB Balantekin, HR Band, D Beavis, W Beriguete, M Bishai, S Blyth, K Boddy, RL Brown, et al. Observation of electron-antineutrino disappearance at daya bay. *Physical Review Letters*, 108(17):171803, 2012.

[88] Peter AR Ade, Nabila Aghanim, Charmaine Armitage-Caplan, Mark Arnaud, M Ashdown, F Atrio-Barandela, J Aumont, C Baccigalupi, Anthony J Banday, RB Barreiro, et al. Planck 2013 results. xvi. cosmological parameters. *Astronomy & Astrophysics*, 571:A16, 2014.

[89] Fritz Zwicky. Die rotverschiebung von extragalaktischen nebeln. *Helvetica physica acta*, 6:110–127, 1933.

[90] Vera C Rubin and W Kent Ford Jr. Rotation of the andromeda nebula from a spectroscopic survey of emission regions. *The Astrophysical Journal*, 159:379, 1970.

[91] Ziro Maki, Masami Nakagawa, and Shoichi Sakata. Remarks on the unified model of elementary particles. *Progress of Theoretical Physics*, 28(5):870–880, 1962.

[92] Stefano Moretti, Claire Shepherd-Themistocleous, and Harri Waltari. Lepton number violation in heavy higgs decays to sneutrinos. *arXiv preprint arXiv:1909.04692*, 2019.

[93] Amit Chakraborty, Stefano Moretti, Claire H Shepherd-Themistocleous, and Harri Waltari. Extraction of neutrino yukawa parameters from displaced vertices of sneutrinos. *Journal of High Energy Physics*, 2021(6):1–20, 2021.

[94] Shaaban Khalil and Stefano Moretti. *Supersymmetry beyond minimality: from theory to experiment*. CRC Press, 2017.

[95] Shrihari Gopalakrishna, André De Gouvêa, and Werner Porod. Right-handed sneutrinos as nonthermal dark matter. *Journal of Cosmology and Astroparticle Physics*, 2006(05):005, 2006.

[96] Hye-Sung Lee, Konstantin T Matchev, and Salah Nasri. Revival of the thermal sneutrino dark matter. *Physical Review D*, 76(4):041302, 2007.

[97] Shaaban Khalil, Hiroshi Okada, and Takashi Toma. Right-handed sneutrino dark matter in supersymmetric b- l model. *Journal of High Energy Physics*, 2011(7):1–21, 2011.

[98] Priyotosh Bandyopadhyay, Eung Jin Chun, and Jong-Chul Park. Right-handed sneutrino dark matter in \mathbf {U (1)'} $seesawmodelsanditssignaturesatthelhc.arXivpreprintarXiv$: 1105.1652, 2011.

[99] G Bélanger, J Da Silva, and A Pukhov. The right-handed sneutrino as thermal dark matter in u (1) extensions of the mssm. *Journal of Cosmology and Astroparticle Physics*, 2011(12):014, 2011.

[100] Lorenzo Basso, Ben O'Leary, Werner Porod, and Florian Staub. Dark matter scenarios in the minimal susy b- l model. *Journal of High Energy Physics*, 2012(9):1–43, 2012.

[101] Katri Huitu, Jari Laamanen, Lasse Leinonen, Santosh Kumar Rai, and Timo Rüppell. Comparison of neutralino and sneutrino dark matter in a model with spontaneous cp violation. *Journal of High Energy Physics*, 2012(11):1–23, 2012.

[102] Arindam Chatterjee, Debottam Das, Biswarup Mukhopadhyaya, and Santosh Kumar Rai. Right sneutrino dark matter and a monochromatic photon line. *Journal of Cosmology and Astroparticle Physics*, 2014(07):023, 2014.

[103] Shankha Banerjee, Genevieve Bélanger, Biswarup Mukhopadhyaya, and Pasquale D Serpico. Signatures of sneutrino dark matter in an extension of the cmssm. *Journal of High Energy Physics*, 2016(7):1–30, 2016.

[104] Mariana Frank, Benjamin Fuks, Katri Huitu, Santosh Kumar Rai, and Harri Waltari. Resonant slepton production and right sneutrino dark matter in left-right supersymmetry. *Journal of High Energy Physics*, 2017(5):1–32, 2017.

[105] Luigi Delle Rose, Shaaban Khalil, Simon JD King, Suchita Kulkarni, Carlo Marzo, Stefano Moretti, and Cem S Un. Sneutrino dark matter in the blssm. *Journal of High Energy Physics*, 2018(7):1–21, 2018.

[106] Shankha Banerjee, Genevieve Bélanger, Avirup Ghosh, and Biswarup Mukhopadhyaya. Long-lived stau, sneutrino dark matter and right-slepton spectrum. *Journal of High Energy Physics*, 2018(9):1–23, 2018.

[107] Junjie Cao, Jie Li, Yusi Pan, Liangliang Shang, Yuanfang Yue, and Di Zhang. A bayesian analysis of sneutrino dm in the nmssm with type-i seesaw mechanism. *arXiv preprint arXiv:1807.03762*, 2018.

[108] Nima Arkani-Hamed, Lawrence Hall, Hitoshi Murayama, David Smith, and Neal Weiner. Small neutrino masses from supersymmetry breaking. *Physical Review D*, 64(11):115011, 2001.

[109] Ryuichiro Kitano and Kin-ya Oda. Neutrino masses in the supersymmetric standard model with right-handed neutrinos and spontaneous r-parity violation. *Physical Review D*, 61(11):113001, 2000.

[110] SA Abel, Subir Sarkar, and PL White. On the cosmological domain wall problem for the minimally extended supersymmetric standard model. *Nuclear Physics B*, 454(3):663–681, 1995.

[111] C Panagiotakopoulos and Kyriakos Tamvakis. Stabilized nmssm without domain walls. *Physics Letters B*, 446(3-4):224–227, 1999.

[112] Anupam Mazumdar, Ken'ichi Saikawa, Masahide Yamaguchi, and Jun'ichi Yokoyama. Possible resolution of the domain wall problem in the nmssm. *Physical Review D*, 93(2):025002, 2016.

[113] A Dedes, C Hugonie, S Moretti, and K Tamvakis. Phenomenology of a new minimal supersymmetric extension of the standard model. *Physical Review D*, 63(5):055009, 2001.

[114] Daniel E López-Fogliani, Andres D Perez, and Roberto Ruiz de Austri. Dark matter candidates in the nmssm with rh neutrino superfields. *Journal of Cosmology and Astroparticle Physics*, 2021(04):067, 2021.

[115] David G Cerdeno, Victor Martin-Lozano, and Osamu Seto. Displaced vertices and long-lived charged particles in the nmssm with right-handed sneutrinos. *Journal of High Energy Physics*, 2014(5):1–30, 2014.

[116] Florian Staub. Exploring new models in all detail with sarah. *Advances in High Energy Physics*, 2015, 2015.

[117] Avelino Vicente. Computer tools in particle physics. *arXiv preprint arXiv:1507.06349*, 2015.

[118] Werner Porod. Spheno, a program for calculating supersymmetric spectra, susy particle decays and susy particle production at e+ e- colliders. *Computer Physics Communications*, 153(2):275–315, 2003.

[119] Werner Porod and Florian Staub. Spheno 3.1: Extensions including flavour, cp-phases and models beyond the mssm. *Computer Physics Communications*, 183(11):2458–2469, 2012.

[120] Johan Alwall, Michel Herquet, Fabio Maltoni, Olivier Mattelaer, and Tim Stelzer. Madgraph 5: going beyond. *Journal of High Energy Physics*, 2011(6):1–40, 2011.

[121] Torbjörn Sjöstrand, Stefan Ask, Jesper R Christiansen, Richard Corke, Nishita Desai, Philip Ilten, Stephen Mrenna, Stefan Prestel, Christine O Rasmussen, and Peter Z Skands. An introduction to pythia 8.2. *Computer physics communications*, 191:159–177, 2015.

[122] J De Favereau, Christophe Delaere, Pavel Demin, Andrea Giammanco, Vincent Lemaitre, Alexandre Mertens, and Michele Selvaggi. Delphes 3: a modular framework

for fast simulation of a generic collider experiment. *Journal of High Energy Physics*, 2014(2):1–26, 2014.

[123] CT Potter. Dsid: a delphes detector for ilc physics studies. *arXiv preprint arXiv:1602.07748*, 2016.

[124] Federico Ambrogi, Chiara Arina, Mihailo Backović, Jan Heisig, Fabio Maltoni, Luca Mantani, Olivier Mattelaer, and Gopolang Mohlabeng. Maddm v. 3.0: a comprehensive tool for dark matter studies. *Physics of the Dark Universe*, 24:100249, 2019.

[125] Eric Conte, Benjamin Fuks, and Guillaume Serret. Madanalysis 5, a user-friendly framework for collider phenomenology. *Computer Physics Communications*, 184(1):222–256, 2013.

[126] T Barklow, J Brau, K Fujii, J Gao, J List, N Walker, and K Yokoya. Ilc operating scenarios. *arXiv preprint arXiv:1506.07830*, 2015.

[127] Abdelhak Djouadi, Y Mambrini, and M Mühlleitner. Chargino and neutralino decays revisited. *The European Physical Journal C-Particles and Fields*, 20(3):563–584, 2001.

[128] R Barate, D Buskulic, D Decamp, P Ghez, C Goy, S Jezequel, J-P Lees, A Lucotte, F Martin, E Merle, et al. Single-and multi-photon production in e+ e- collisions at a centre-of-mass energy of 183 gev. *Physics Letters B*, 429(1-2):201–214, 1998.

[129] J Abdallah, DELPHI Collaboration, et al. Photon events with missing energy in e+ e-collisions at sqrt {s}= 130 to 209 gev. *arXiv preprint hep-ex/0406019*, 2004.

[130] Murray Gell-Mann, Pierre Ramond, and Richard Slansky. Complex spinors and unified theories. In *Murray Gell-Mann: Selected Papers*, pages 266–272. World Scientific, 2010.

[131] Rabindra N Mohapatra and Goran Senjanović. Neutrino masses and mixings in gauge models with spontaneous parity violation. *Physical Review D*, 23(1):165, 1981.

[132] Shaaban Khalil and Stefano Moretti. *Standard model phenomenology*. CRC Press, 2022.

[133] Albert M Sirunyan, Armen Tumasyan, Wolfgang Adam, Federico Ambrogi, Ece Asilar, Thomas Bergauer, Johannes Brandstetter, Erica Brondolin, Marko Dragicevic, Janos Erö, et al. Search for evidence of the type-iii seesaw mechanism in multilepton final states in proton-proton collisions at s= 13 tev. *Physical review letters*, 119(22):221802, 2017.

[134] CMS collaboration et al. Search for heavy majorana neutrinos in same-sign dilepton channels in proton-proton collisions at $\sqrt{s}$ =13 tev. *arXiv preprint arXiv:1806.10905*, 2018.

[135] Georges Aad, Brad Abbott, Dale Charles Abbott, A Abed Abud, K Abeling, DK Abhayasinghe, SH Abidi, OS AbouZeid, NL Abraham, H Abramowicz, et al. Search for heavy neutral leptons in decays of w bosons produced in 13 tev pp collisions using prompt and displaced signatures with the atlas detector. *Journal of high energy physics*, 2019(10):1–47, 2019.

[136] Georges Aad, Brad Abbott, Dale C Abbott, A Abed Abud, Kira Abeling, Deshan Kavishka Abhayasinghe, Syed Haider Abidi, OS AbouZeid, Nadine L Abraham, Halina Abramowicz, et al. Search for type-iii seesaw heavy leptons in dilepton final states in pp collisions at s= 13 tev with the atlas detector. *The European Physical Journal C*, 81(3):218, 2021.

[137] Alexey A Petrov and William Shepherd. Searching for dark matter at lhc with mono-higgs production. *Physics Letters B*, 730:178–183, 2014.

[138] Asher Berlin, Tongyan Lin, and Lian-Tao Wang. Mono-higgs detection of dark matter at the lhc. *Journal of High Energy Physics*, 2014(6):1–20, 2014.

[139] Georges Aad, Brad Abbott, Dale Charles Abbott, A Abed Abud, K Abeling, DK Abhayasinghe, SH Abidi, OS AbouZeid, NL Abraham, H Abramowicz, et al. Search for electroweak production of charginos and sleptons decaying into final states with two leptons and missing transverse momentum in $\sqrt{s} = 13$ tev pp collisions using the atlas detector. *The European Physical Journal C*, 80(2):1–33, 2020.

[140] Fabiola Gianotti, Michelangelo L Mangano, T Virdee, S Abdullin, G Azuelos, A Ball, D Barberis, A Belyaev, P Bloch, M Bosman, et al. Physics potential and experimental

challenges of the lhc luminosity upgrade. *The European Physical Journal C-Particles and Fields*, 39:293–333, 2005.

[141] ATLAS collaboration et al. Search for heavy resonances decaying into a z or w boson and a higgs boson in final states with leptons and b-jets in 139 fb $^{-1}$ of pp collisions at $\sqrt{s} = 13$ tev with the atlas detector. *arXiv preprint arXiv:2207.00230*, 2022.

[142] CMS collaboration et al. Identification of b-quark jets with the cms experiment. *Journal of Instrumentation*, 8(04):P04013, 2013.

[143] FCC collaboration et al. Fcc physics opportunities: future circular collider conceptual design report volume 1. *European Physical Journal C*, 79(6):474, 2019.

[144] Alakabha Datta, Murugeswaran Duraisamy, and David London. Searching for new physics with b-decay fake triple products. *Physics Letters B*, 701(3):357–362, 2011.

[145] A Elsayed, S Khalil, and S Moretti. Higgs mass corrections in the susy b- l model with inverse seesaw. *Physics Letters B*, 715(1-3):208–213, 2012.

[146] Rene Brun and Fons Rademakers. Root—an object oriented data analysis framework. *Nuclear instruments and methods in physics research section A: accelerators, spectrometers, detectors and associated equipment*, 389(1-2):81–86, 1997.

[147] A Abada et al. Future circular collider conceptual design report. *The Eur. Phys. J. Spec. Top*, 228, 2019.